Supplementary Information for Cobalt complexes with α-amino acid ligands catalyzes incorporation of CO_2 into cyclic carbonates.

Andrés Castro Ruiz[1], Lea Grefe[2], Esteban Mejía[2], Sigridur G. Suman[1]

[1]Science Institute, University of Iceland, Dunhagi 3, 107 Reykjavik, Iceland

[2]Leibniz Institute for Catalysis, Albert-Einstein-Str. 29a, 18059 Rostock, Germany

Contents

Table S1. *Summary of crystal data and structural refinement parameters for* ***6****.*

Parameter	**6**
Empirical formula	$C_{20}H_{24}N_4O_4CoCl$
Colour	Red block
Formula weight ($gmol^{-1}$)	478.81
Crystal size (mm)	0.45 × 0.35 × 0.30
Crystal system	Orthorhombic
Space group	P $2_12_12_1$
a (Å)	8.3459(6)
b (Å)	12.9372(9)
c (Å)	19.0279(14)
α (°)	
β (°)	
γ (°)	
Volume ($Å^3$)	2054.5(3)
Z	4
$\rho_{calc.}(g/cm^3)$	1.548
F(000)	992.0
μ K_α (mm^{-1})	1.001
Temperature (K)	296(2) K
Reflections collected/unique/ observed [$I > 2\sigma(I)$]	74894/8384/
Data/restraints/parameters	8384/0/279
Goodness of fit on F^2	1.042
Final R indices [I>2σ(I)]	R_1 = 0.0279, wR_2 = 0.0770
R indices (all data)	R_1 = 0.0302, wR_2 = 0.0796

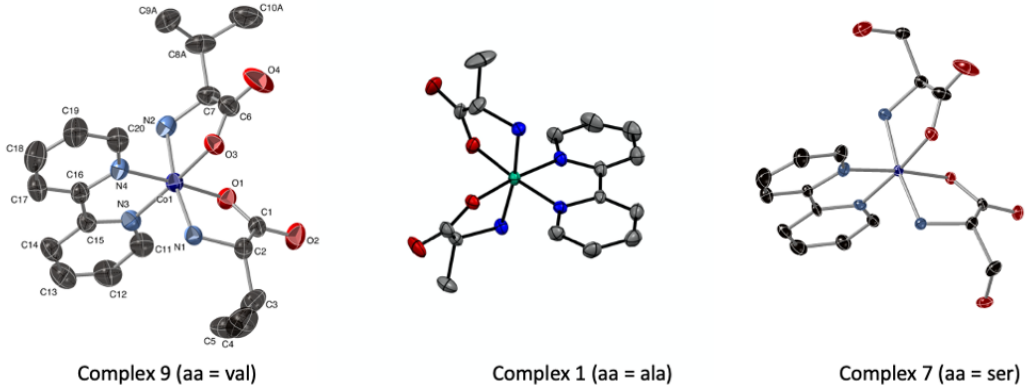

Figure S1A Structural connectivity of **1**, **7** and **9**. Figures obtained after partial refinement described in the main text.

SI Table 2. Unit cell parameters for **1**, **7** and **9**.

Parameter/compound	**1**	**7**	**9**
Empirical formula	$C_{16}H_{24}N_4O_6CoCl$	$C_{17}H_{21}N_4O_7CoCl$	$C_{16}H_{24}N_4O_6CoCl$
Colour	pink block	pink block	pink needle
Formula weight ($gmol^{-1}$)	462.77	463.74	489.77
Crystal size (mm)	0.40 × 0.30 × 0.20	0.45 × 0.35 × 0.30	0.52 × 0.14 × 0.12
Crystal system	Monoclinic	Monoclinic	Hexagonal
Space group	P 2_1	P 2_1	P 6_5
a (Å)	11.788(2)	11.7639(15)	16.5159(11)
b (Å)	10.3789(18)	12.3920(15)	16.5159(11)
c (Å)	19.083(3)	15.4726(19)	16.5811(11)
α (°)	90	90	90
β (°)	107.52(6)	111.65(4)	90
γ (°)	90	90	120
Volume ($Å^3$)	2226.4(7)	2096.4(5)	3917.0(5)
Z	4	4	6
$\rho_{calc.}(g/cm^3)$	1.396	1.497	1.291
Temperature (K)	296(2) K	150(2) K	296(2) K

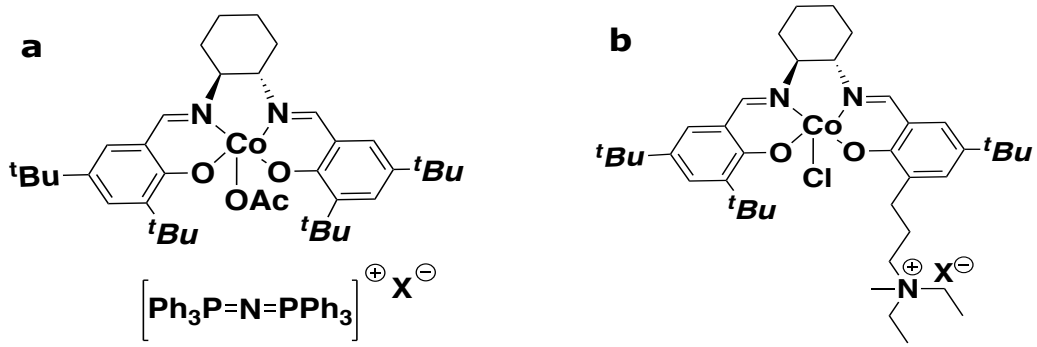

Figure S1. a) binary Co(III) salen/PPNCl catalyst. b) bifunctional Co(III) salen

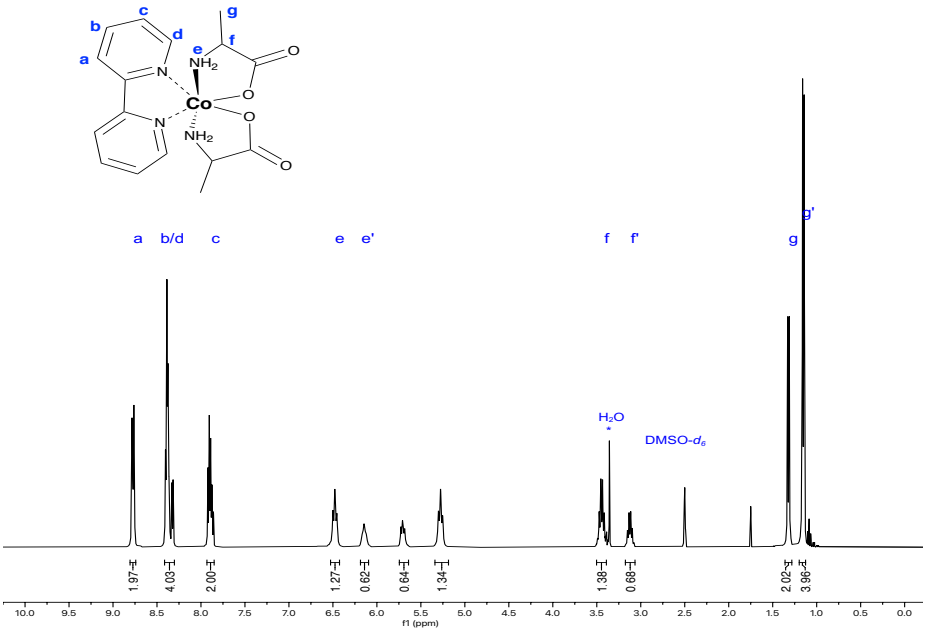

Figure S2. ^{1}H NMR of **1** in DMSO-d_6 mixture of diastereomers major product Δ-*RR*/*Λ*-*SS* and minor product Δ-*SS*/*Λ*-*RR* 2:1

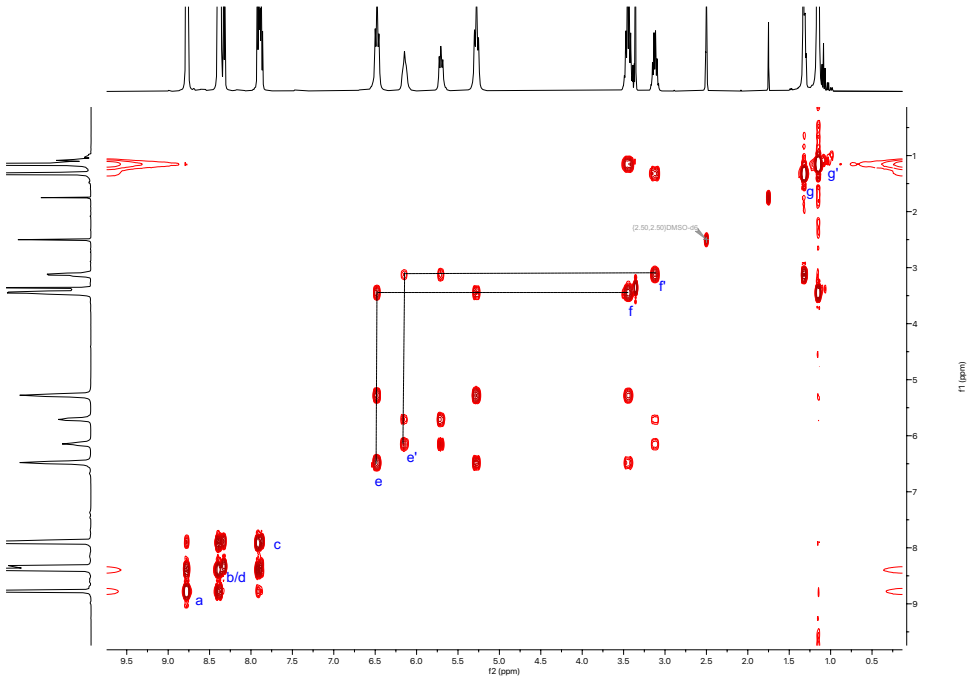

Figure S3. 2D COSY NMR of **1** (DMSO-d_6, 298 K)

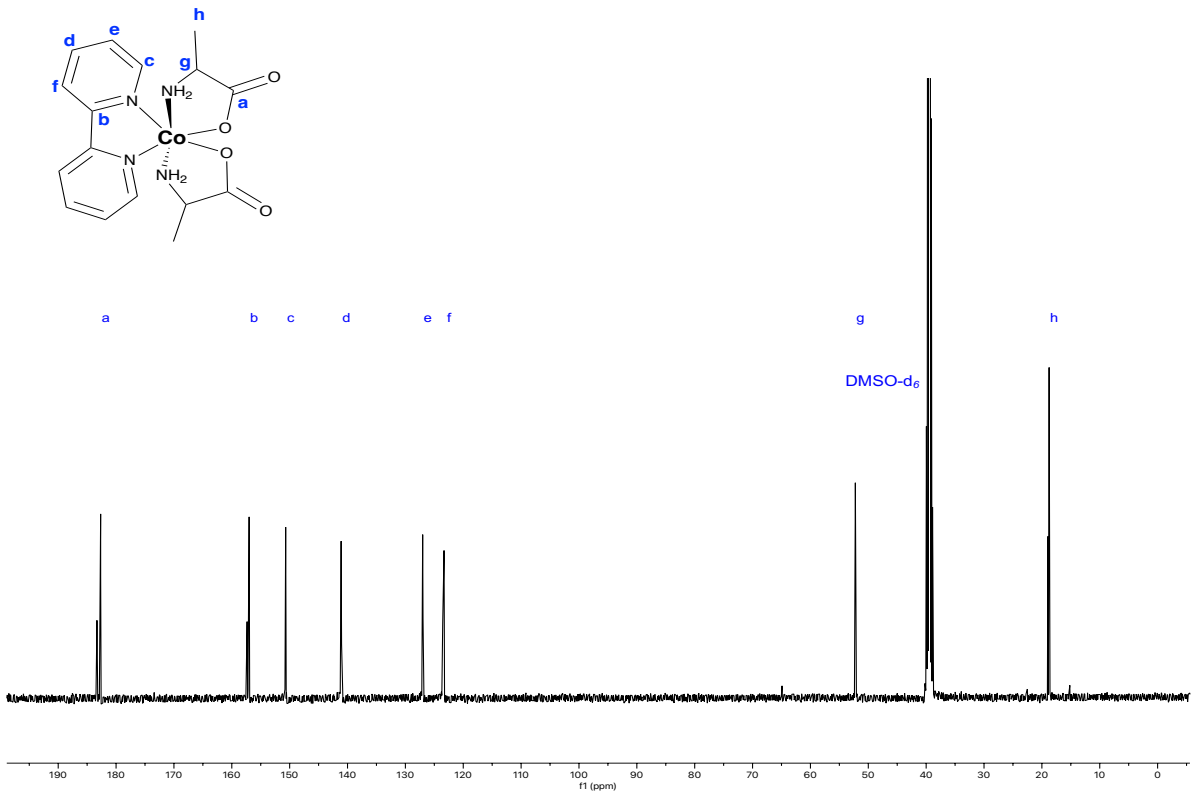

Figure S4. $^{13}C\{1H\}$ NMR of **1** (DMSO-*d*6, 298 K)

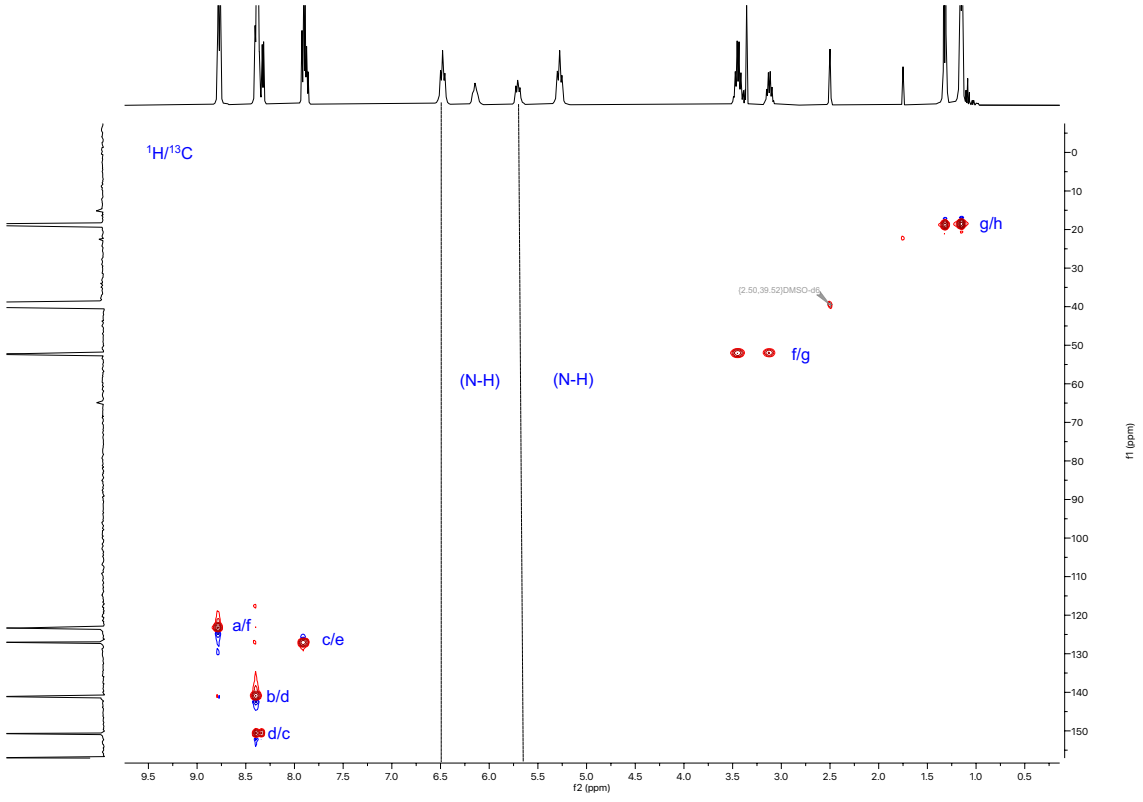

Figure S5. 2D HSQC NMR of **1** (DMSO-d_6, 298 K)

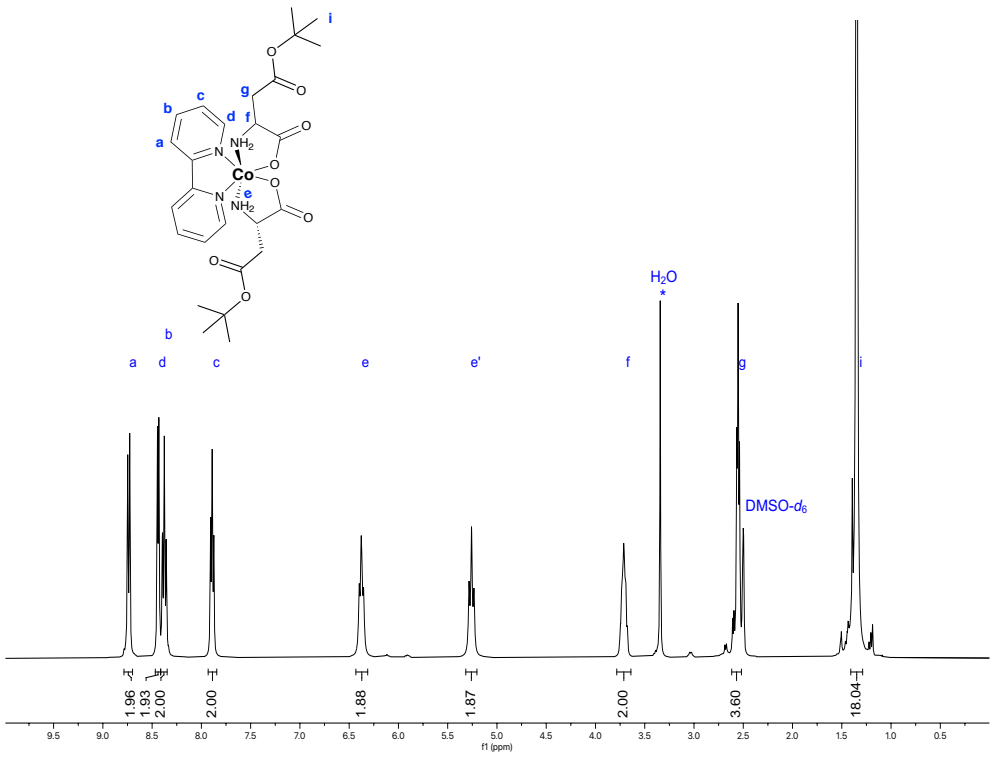

Figure S6. ^{1}H NMR of **2** in (DMSO-d_6, 298 K)

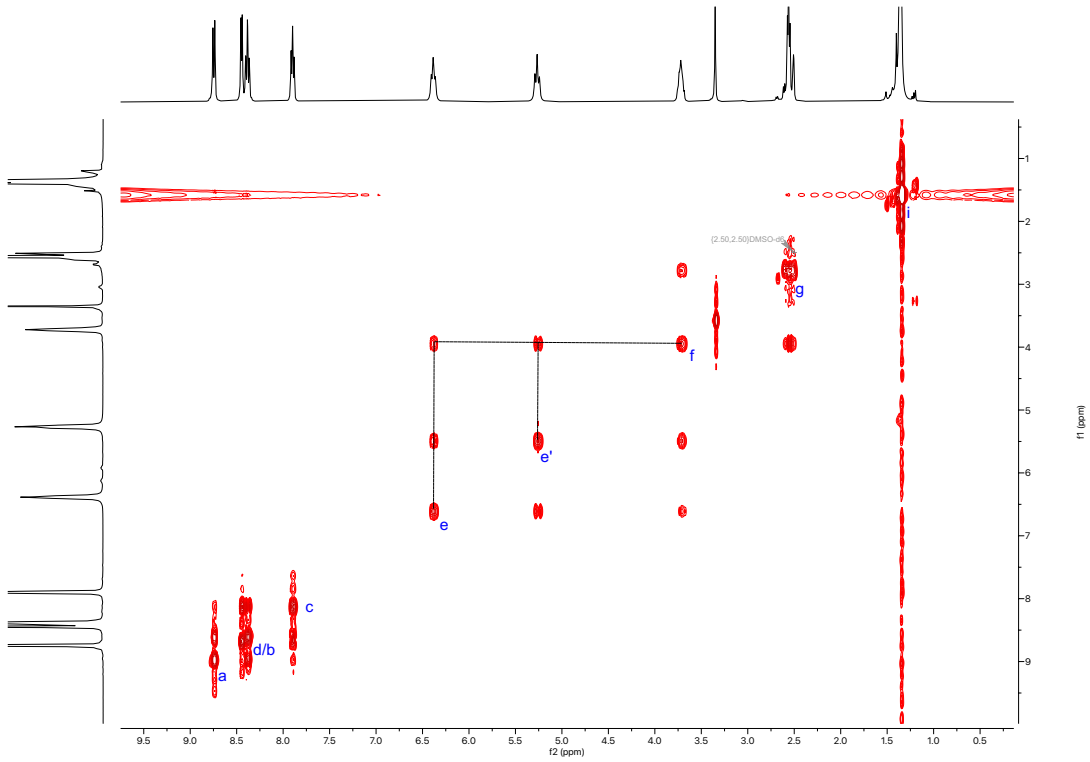

Figure S7. 2D COSY NMR of **2** (DMSO-d_6, 298 K)

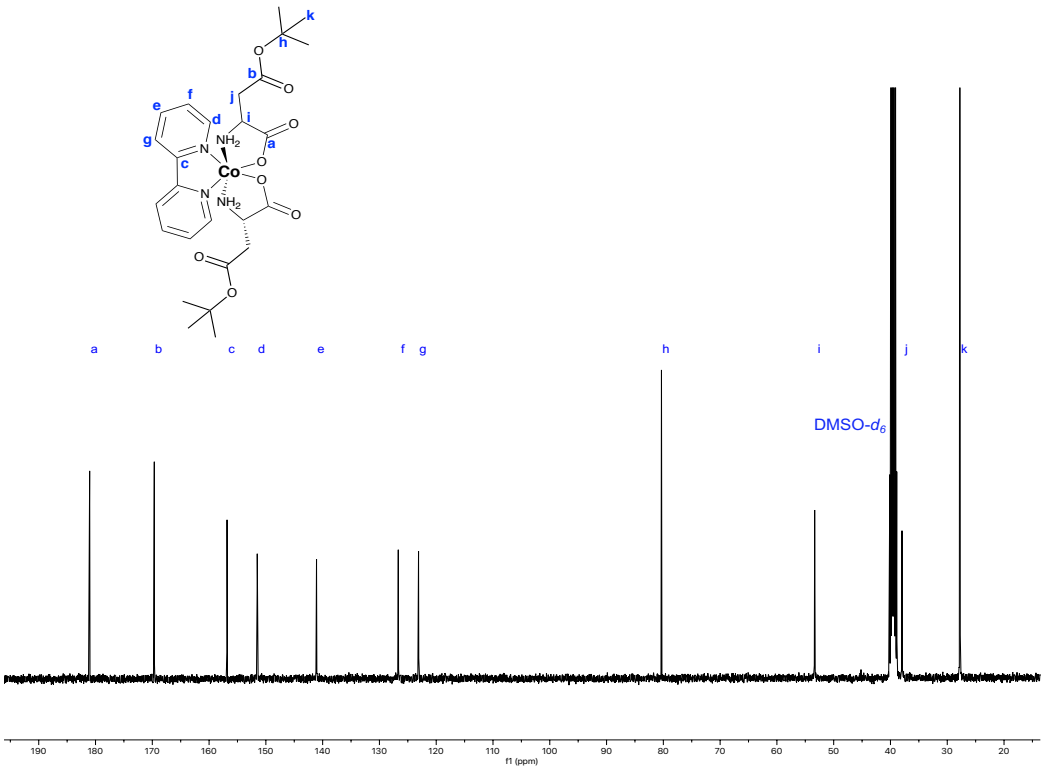

Figure S8. $^{13}C\{1H\}$ NMR of **2** (DMSO-d_6, 298 K)

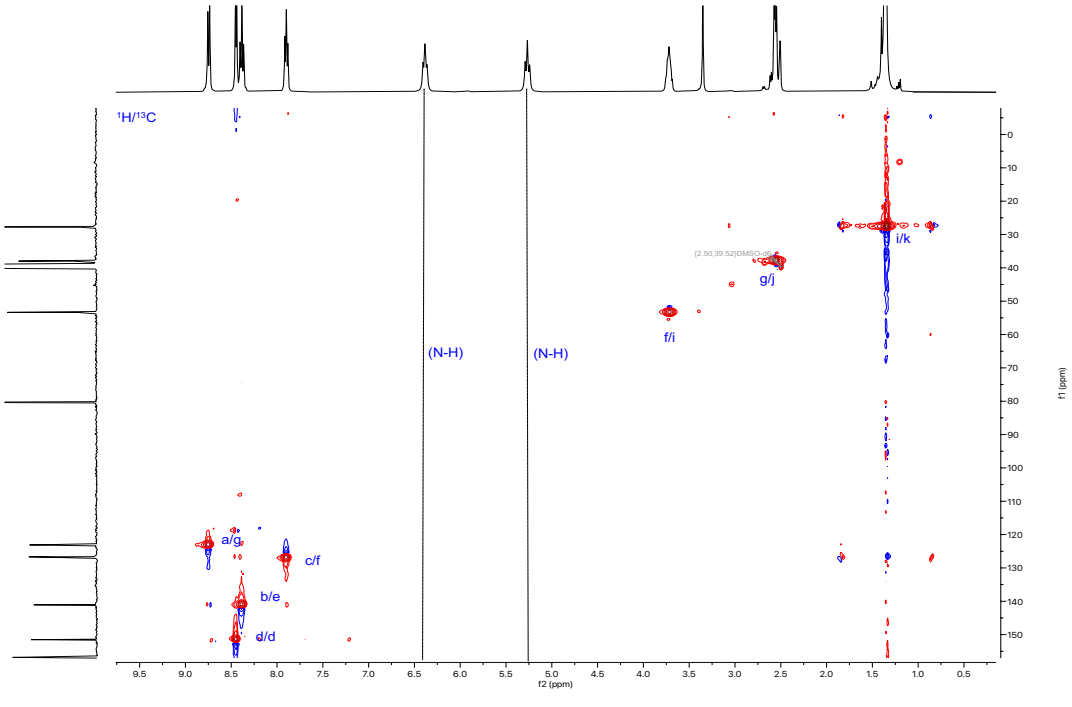

Figure S9. 2D HSQC NMR of **2** (DMSO-d_6, 298 K)

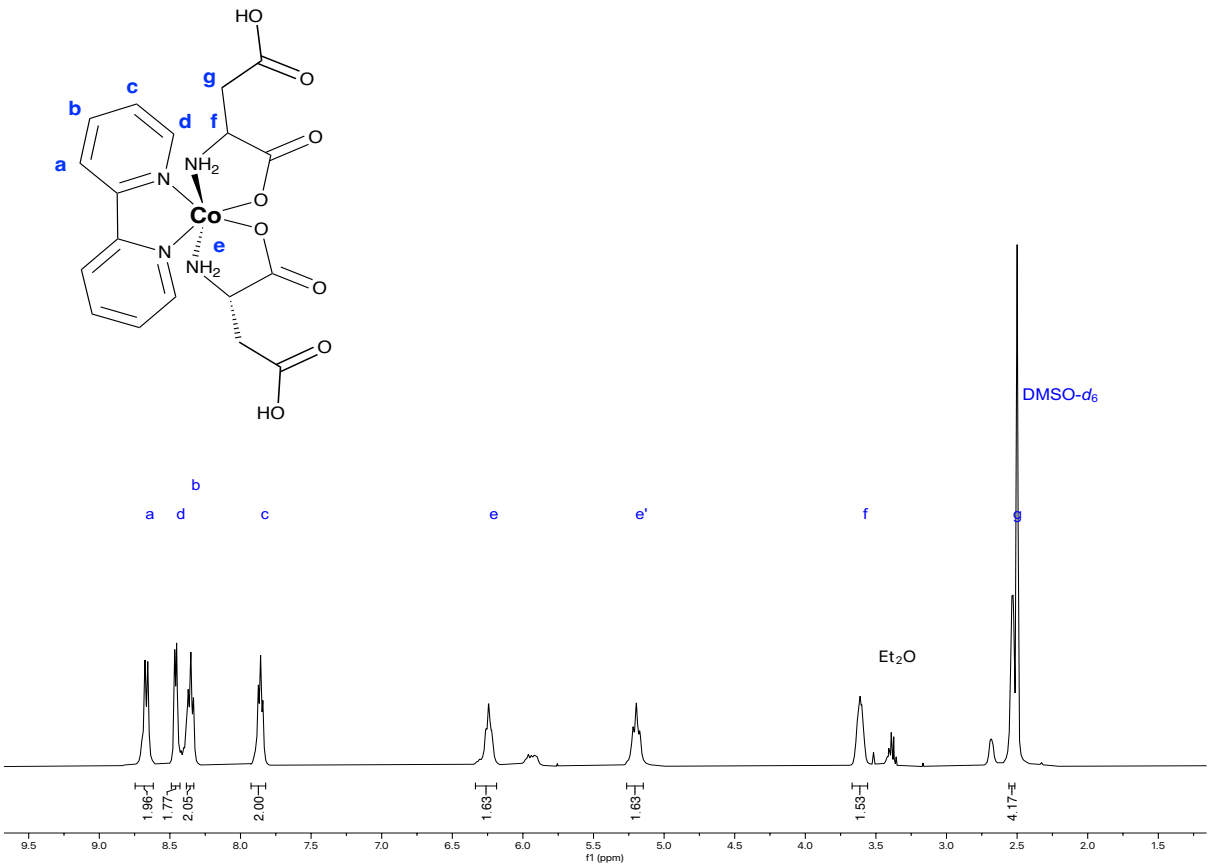

Figure S10. ^{1}H NMR of **2a** in (DMSO-d_6, 298 K)

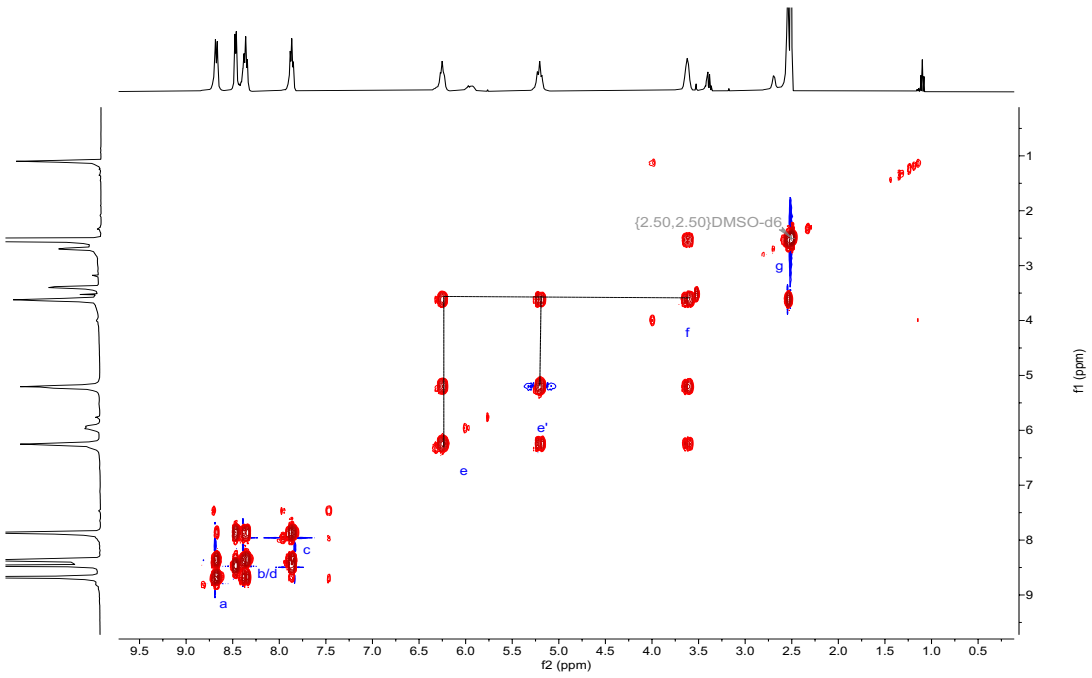

Figure S11. 2D COSY NMR of **2a** (DMSO-d_6, 298 K)

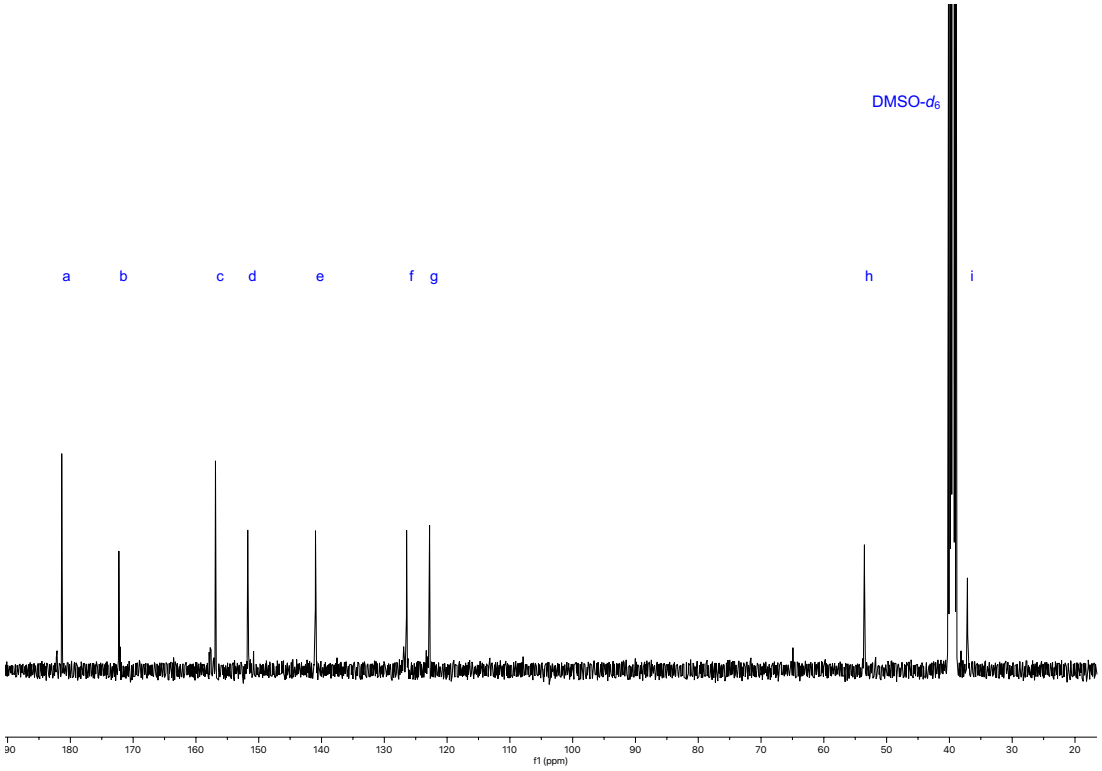

Figure S12. $^{13}C\{1H\}$ NMR of **2a** (DMSO-d_6, 298 K)

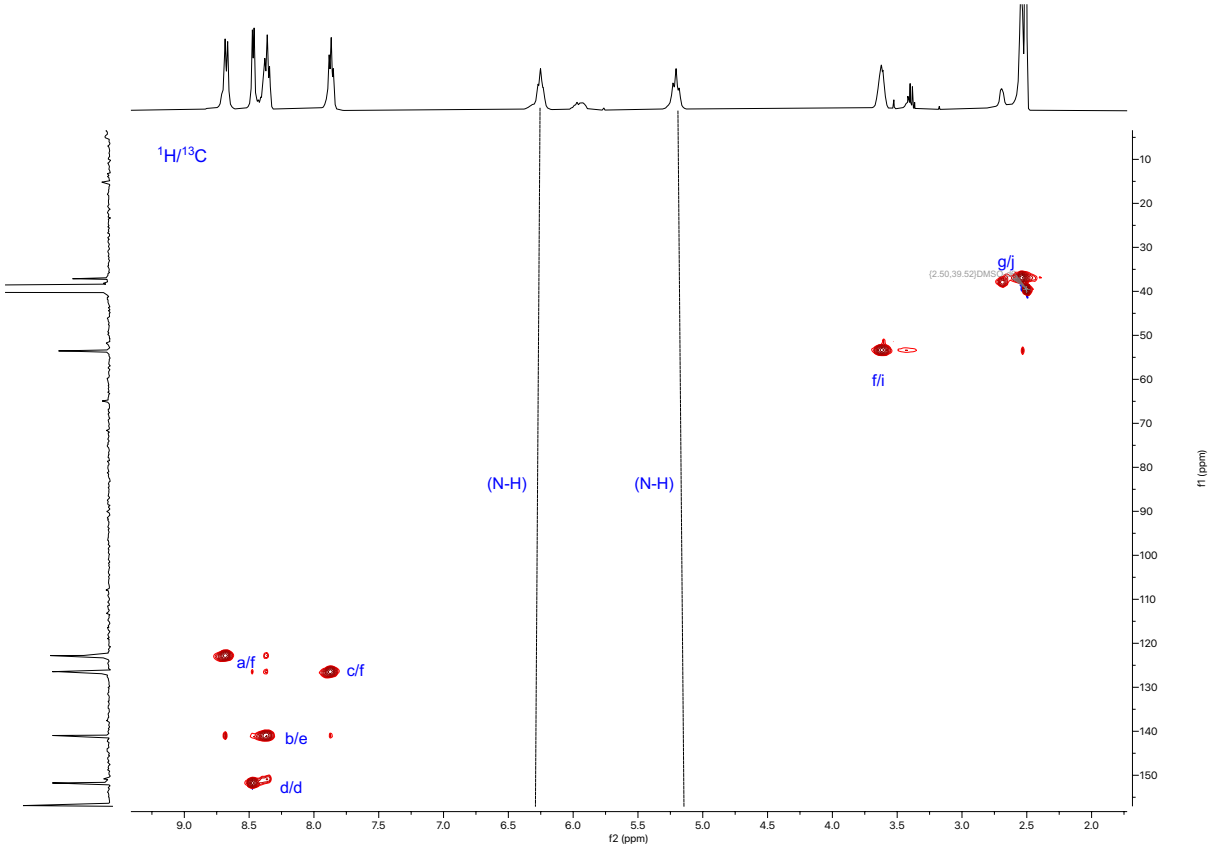

Figure S13. 2D HSQC NMR of **2a** (DMSO-d_6, 298 K)

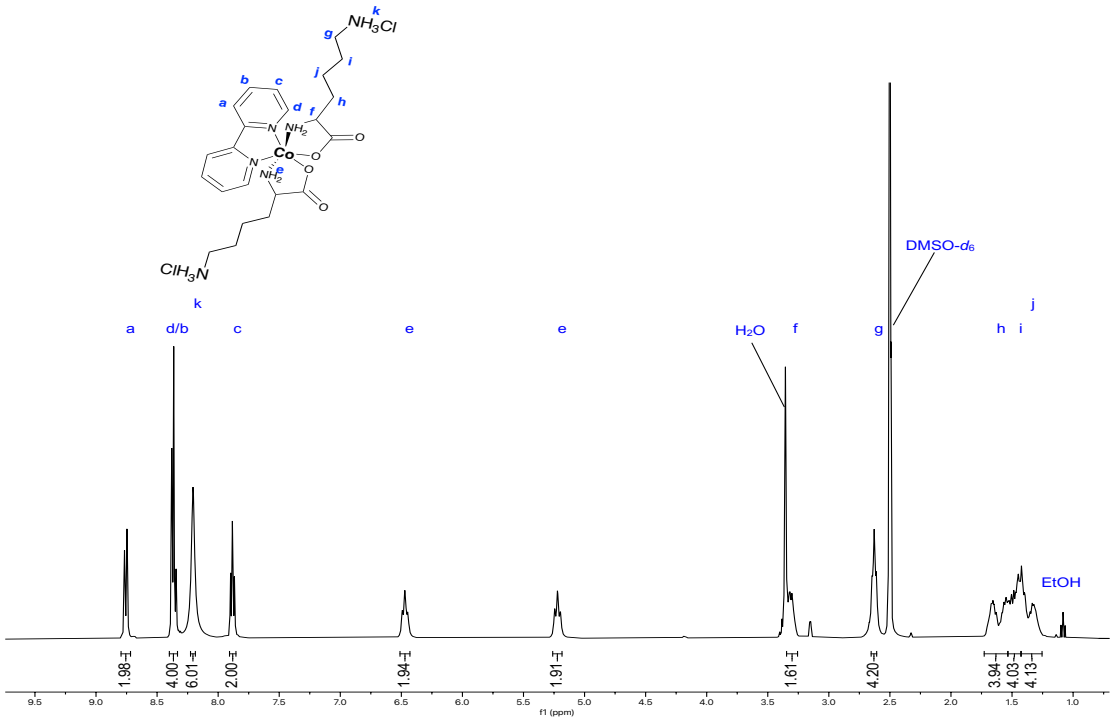

Figure S14. ^{1}H NMR of **3** in (DMSO-d_6, 298 K)

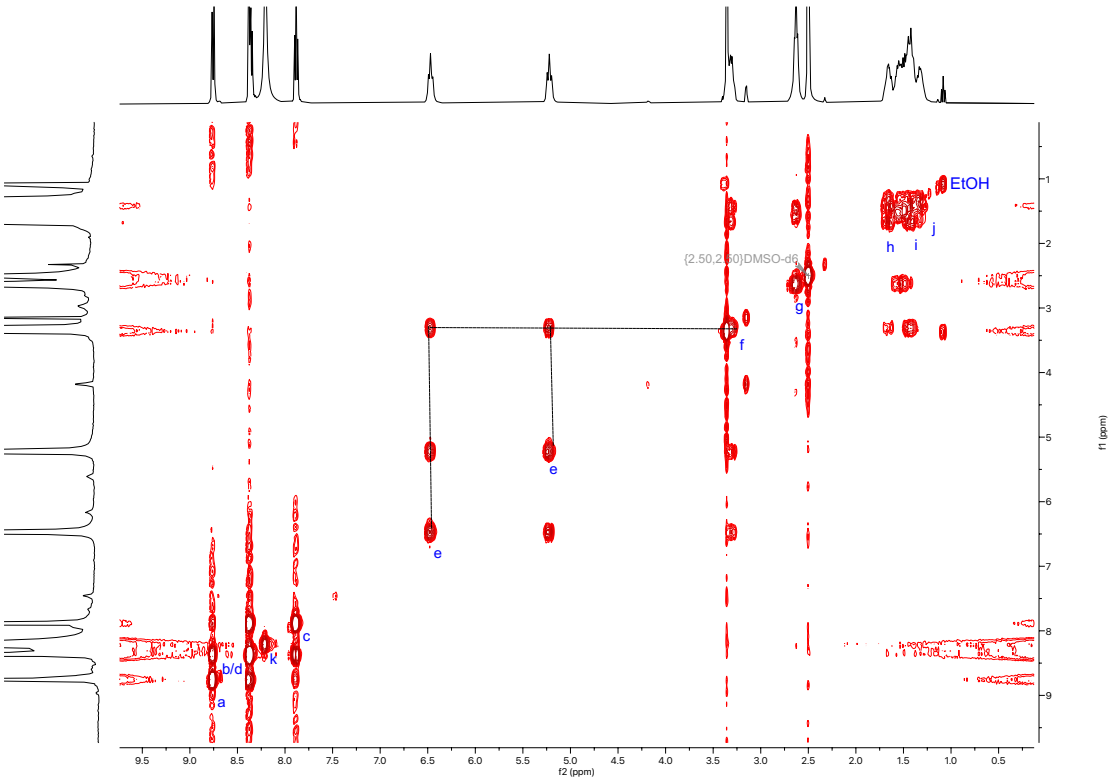

Figure S15. 2D COSY NMR of **3** (DMSO-d_6, 298 K)

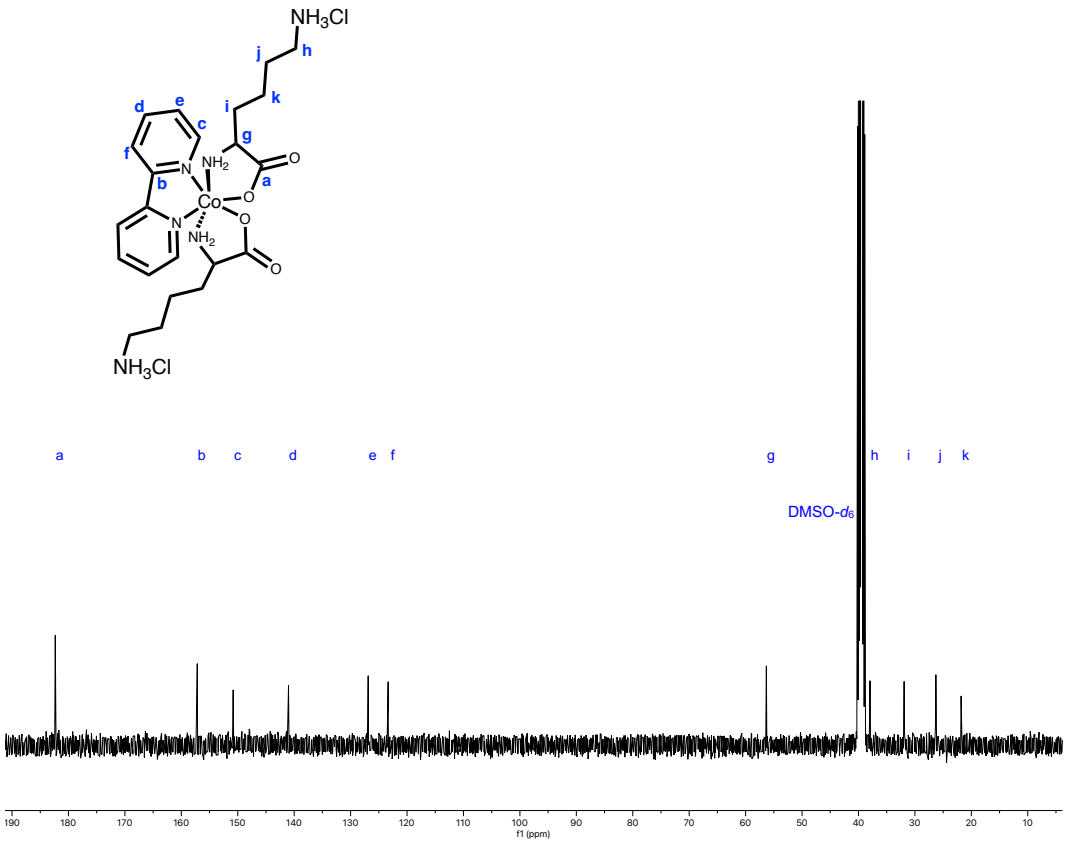

Figure S16. $^{13}C\{1H\}$ NMR of **3** (DMSO-d_6, 298 K)

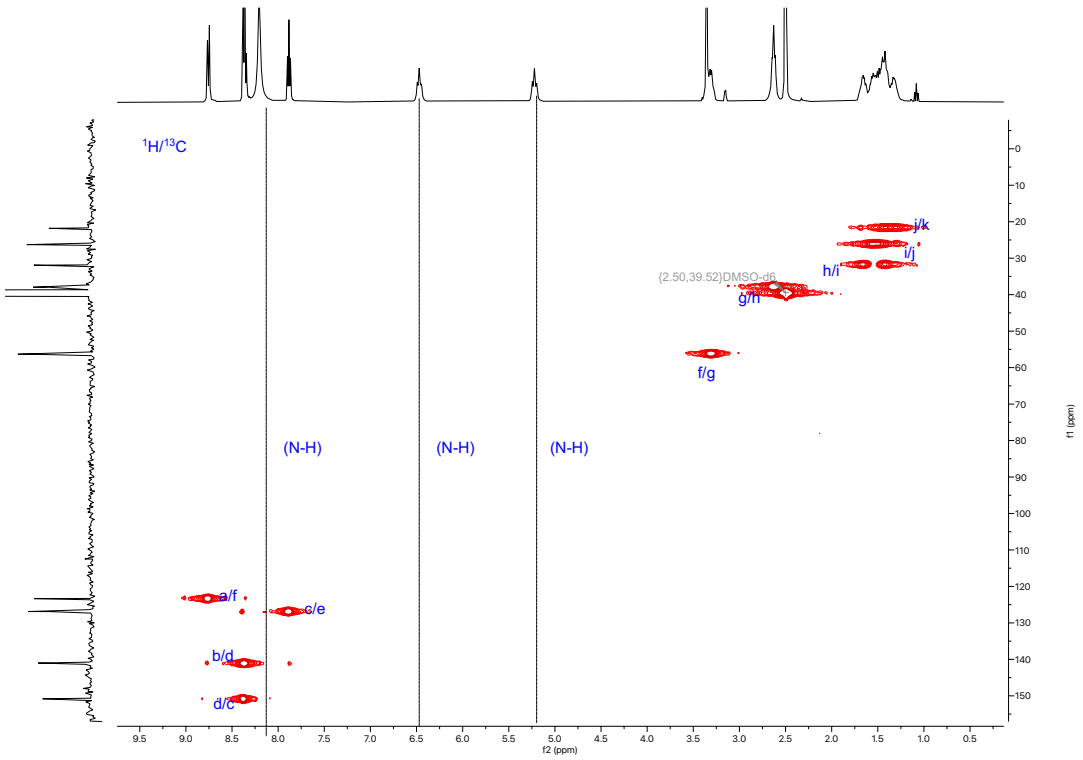

Figure S17. 2D HSQC NMR of **3** (DMSO-d_6, 298 K)

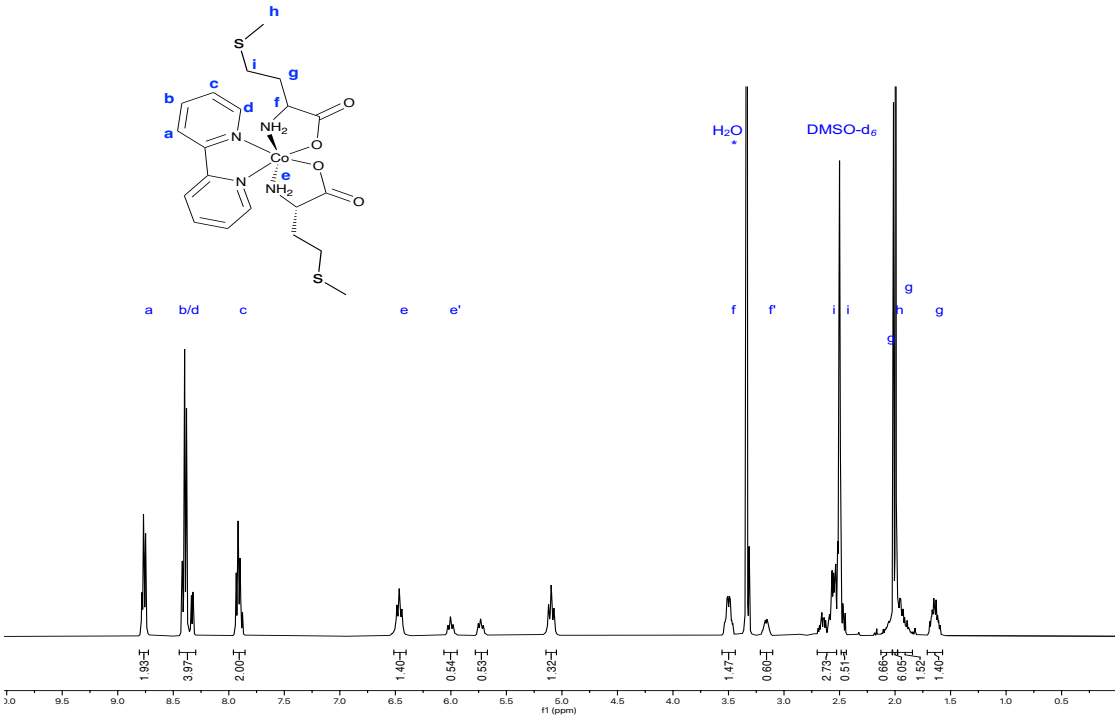

Figure S18. ^{1}H NMR of **4** in (DMSO-d_6, 298 K) mixture of diastereomers major product Δ-*RR*/*Λ*-*SS* and minor product Δ-*SS*/*Λ*-*RR* 2.4:1

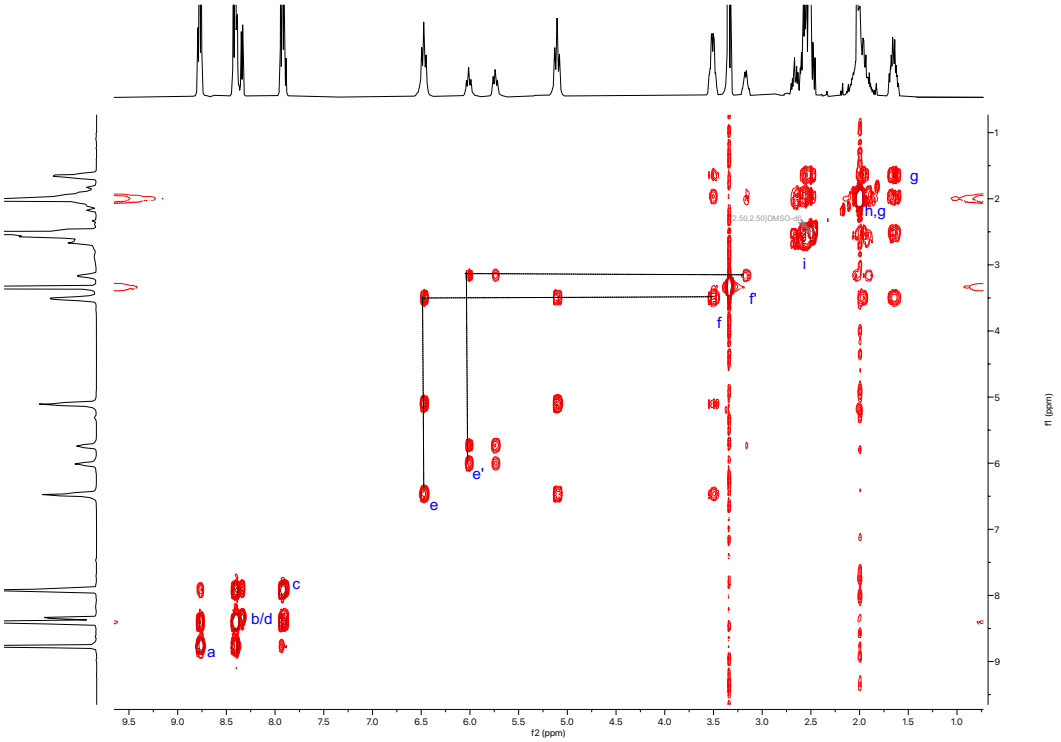

Figure S19. 2D COSY NMR of **4** (DMSO-d_6, 298 K)

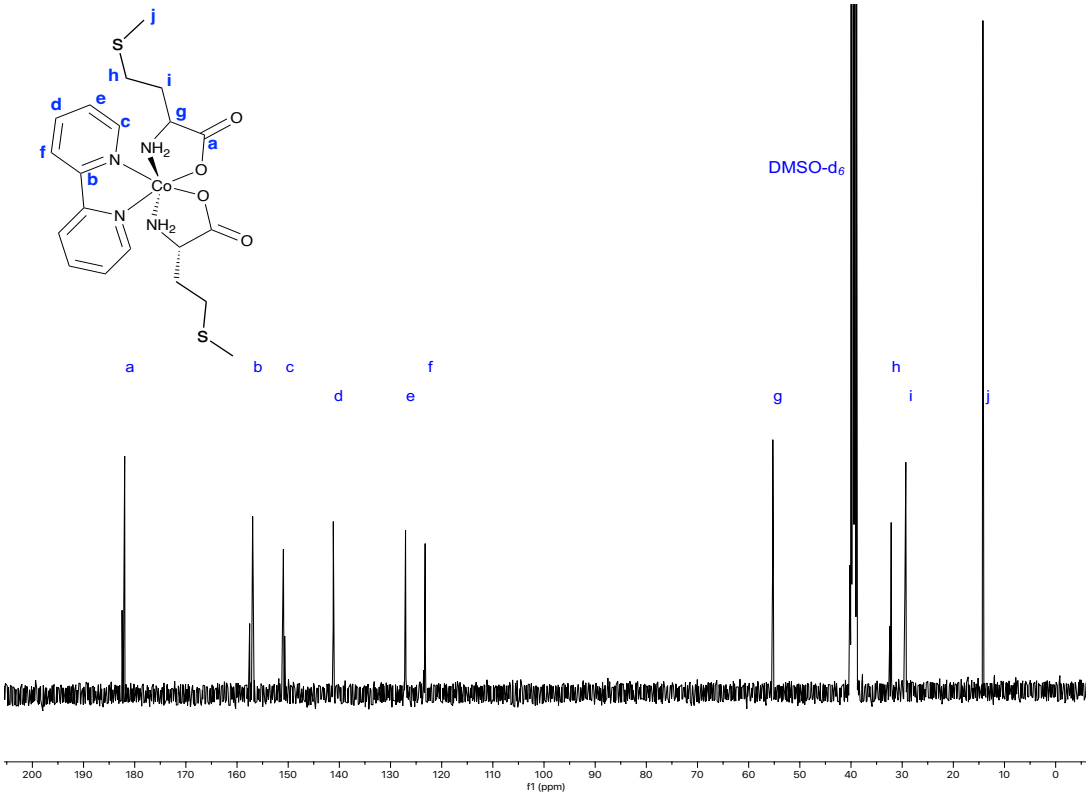

Figure S20. $^{13}C\{1H\}$ NMR of **4** (DMSO-*d*6, 298 K)

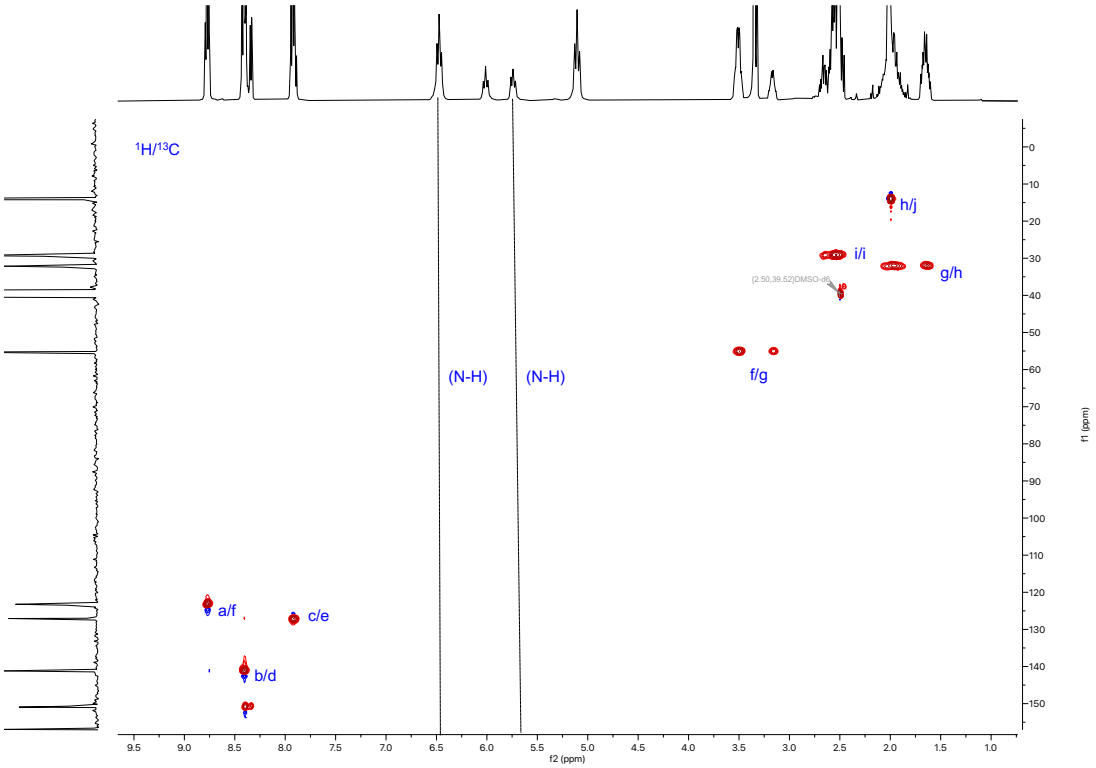

Figure S21. 2D HSQC NMR of **4** (DMSO-d_6, 298 K)

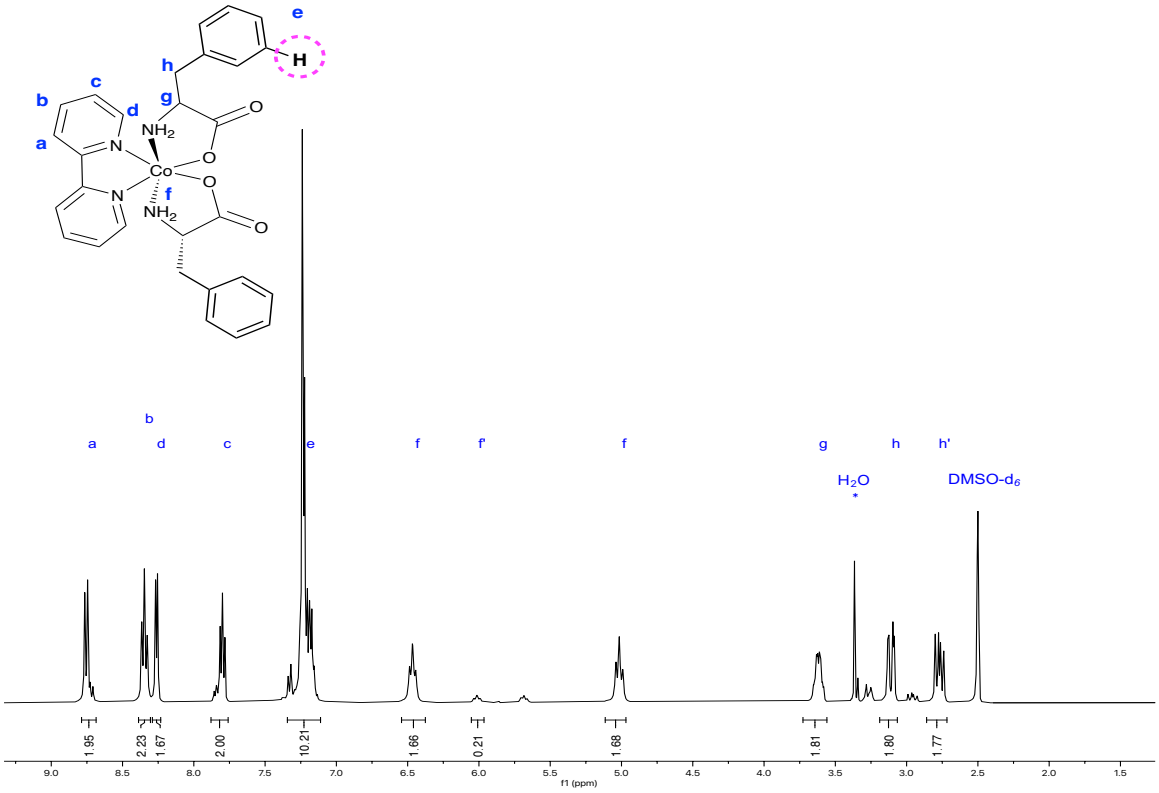

Figure S22. ^{1}H NMR of **5** in (DMSO-d_6, 298 K) precise signal integration could not be obtained for protons **e** due to overlapping with neighboring signal. In this case signals were integrated together. 4.15:1

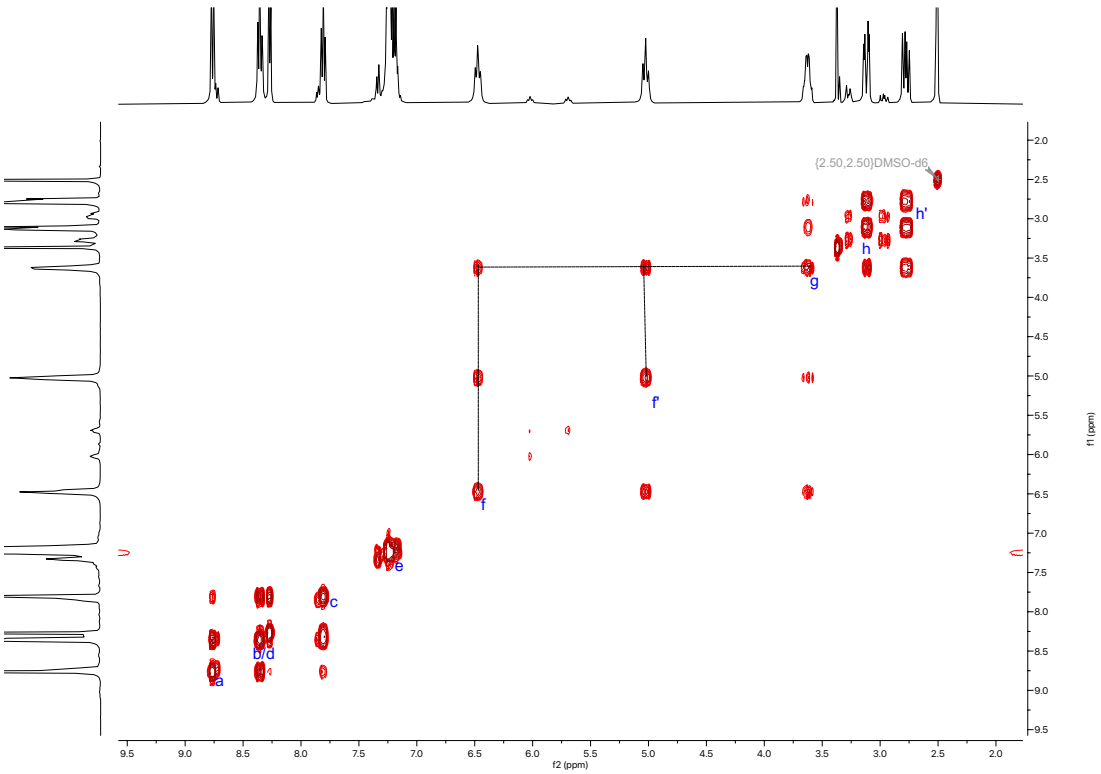

Figure S23. 2D COSY NMR of **5** (DMSO-d_6, 298 K)

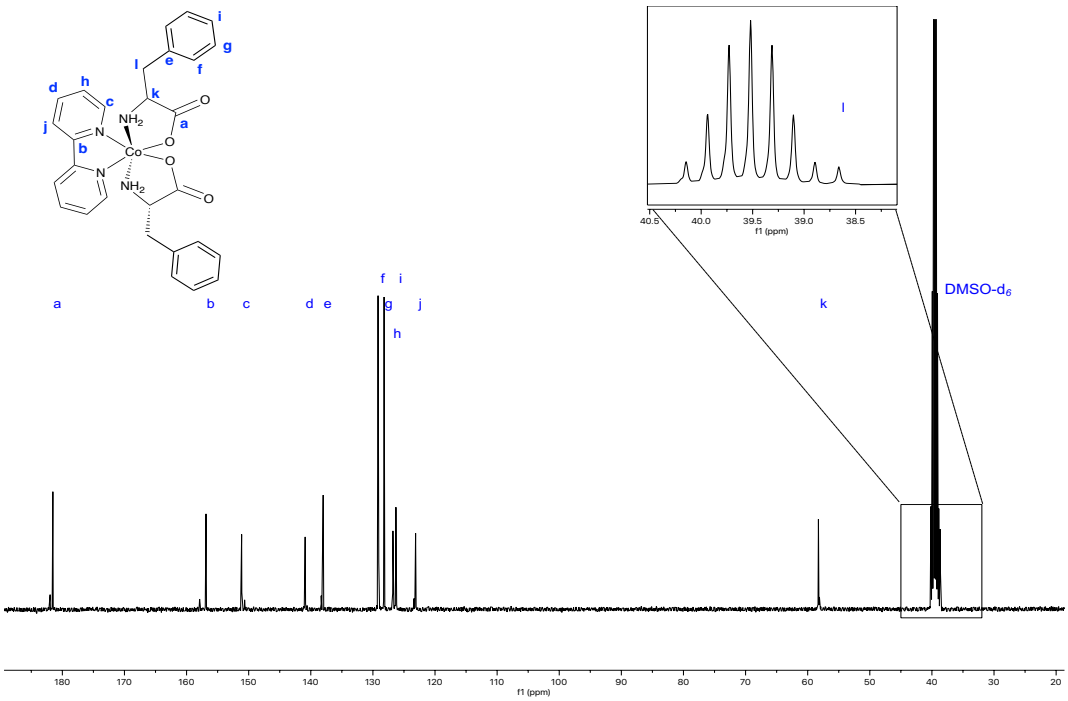

Figure S24. $^{13}C\{1H\}$ NMR of **5** (DMSO-*d*6, 298 K)

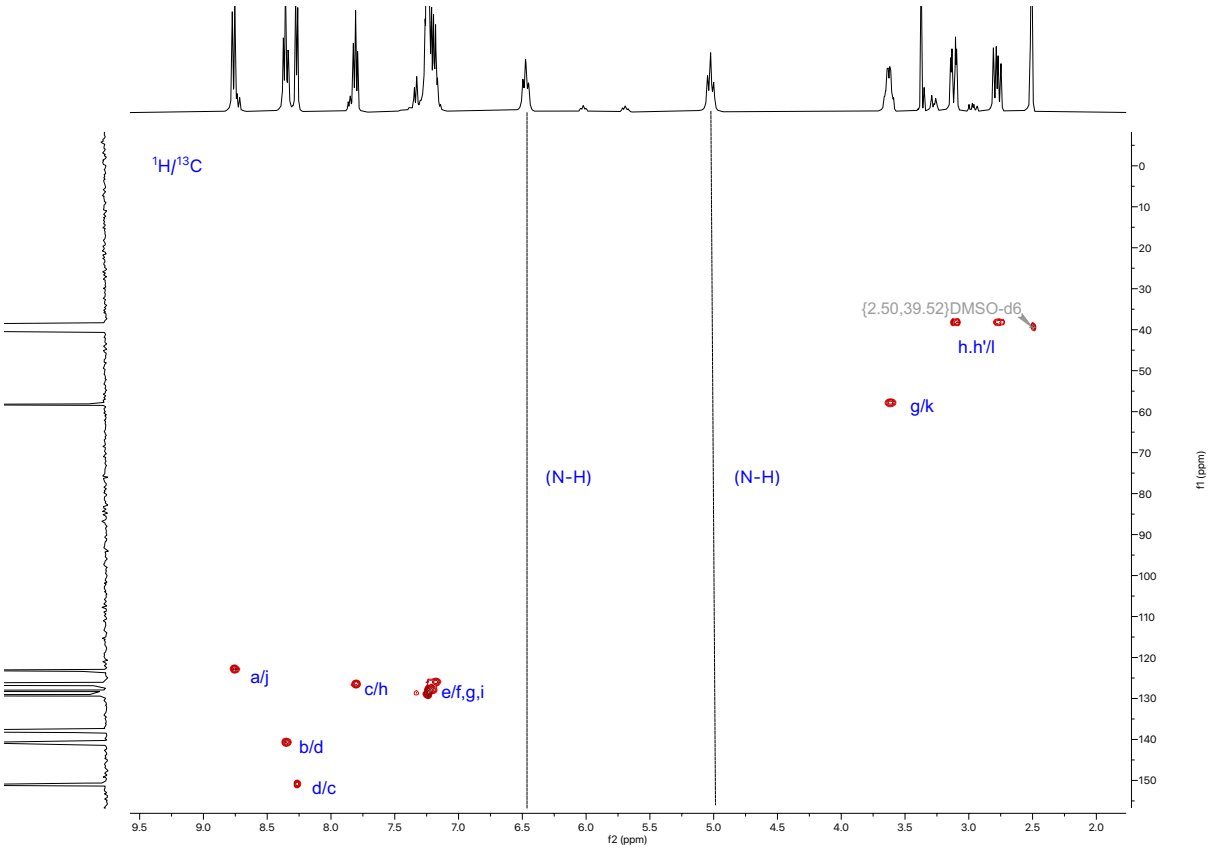

Figure S25. 2D HSQC NMR of **5** (DMSO-d_6, 298 K)

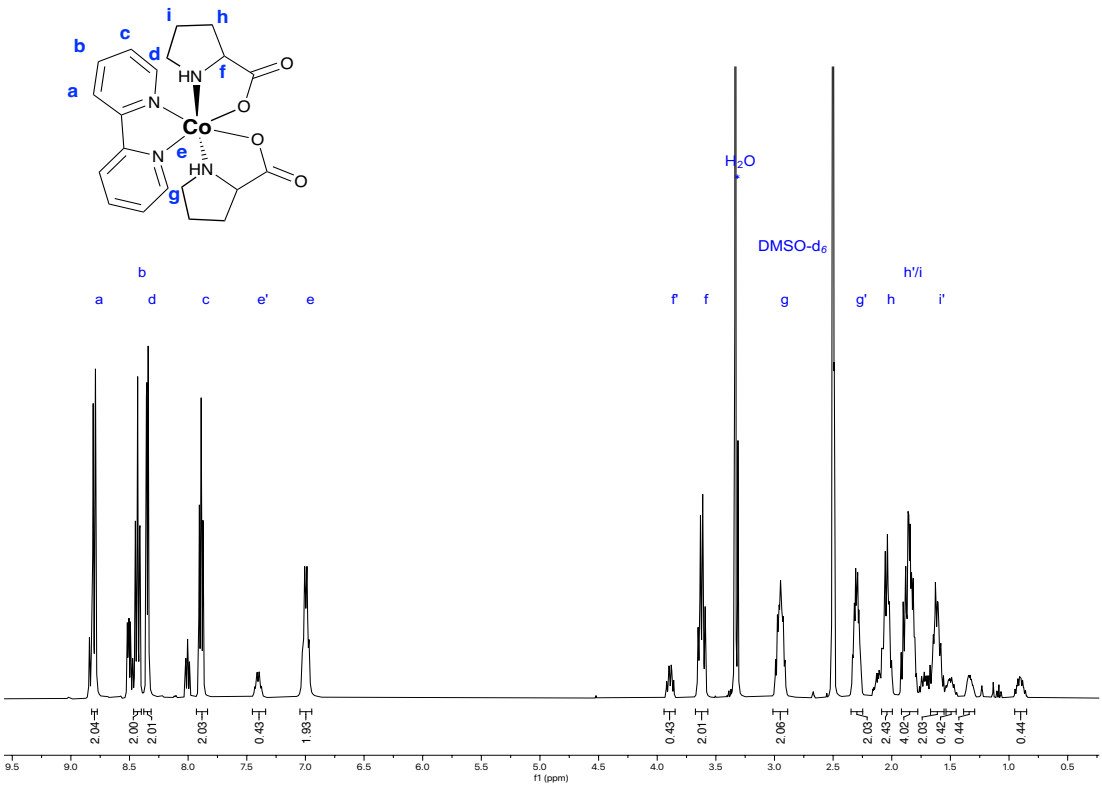

Figure S26. ^{1}H NMR of **6** in (DMSO-d_6, 298 K) 4.7:1

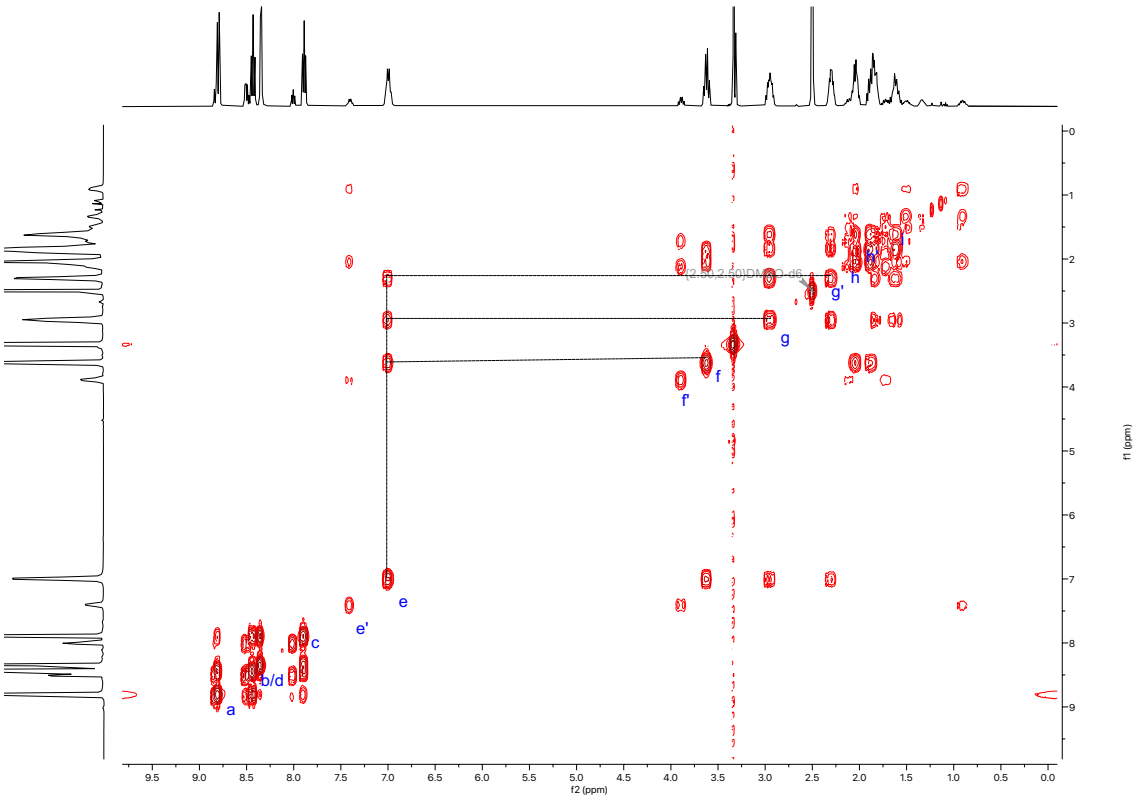

Figure S27. 2D COSY NMR of **6** (DMSO-d_6, 298 K)

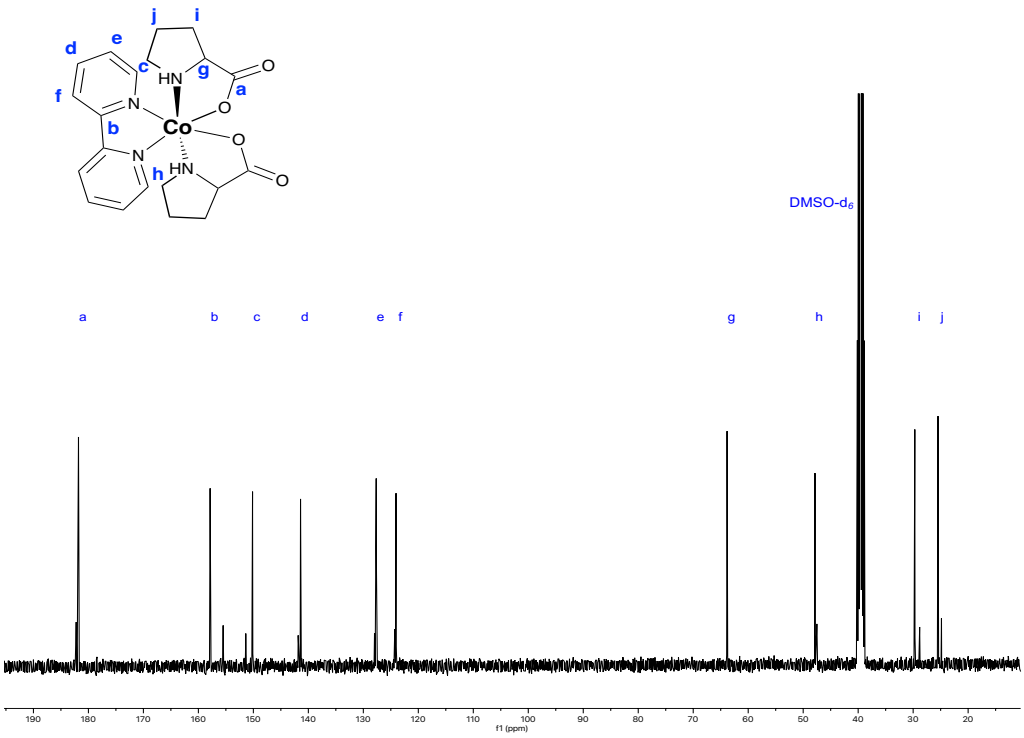

Figure S28. $^{13}C\{1H\}$ NMR of **6** (DMSO-*d*6, 298 K)

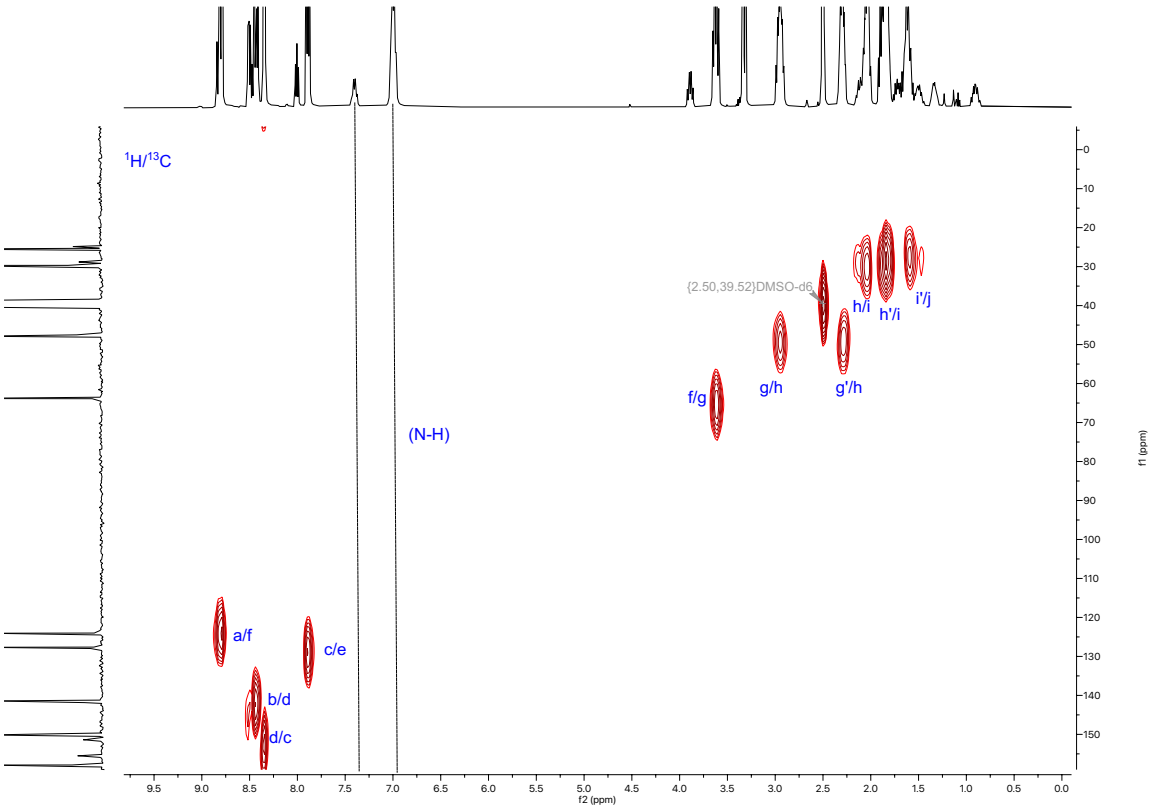

Figure S29. 2D HSQC NMR of **6** (DMSO-d_6, 298 K)

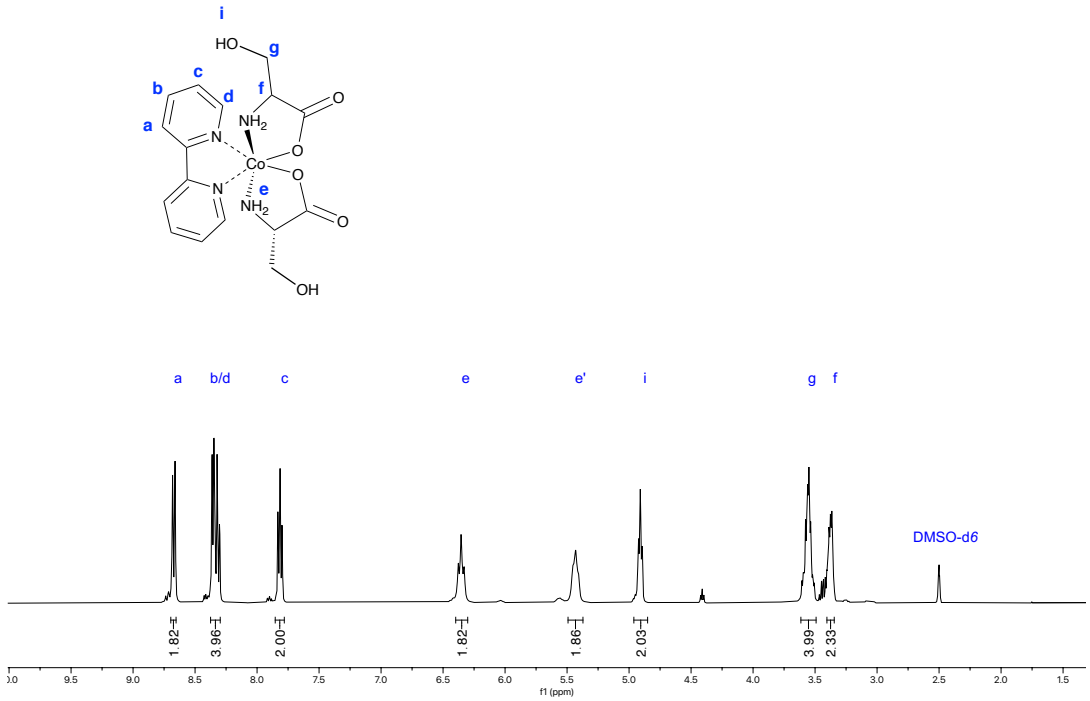

Figure S30. ^{1}H NMR of **7** in (DMSO-d_6, 298 K)

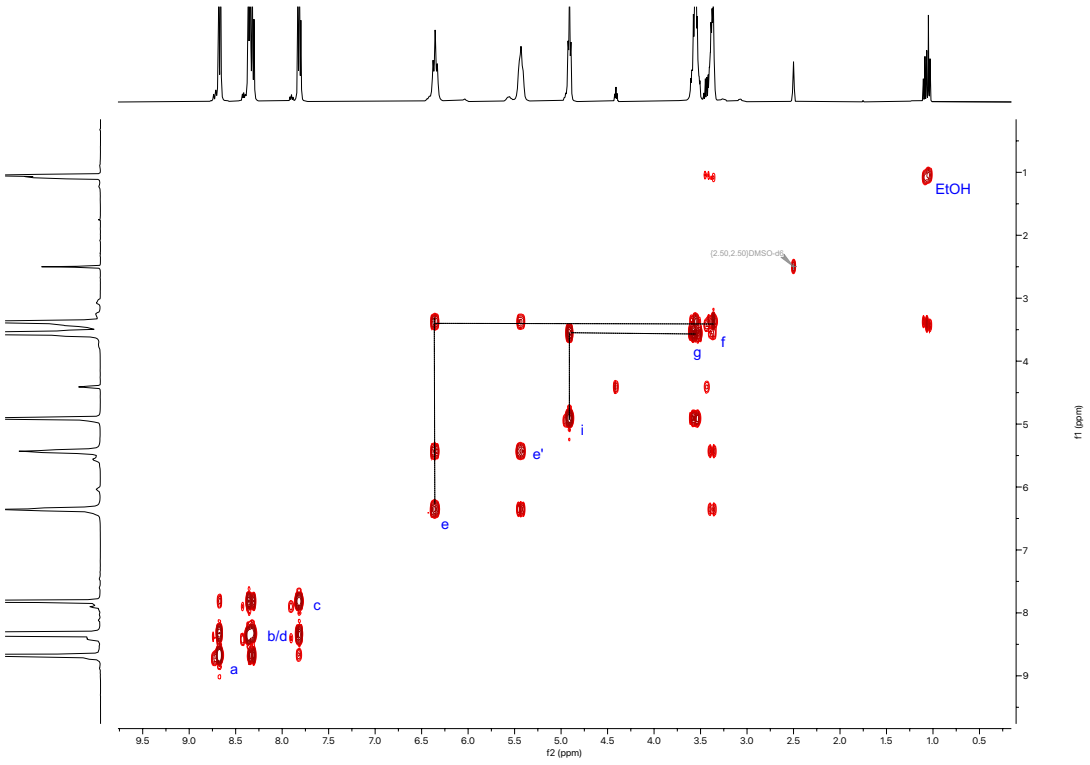

Figure S31. 2D COSY NMR of **7** (DMSO-d_6, 298 K)

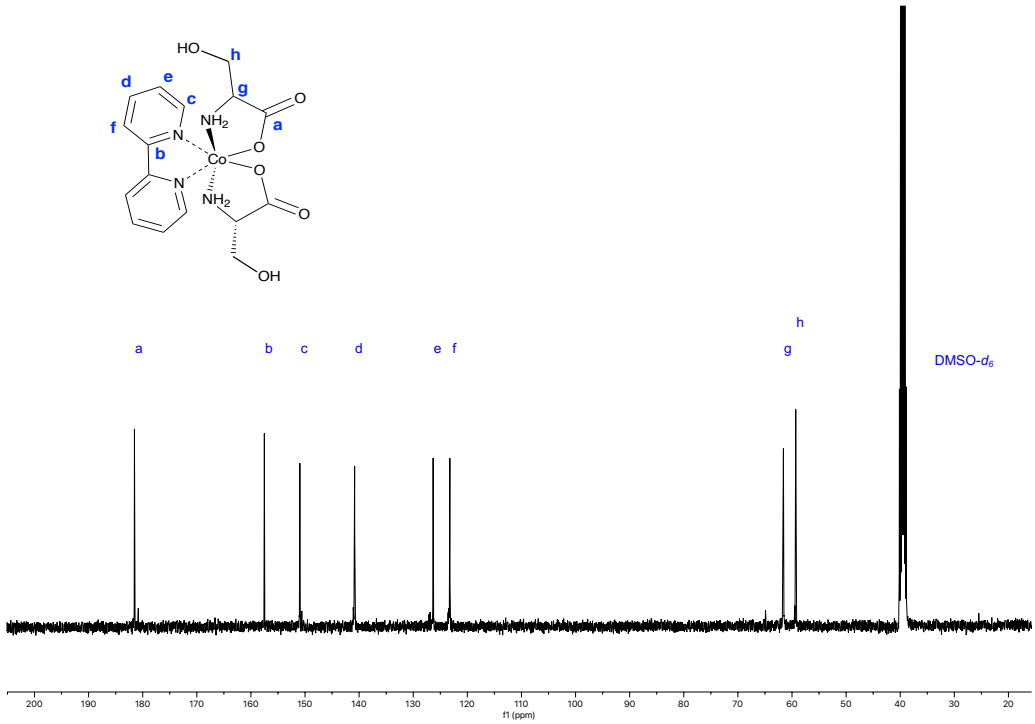

Figure S32. $^{13}C\{1H\}$ NMR of **7** (DMSO-*d*6, 298 K)

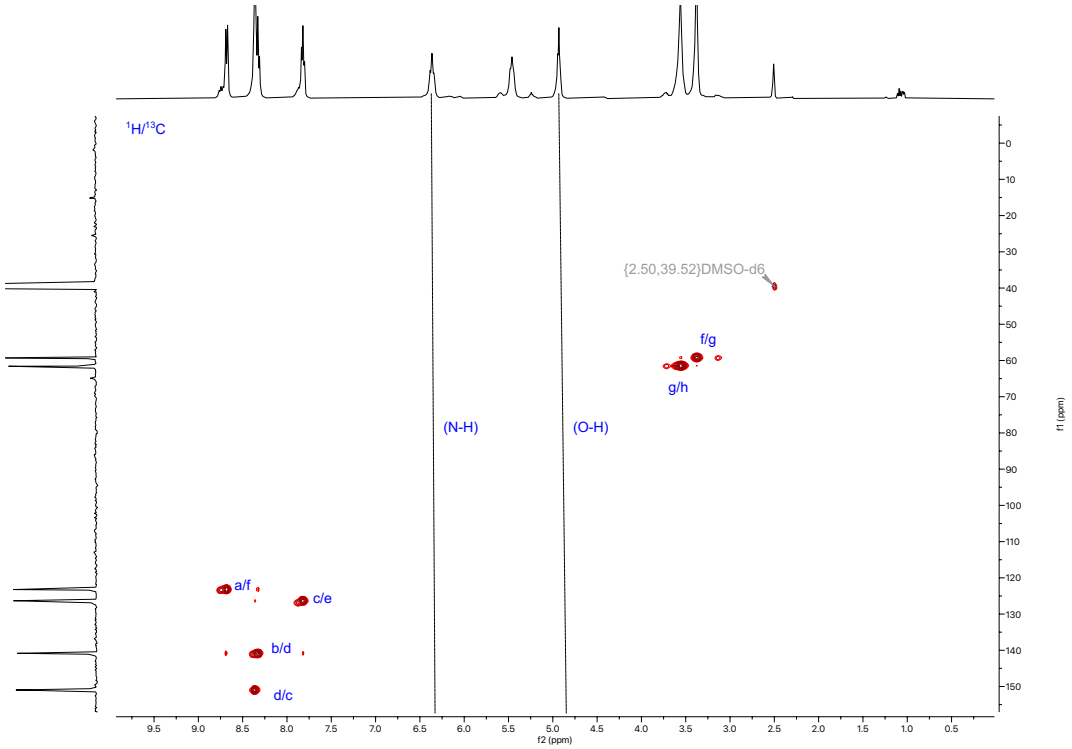

Figure S33. 2D HSQC NMR of **7** (DMSO-d_6, 298 K)

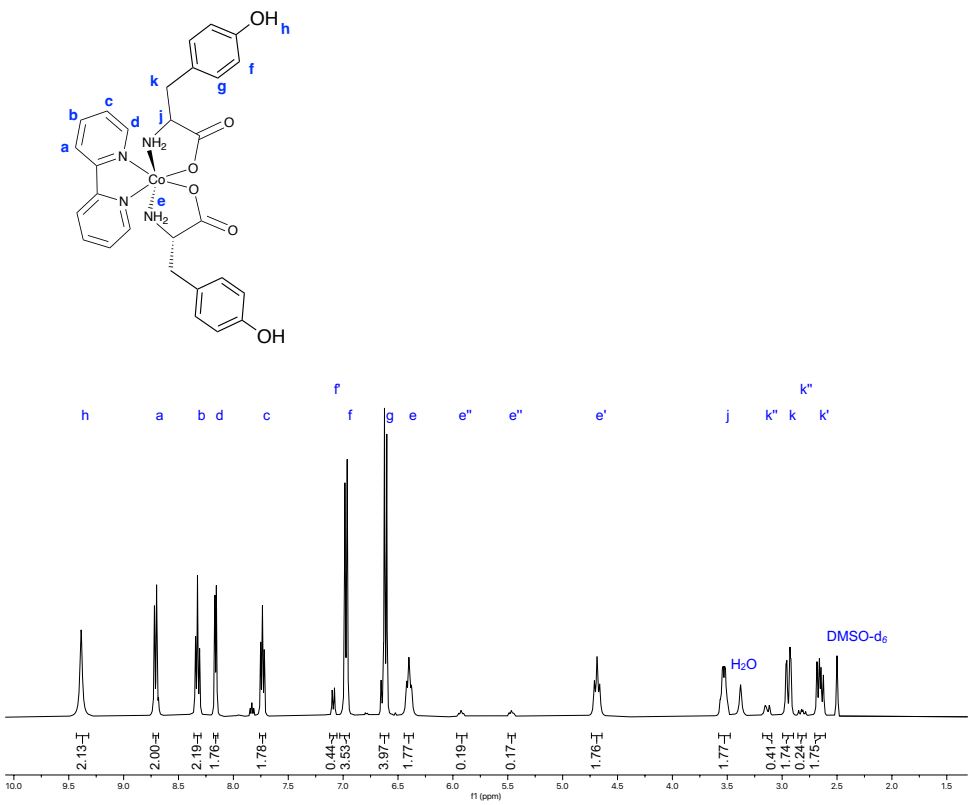

Figure S34. ^{1}H NMR of **8** in (DMSO-d_6, 298 K) mixture of diastereomers major product Δ-*RR*/*Λ*-*SS* and minor product Δ-*SS*/*Λ*-*RR* 8.1:1

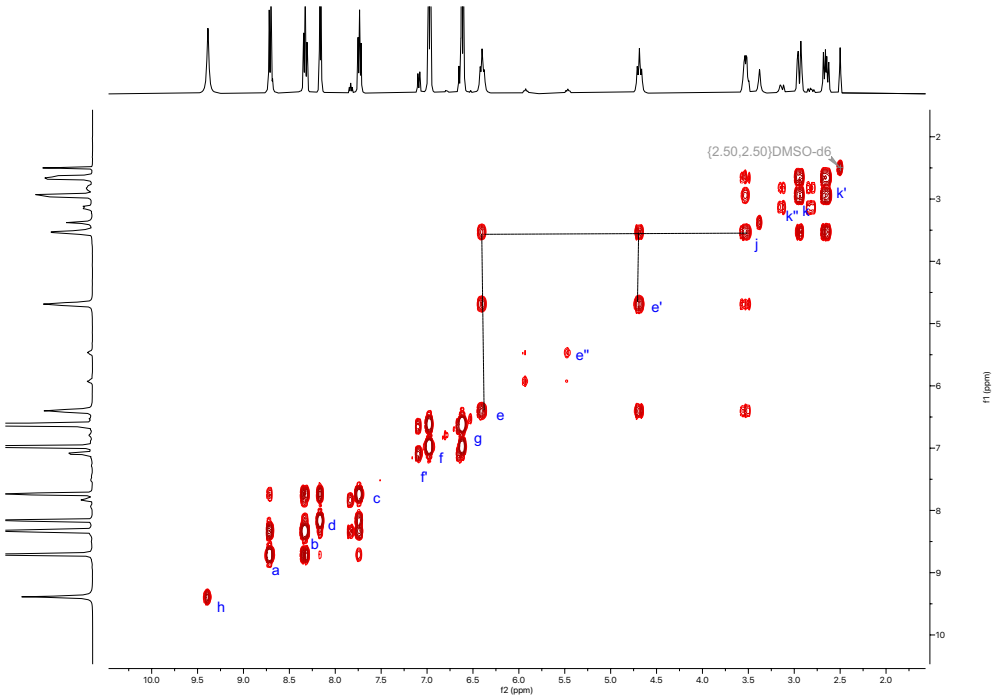

Figure S35. 2D COSY NMR of **8** (DMSO-d_6, 298 K)

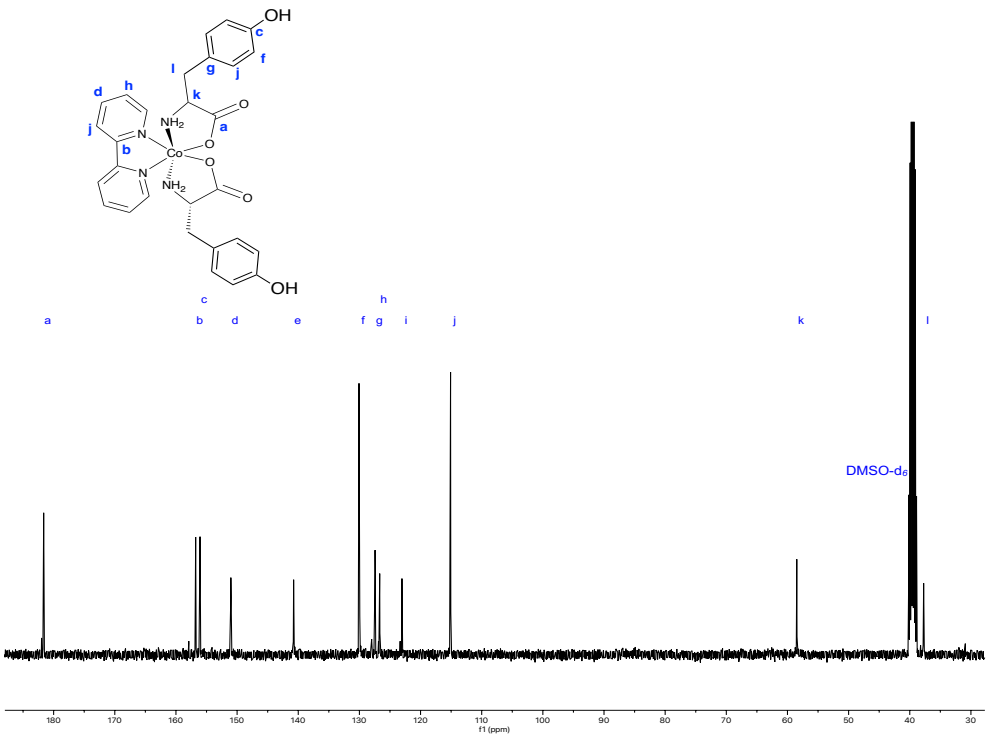

Figure S36. $^{13}C\{1H\}$ NMR of **8** (DMSO-*d*6, 298 K)

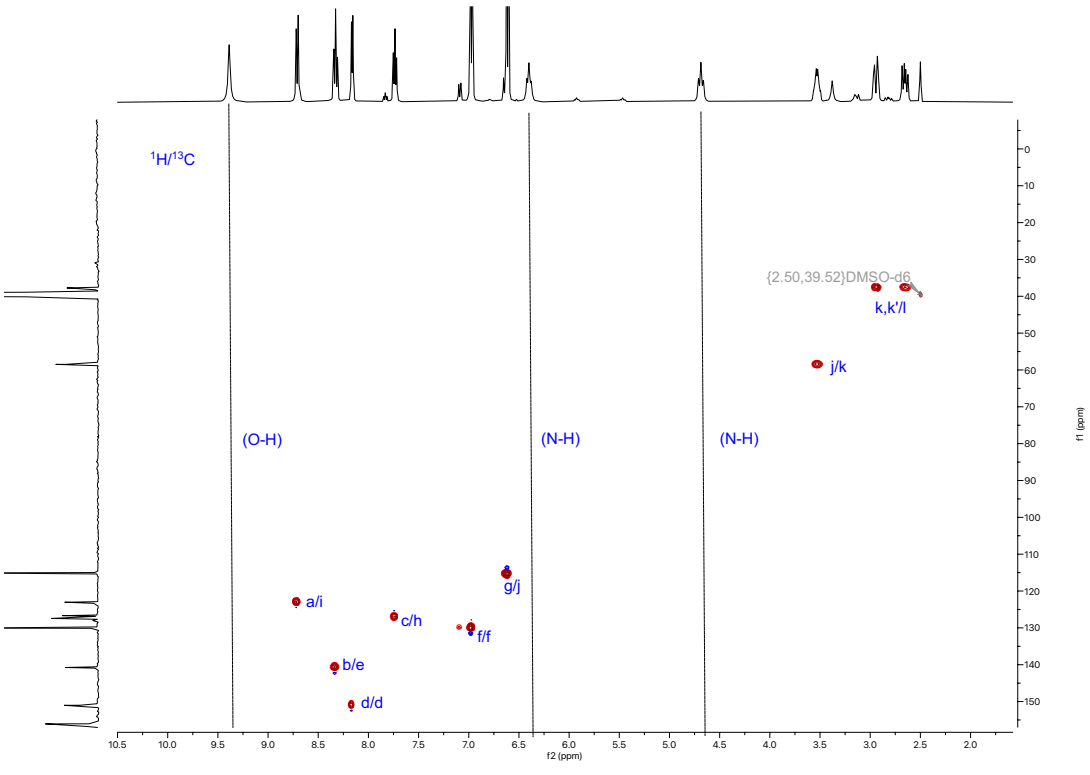

Figure S37. 2D HSQC NMR of **8** (DMSO-d_6, 298 K)

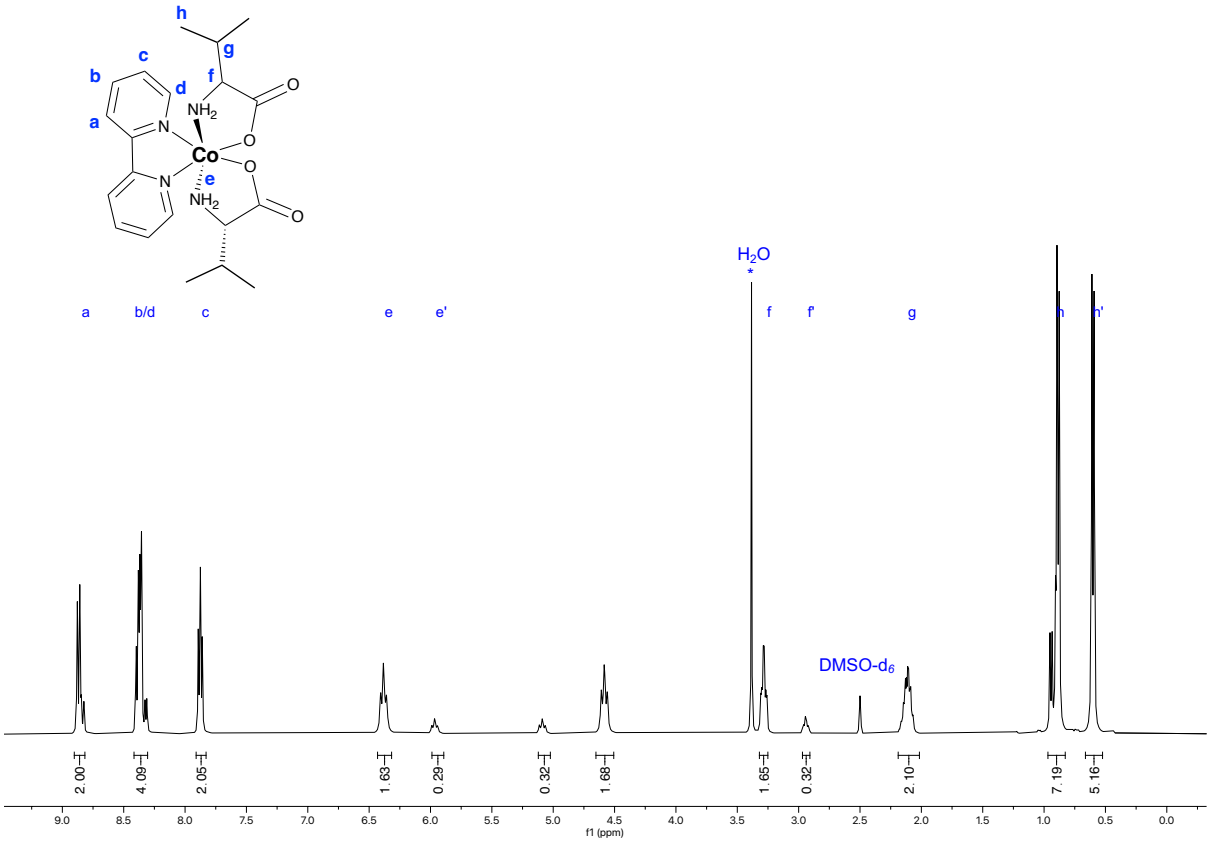

Figure S38. ^{1}H NMR of **9** in (DMSO-d_6, 298 K) mixture of diastereomers major product Δ-*RR*/*Λ*-*SS* and minor product Δ-*SS*/*Λ*-*RR* 5.1:1

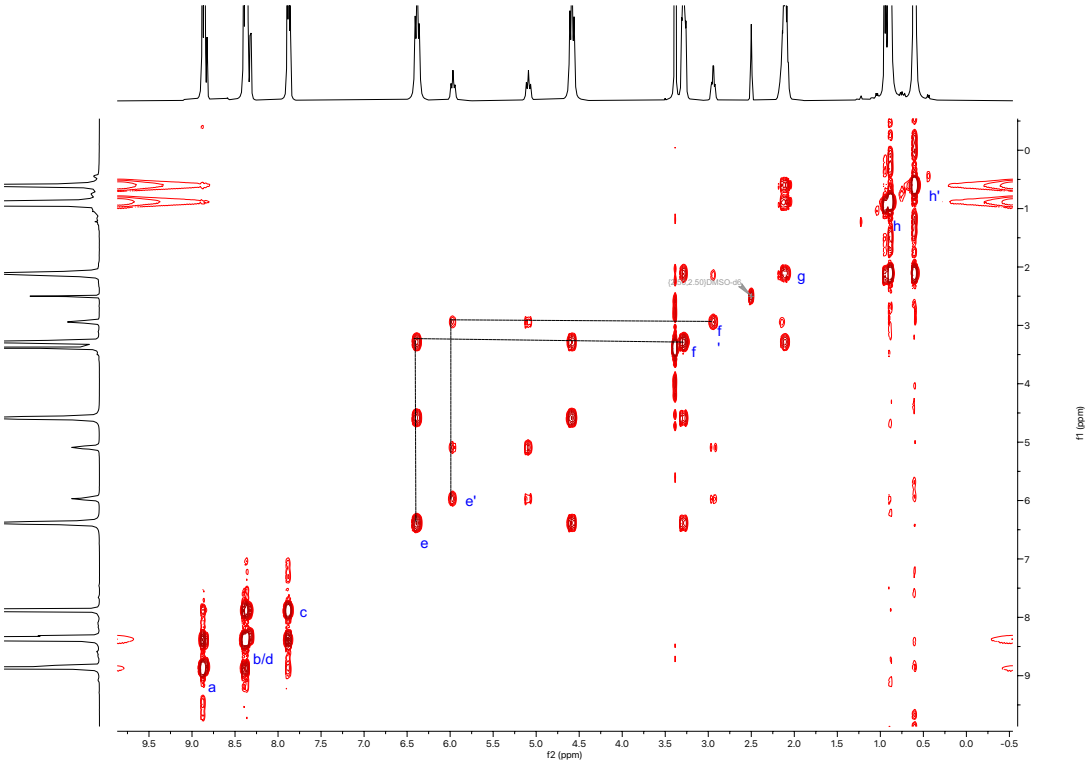

Figure S39. 2D COSY NMR of **9** (DMSO-d_6, 298 K)

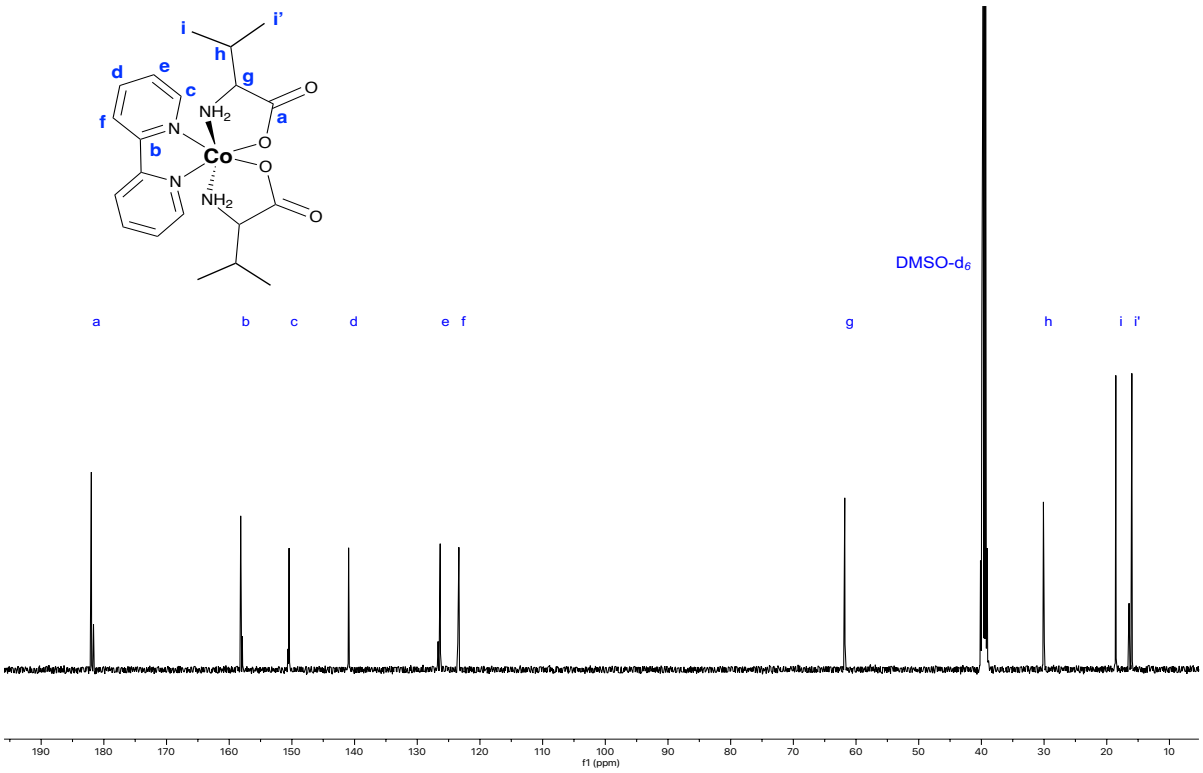

Figure S40. $^{13}C\{1H\}$ NMR of **9** (DMSO-d_6, 298 K)

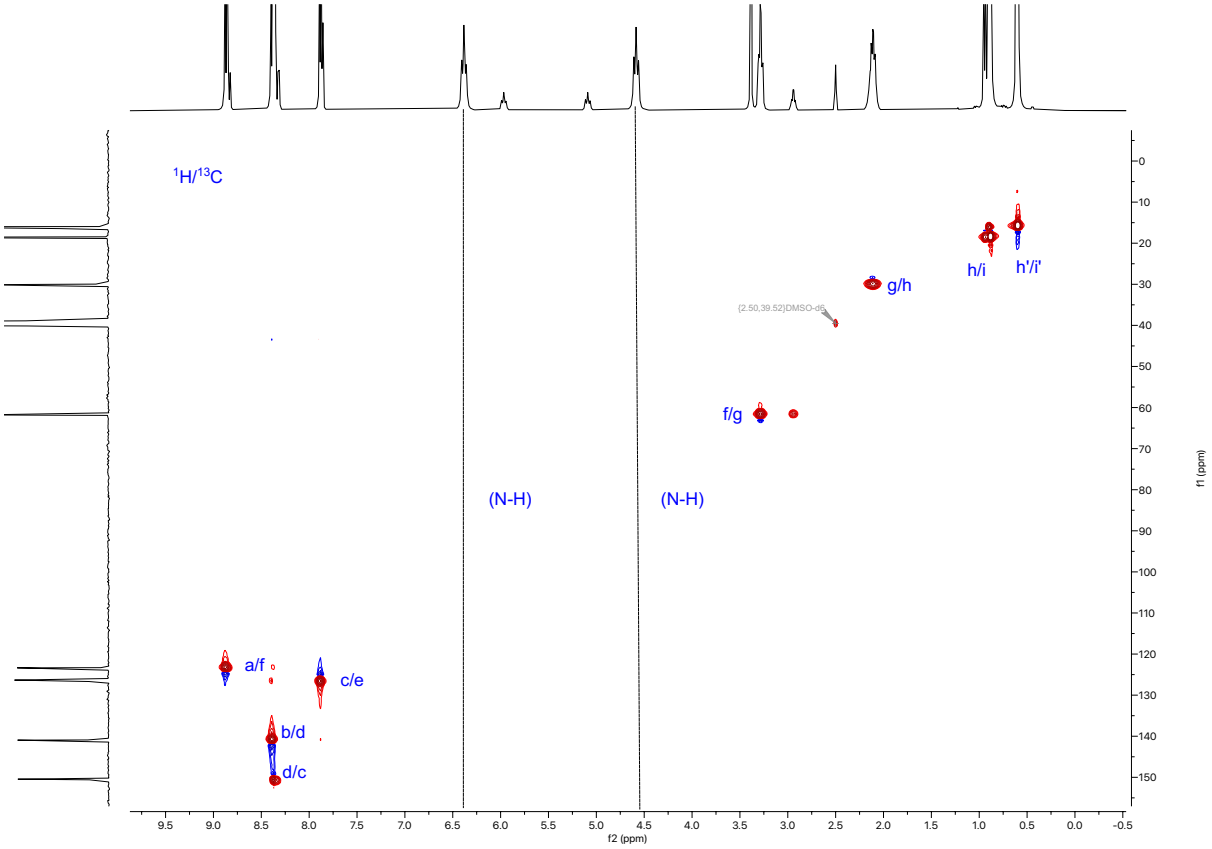

Figure S41. 2D HSQC NMR of **9** (DMSO-d_6, 298 K)

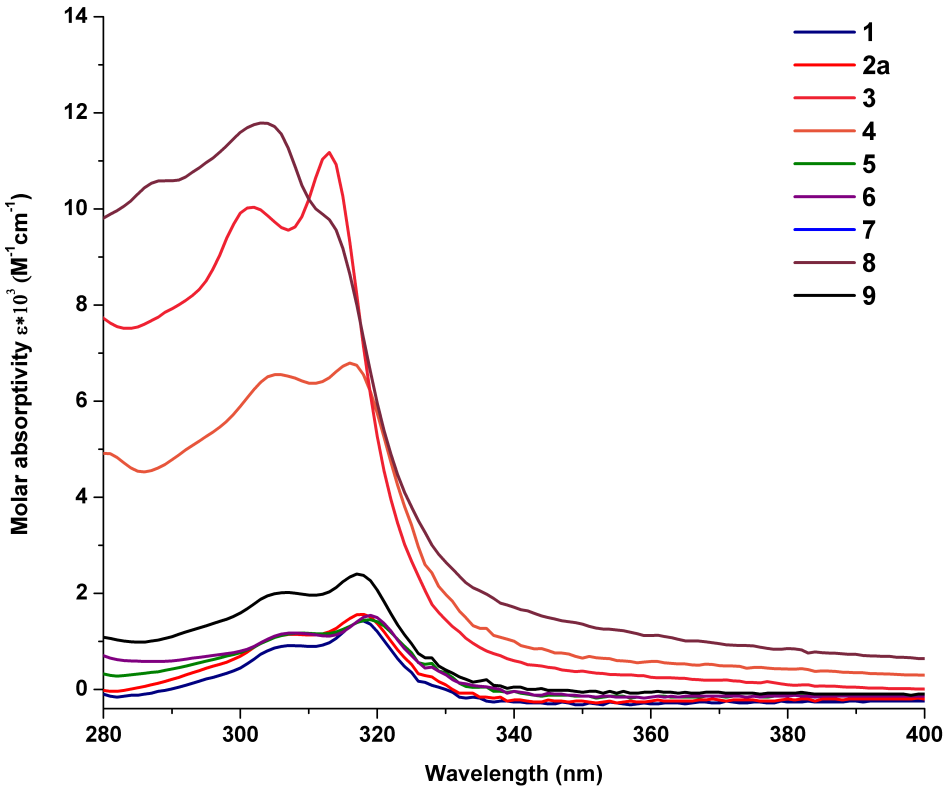

Figure S42. UV-vis absorption spectra of **1-9** in EtOH ($1x10^{-5}$ M).

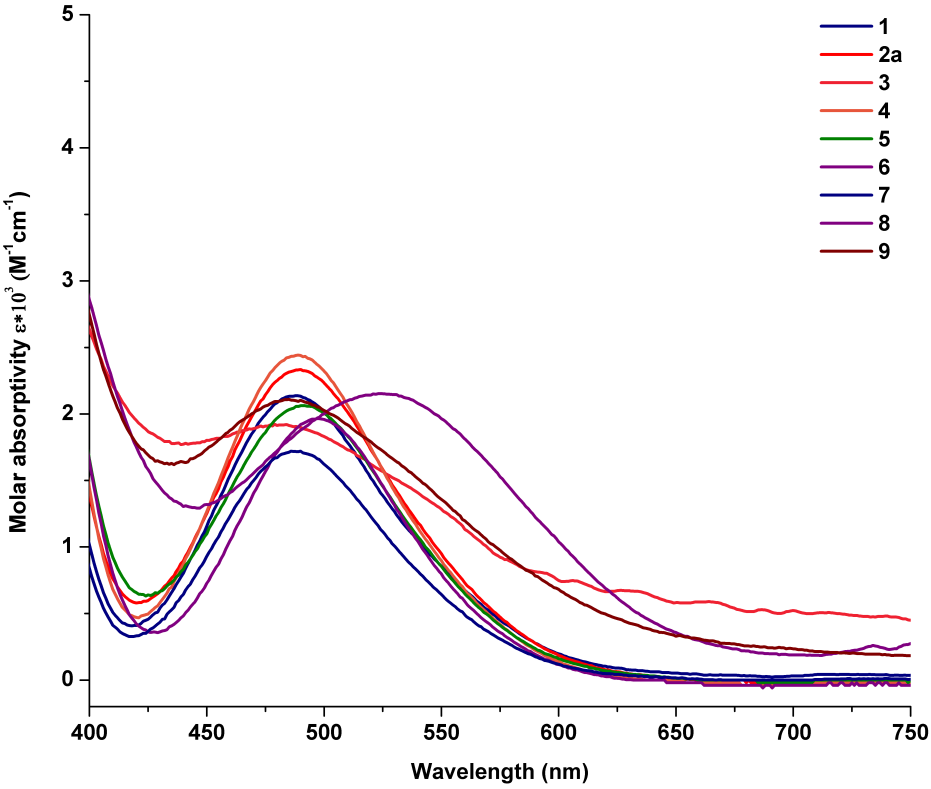

Figure S43. UV-vis absorption spectra of **1-9** in EtOH ($1x10^{-3}$ M).

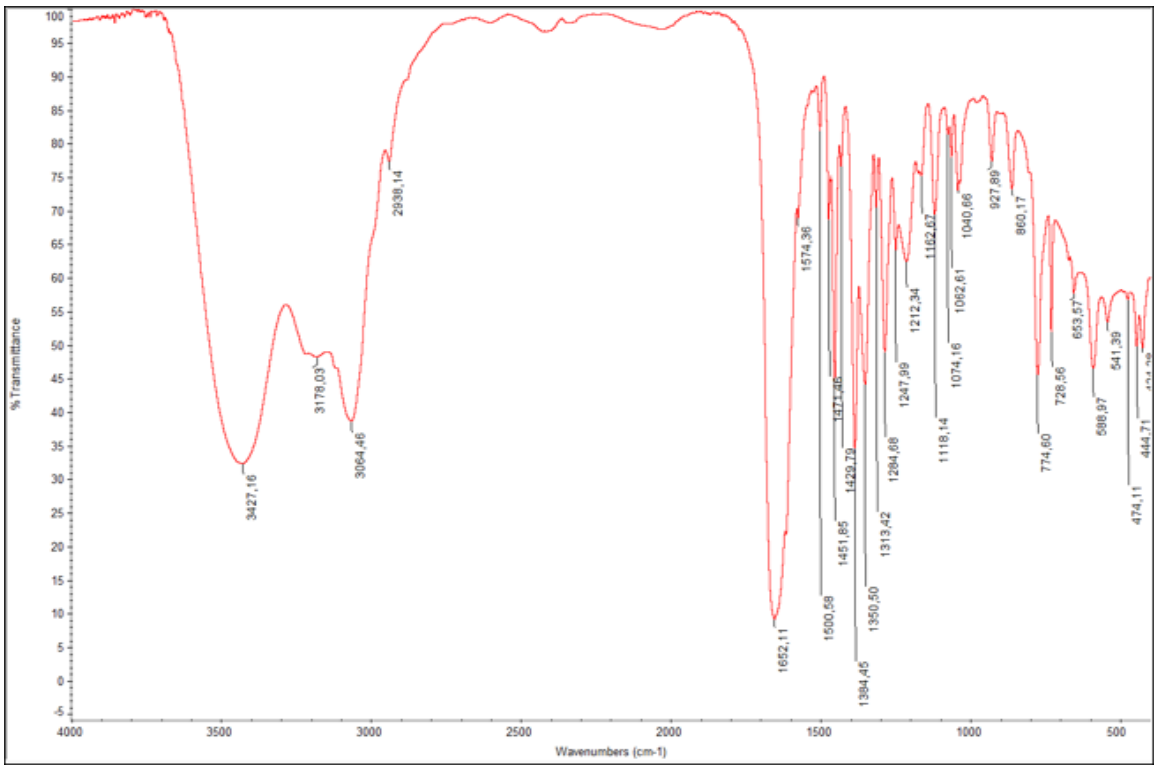

Figure S44. FT-IR of **1**

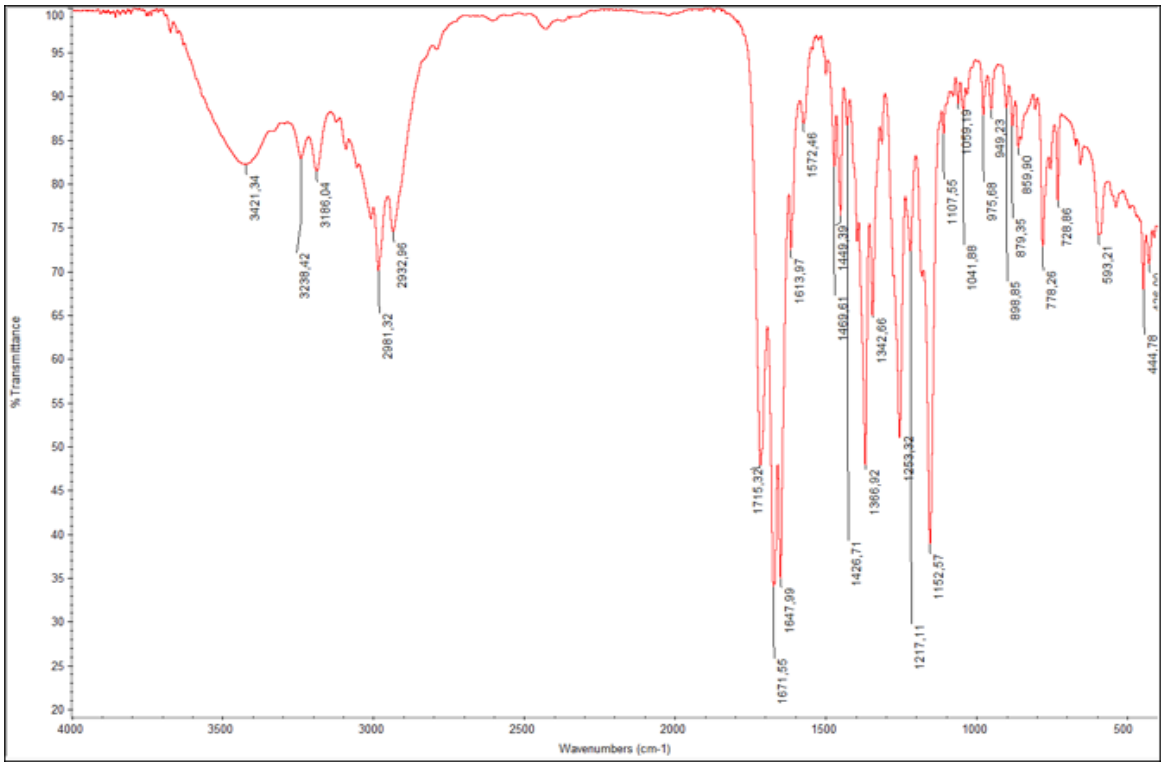

Figure S45. FT-IR of **2**

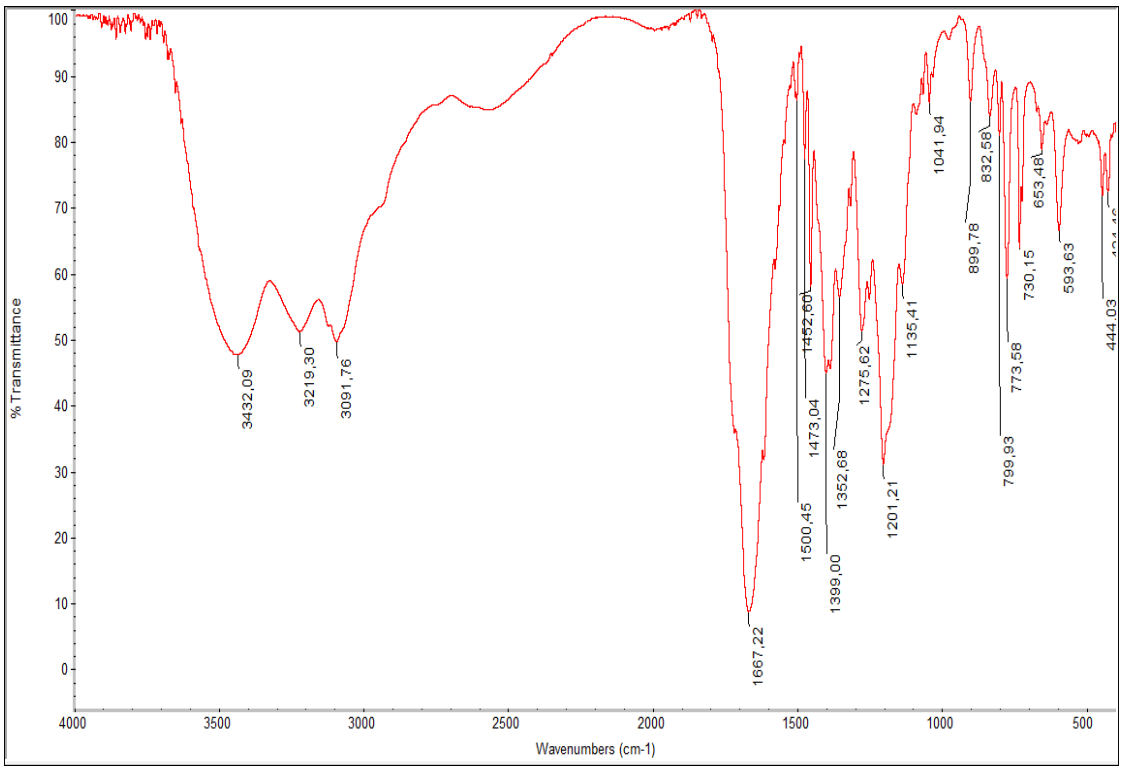

Figure S46. FT-IR of **2a**

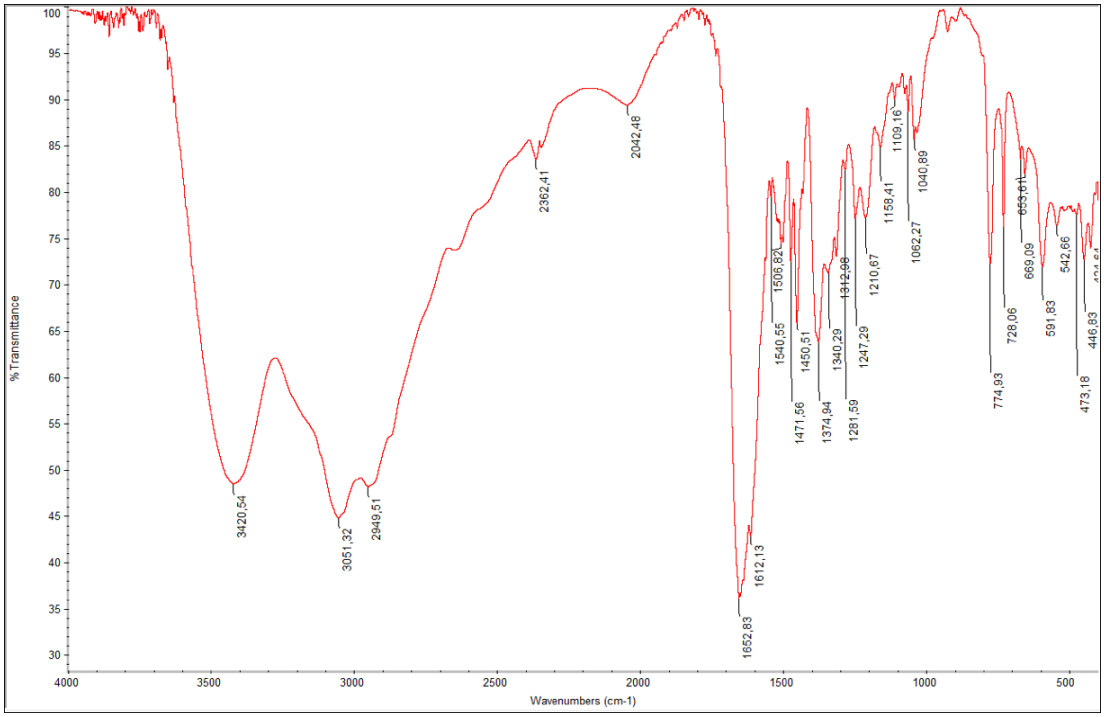

Figure S47. FT-IR of **3**

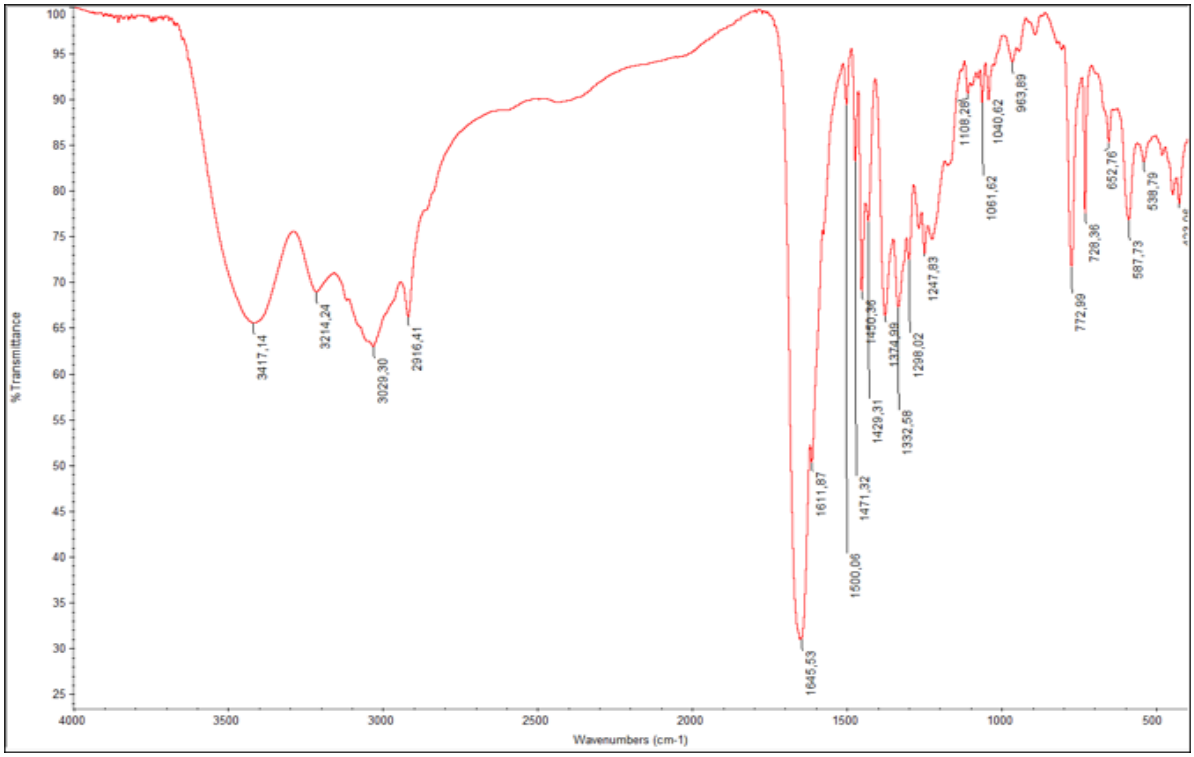

Figure S48. FT-IR of **4**

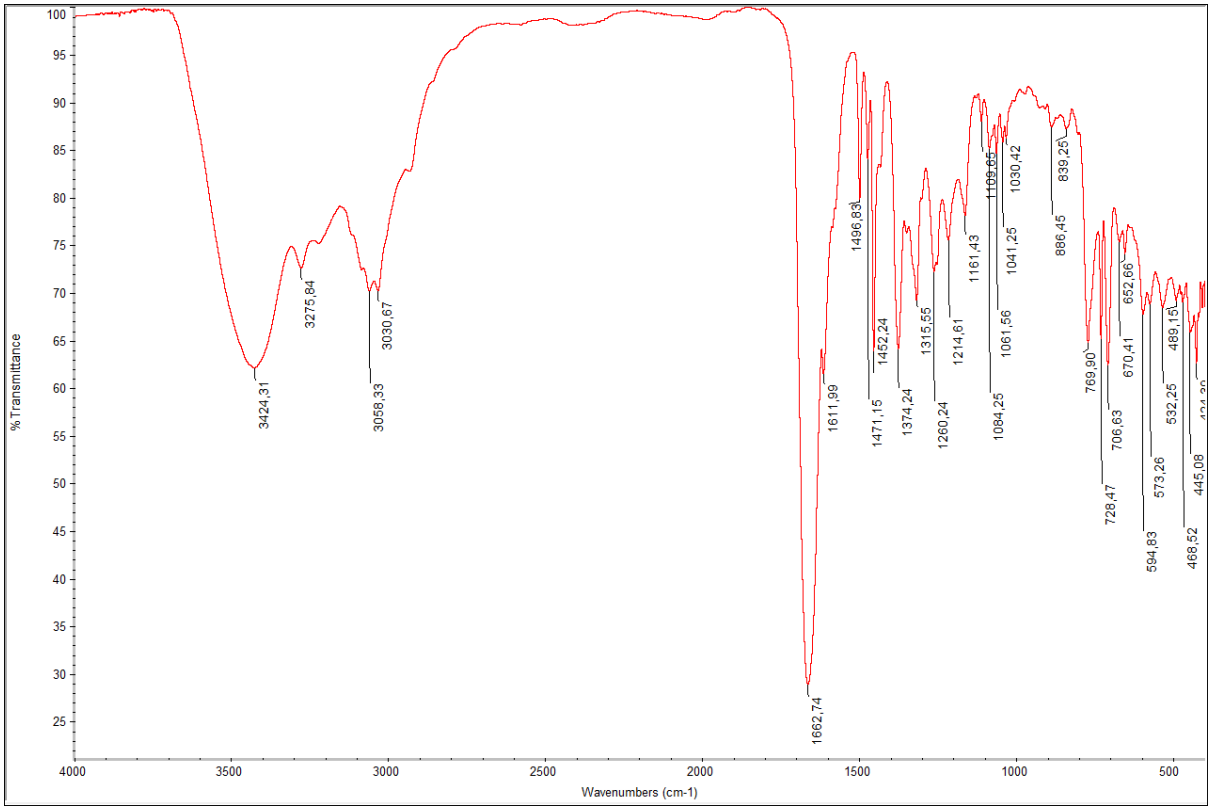

Figure S49. FT-IR of **5**

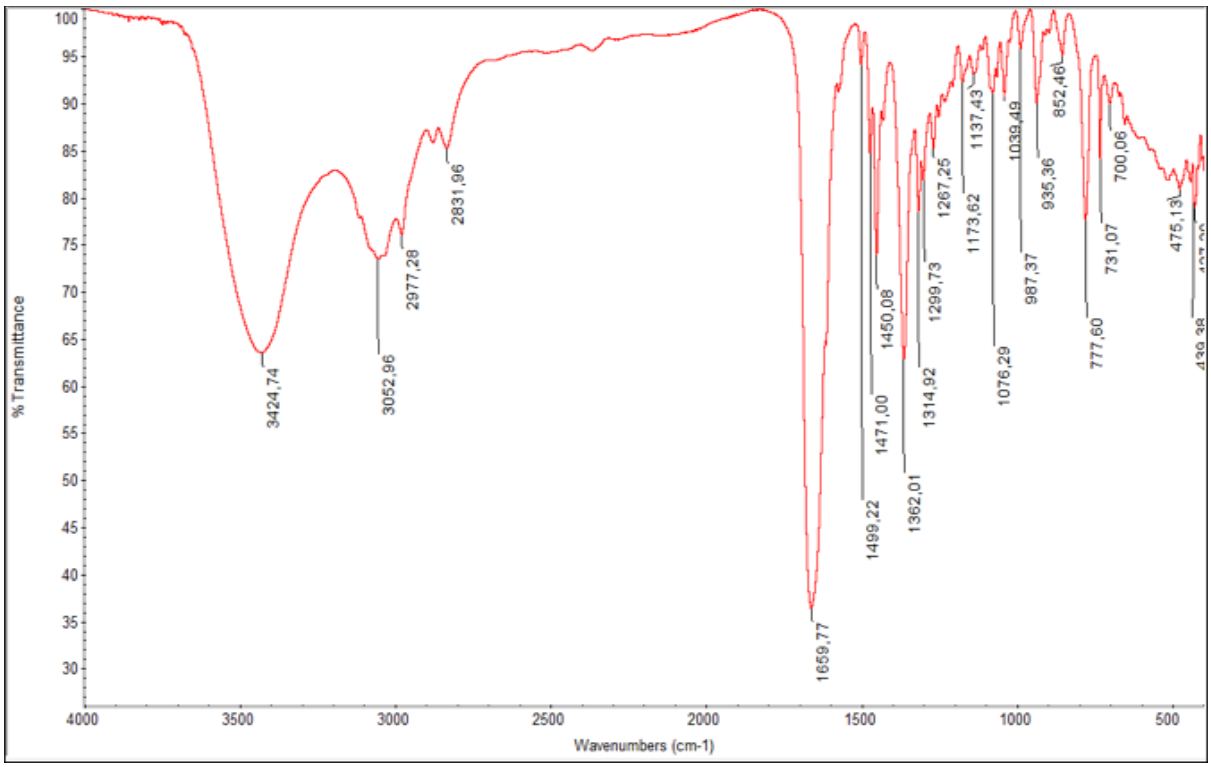

Figure S50. FT-IR of **6**

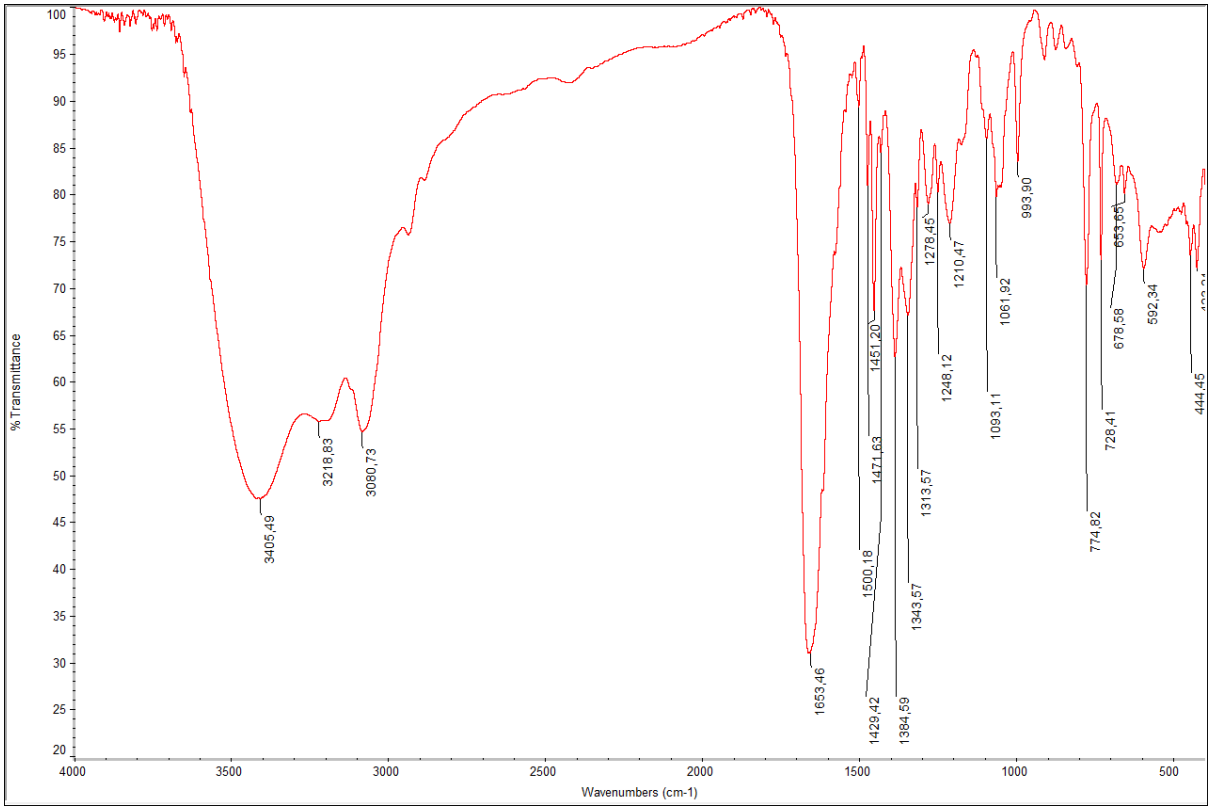

Figure S51. FT-IR of **7**

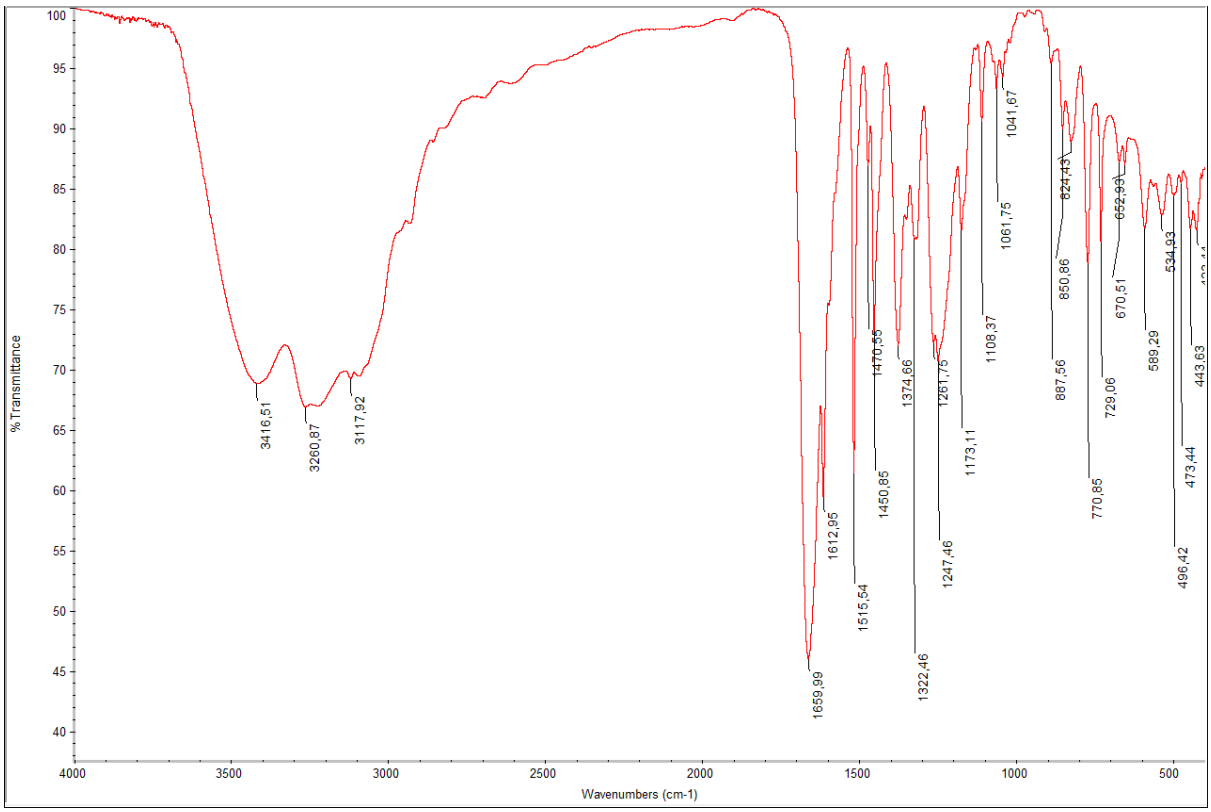

Figure S52. FT-IR of **8**

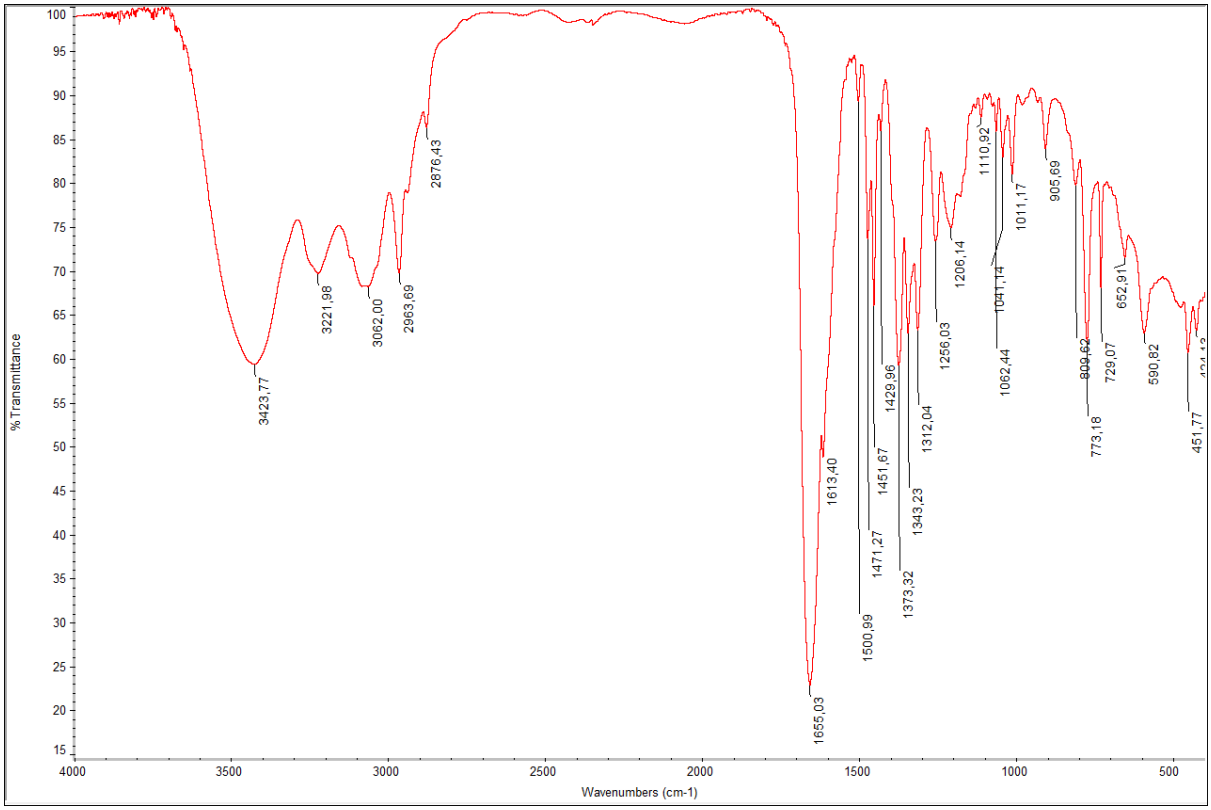

Figure S53. FT-IR of **9**

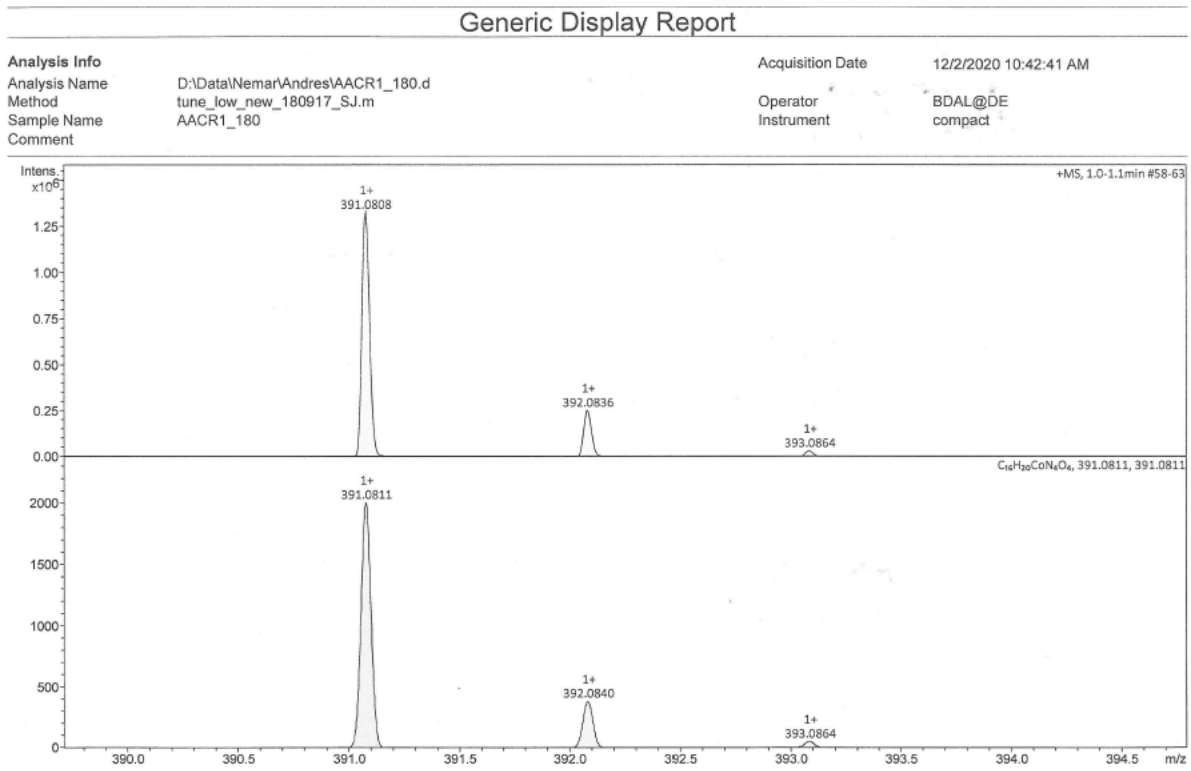

Figure S54. HRMS of **1**

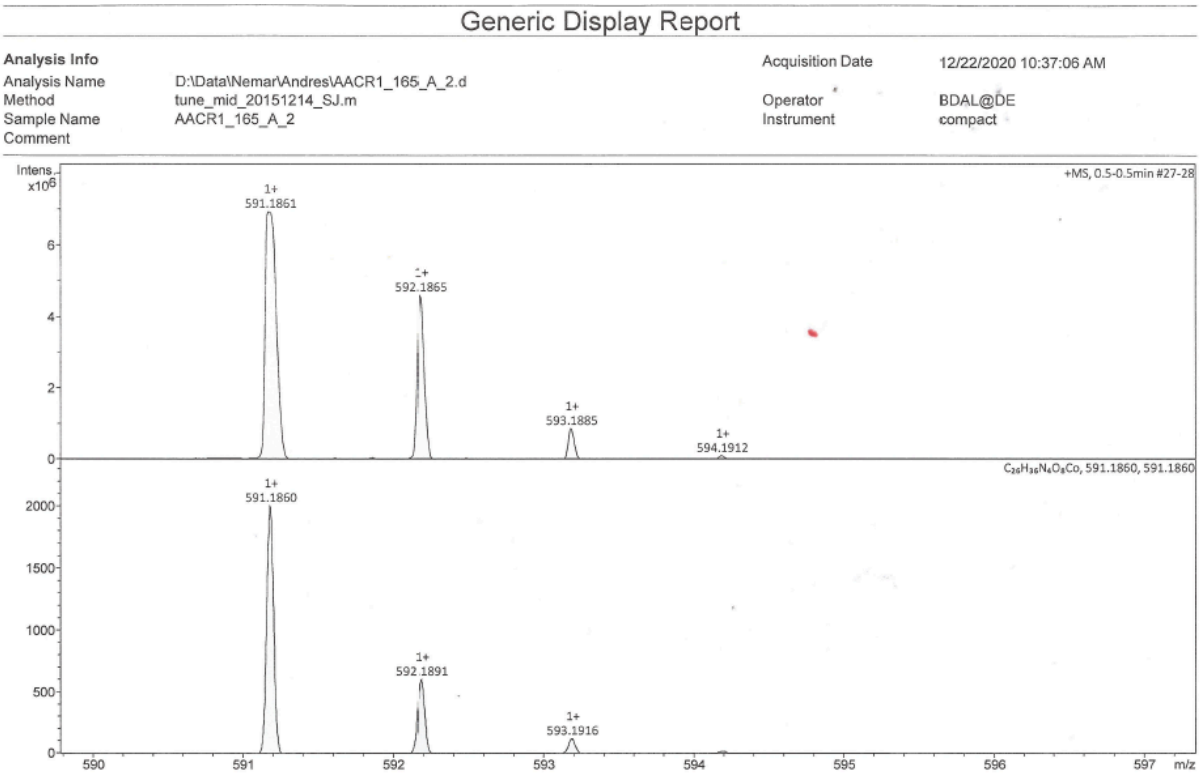

Figure S55. HRMS of **2**

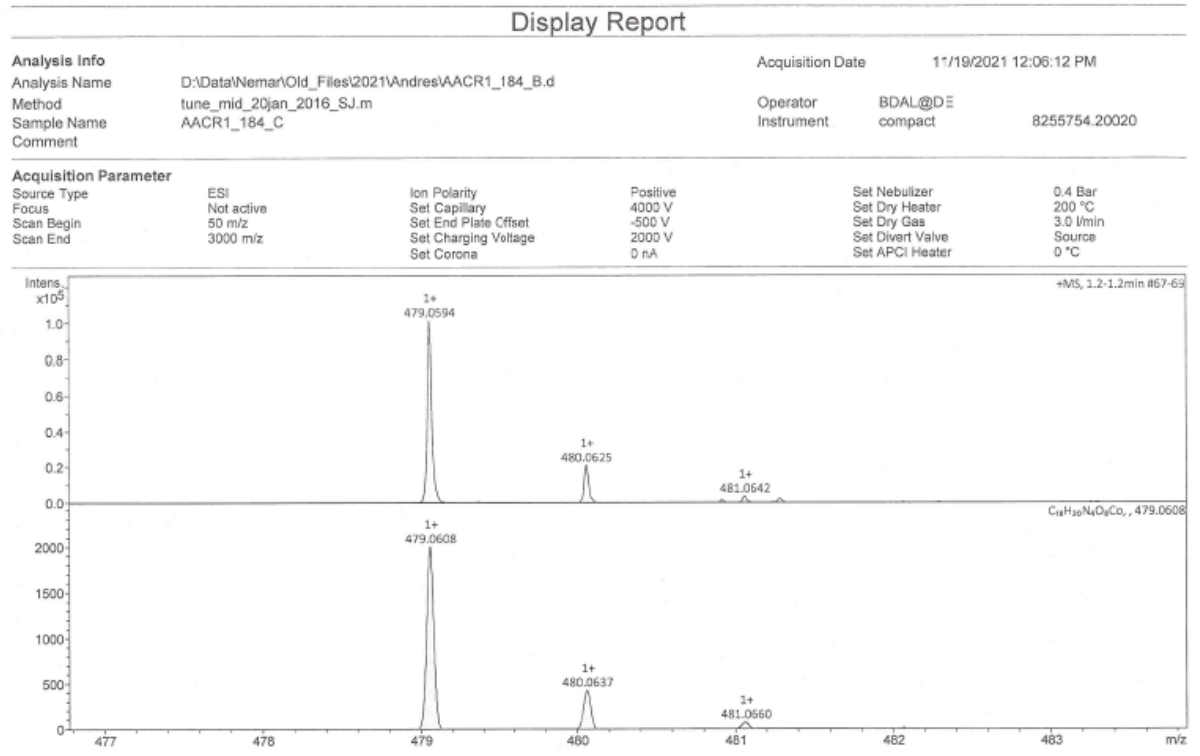

Figure S56. HRMS of **2a**

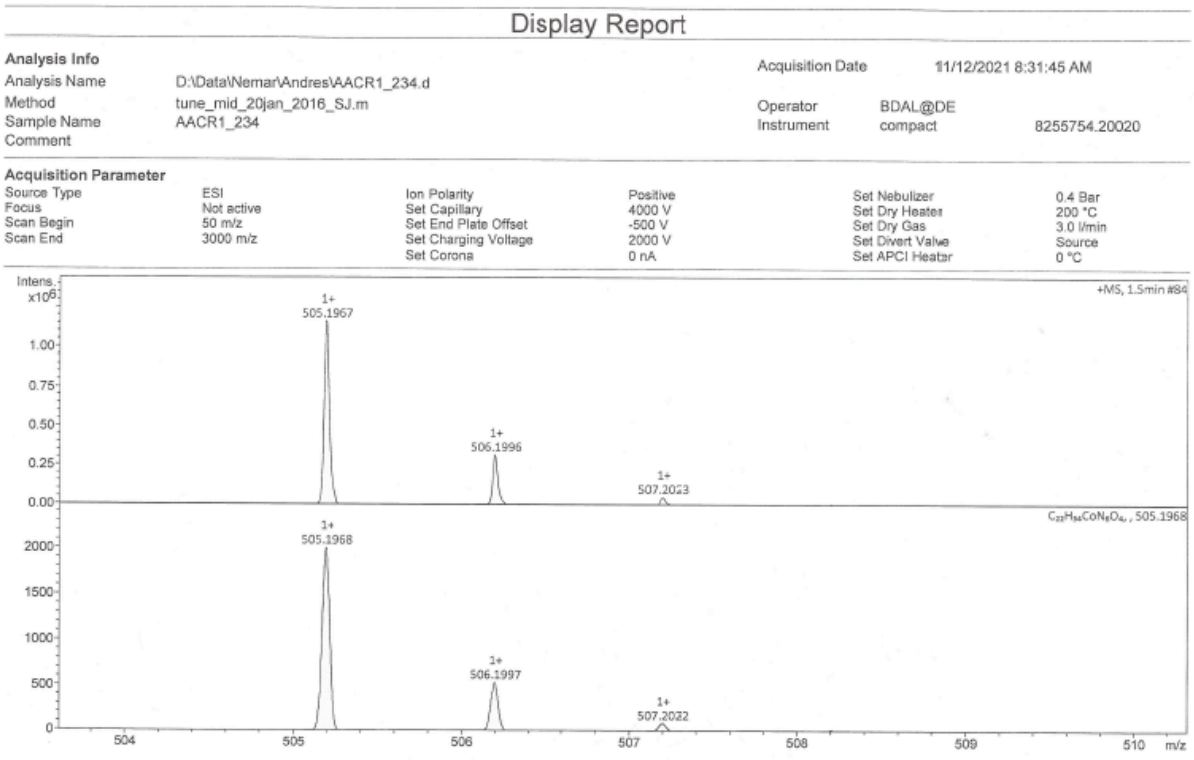

Figure S57. HRMS of **3**

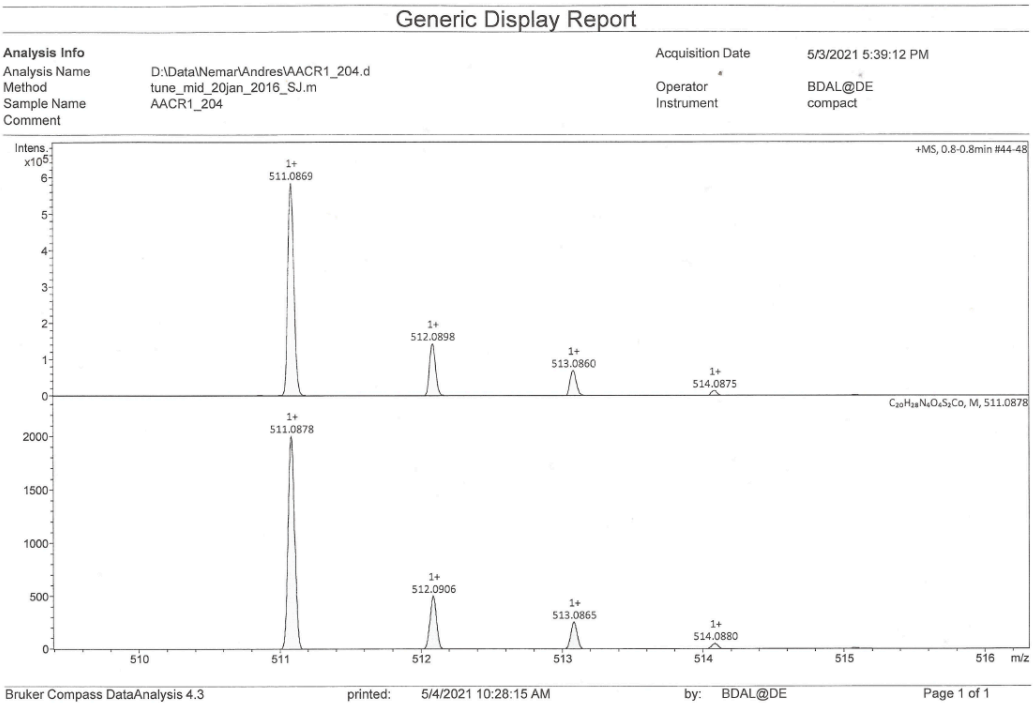

Figure S58. HRMS of **4**

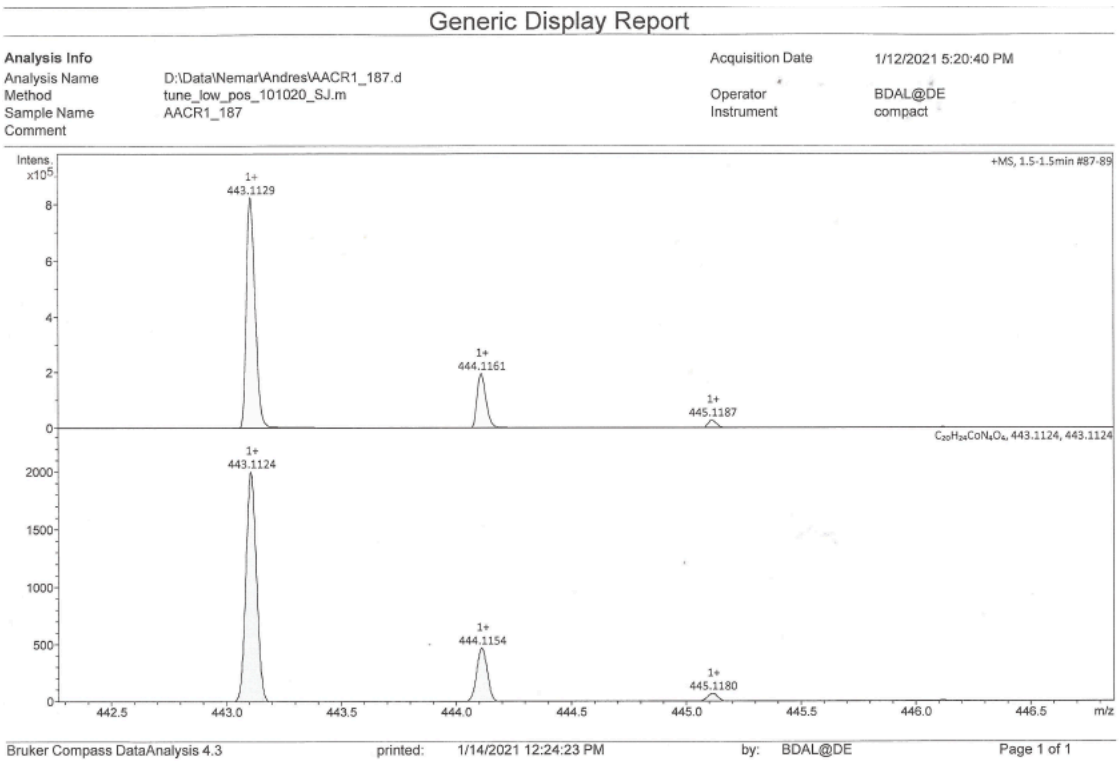

Figure S59. HRMS of **5**

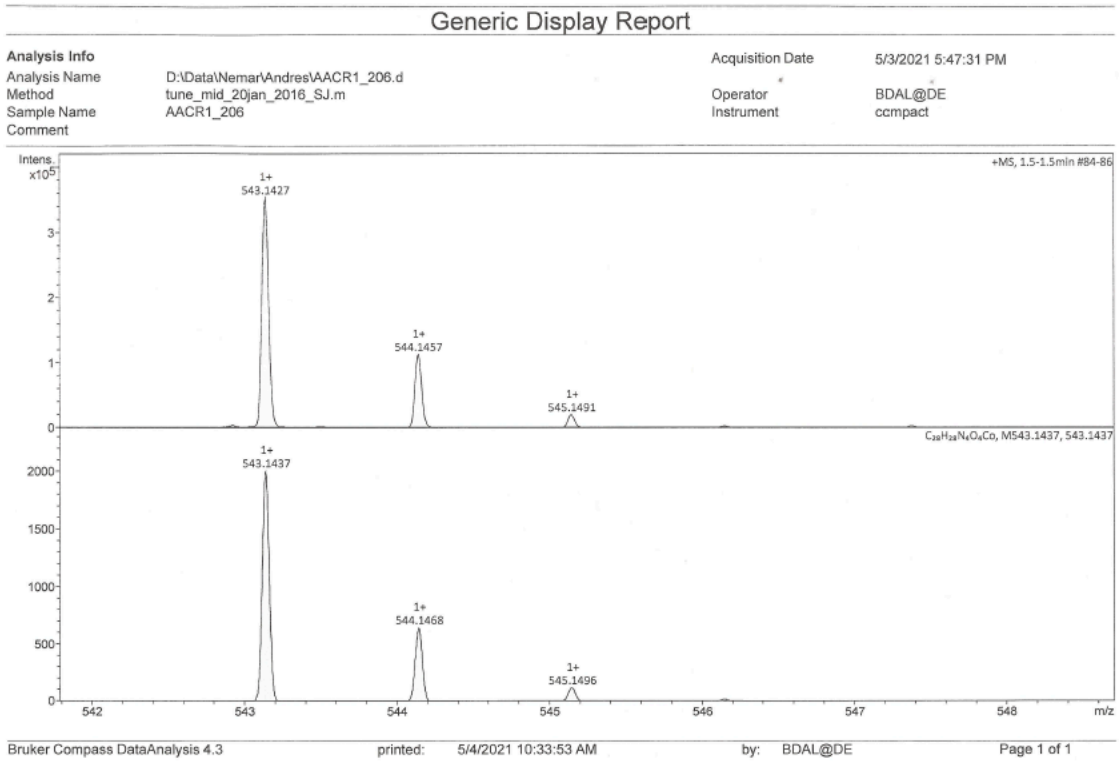

Figure S60. HRMS of **6**

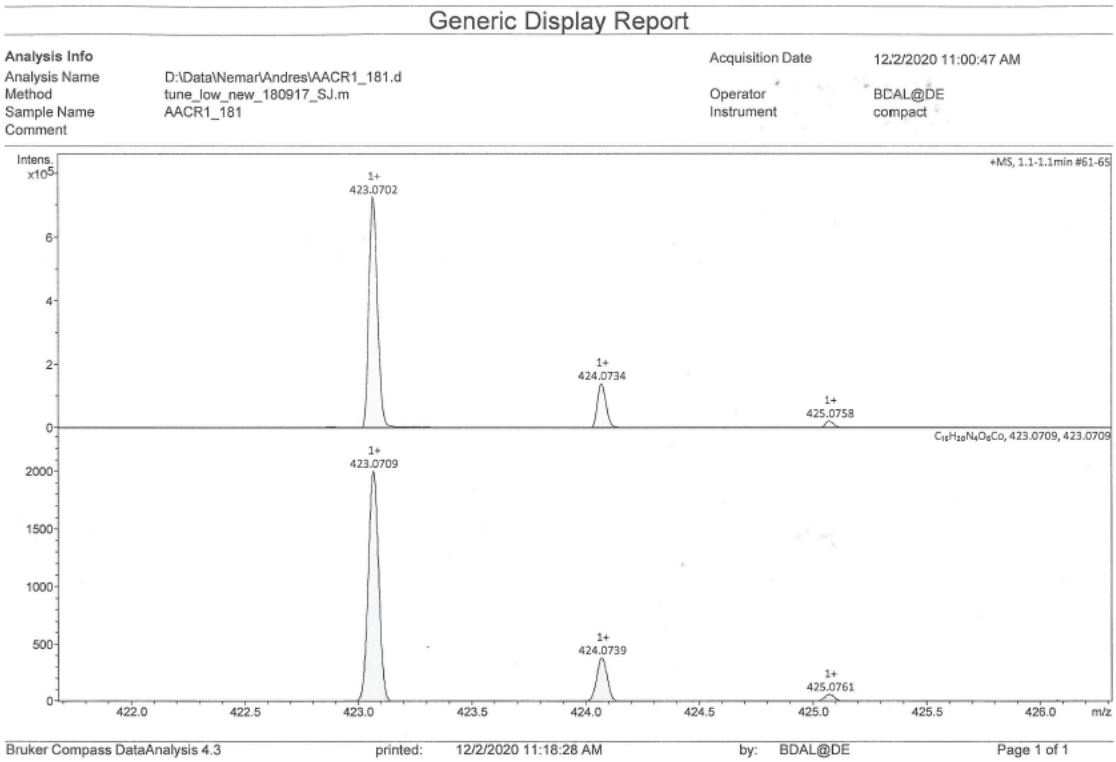

Figure S61. HRMS of **7**

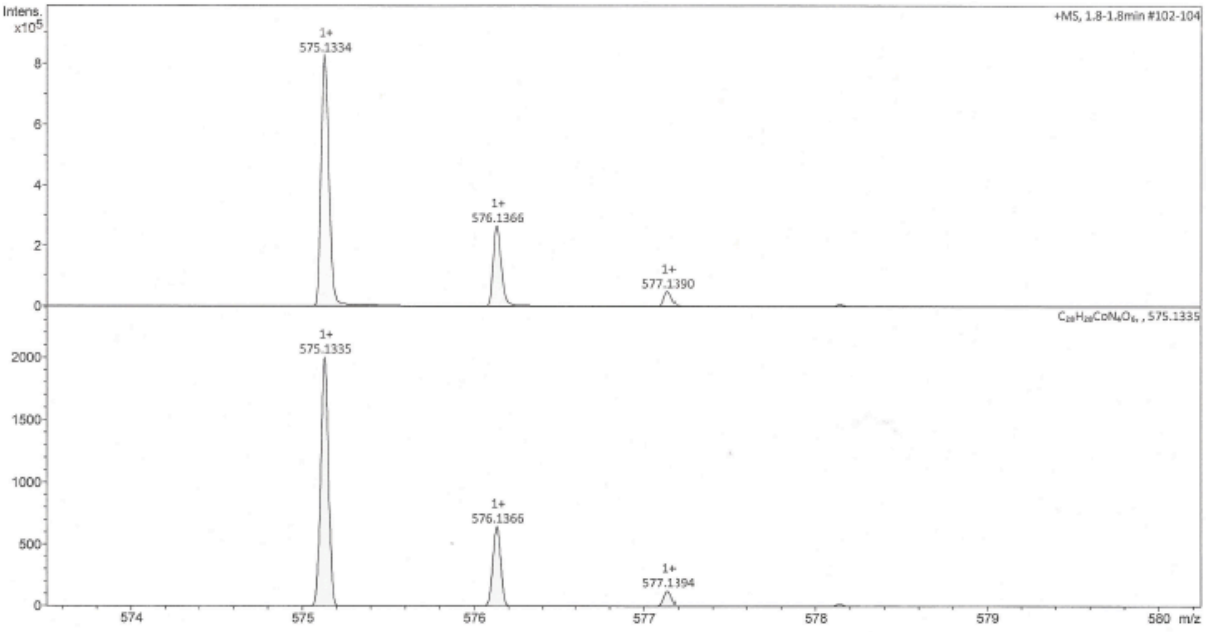

Figure S62. HRMS of **8**

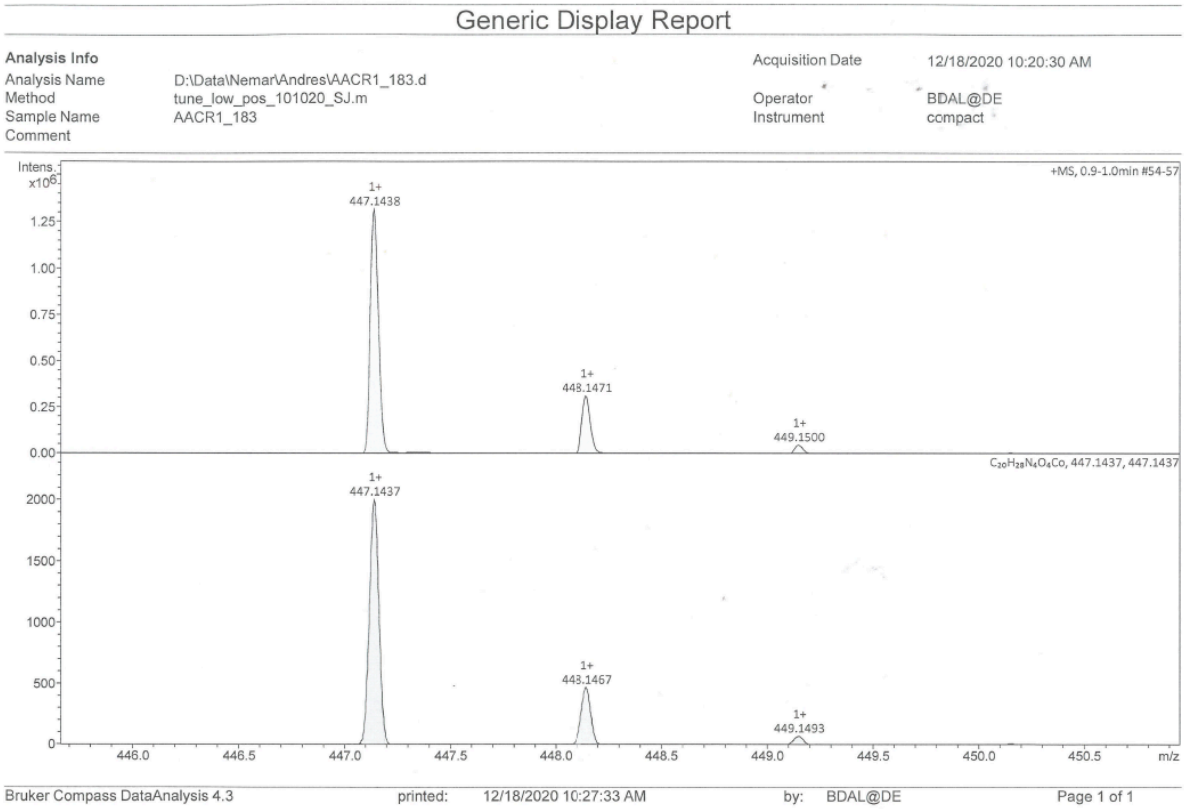

Figure S63. HRMS of **9**

Table S3. Catalytic activity of and Styrene Oxide

Entry	**Catalyst (mol %)**	**Co-catalyst (mol %)**	**Conv. (%)**	**TON**	**TOF (h^{-1})**	**Time (h)**
1	2a	PPNCl	34	675	338	2
2	4	PPNCl	32	649	324	2
3	7	PPNCl	29	582	291	2
4	3	PPNCl	36	720	360	2
5	2a	PPNCl	>99	1980	396	5
6[a]	4	PPNCl	>99	1980	396	5

7	7	PPNCl	>98	1960	392	5
8	3	PPNCl	>99	1980	396	5

Reaction conditions: $[cat]_0:[co\text{-}cat]_0:[PO]_0$ [a] 1:1:2000, (0.015 mmol, 0.015 mmol, 30 mmol) 120 °C, P_{CO2} = 20 bar, PO conversion determined from the relative integrals in the ^{1}H NMR spectrum using mesitylene as the internal standard, Turnover number (TON) = number of moles of PO consumed/number of moles of catalyst. Turnover frequency (TOF) = TON/ time (h).

Table S4. Coupling of PO and CO_2 with catalysts 1-9

Entry	**Catalyst (mol %)**	**Co-catalyst (mol %)**	**Conv. (%)**	**TON**	**TOF (h^{-1})**	**Time (h)**
1[a]	9 (0.025)	KI (0.025)	98	3920	490	8
2[a]	7 (0.025)	KI (0.025)	97	3876	485	8
3[a]	4 (0.025)	KI (0.025)	71	2840	355	8
4[b]	9 (0.016)	KI (0.016)	71	4235	529	8
5[b]	9 (0.016)	PPNCl (0.016)	98	5880	735	8
6	9 (0.025)	-	18	720	36	20
7[b]	3 (0.016)	PPNCl (0.016)	99	5940	742	4.5-5
8	3 (0.016)	-	63	2520	126	20
9	-	-	0	0	0	0
8	3 (0.016)	-	54	3180	162	20
9[b]	8 (0.016)	PPNCl (0.016)	81	4878	243	20
10[b]	7 (0.016)	PPNCl (0.016)	64	3840	768	5

11[b]	4 (0.016)	PPNCl (0.016)	63	3780	756	5
12[b]	2a (0.016)	PPNCl (0.016)	72	4333	866	5
13	3 (0.016)	H_2O 100equiv:PPNCl (0.016)	30	1775	1775	1
14	3 (0.016)	H_2O 100equiv:PPNCl (0.016)	29	1774	1774	1
15	2a (0.016)	PPNCl (0.016)	35	2129	1064	2
16	3 deprotected (0.016)	PPNCl (0.016)	38	2250	1125	1
17[b]	3 deprotected (0.016)	PPNCl (0.016)	80	4785	957	5
18	3 140 °C (0.016)	PPNCl (0.016)	70	4204	2102	2
19	3 (0.016) 1 atm	PPNCl (0.016)	29	1680	1680	1
20	3 (0.016) 10 bar	PPNCl (0.016)	38	2280	2280	1

Reaction conditions: $[cat]_0$:$[co\text{-}cat]_0$:$[PO]_0$ [a]1:1:6000 120 °C, P_{CO2} = 20 bar, PO conversion determined from the relative integrals in the ^1H NMR spectrum using mesitylene as the internal standard, Turnover number (TON) = number of moles of PO consumed/number of moles of catalyst. Turnover frequency (TOF) = TON/ time (h).

Table S5 NMR of cyclic carbonates

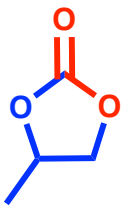

^1H NMR, 400 MHz, CDCl3: δ/ppm = 4.85−4.71(1H, m, OCH), 4.48 (1H, m, *J* = 8.4, 7.2 Hz OCH_2), 4.01 (1H, dd, OCH_2), 1.47 (3H, d, *J* = 6.3 Hz, CH_3); $^{13}C\{1H\}$ NMR, 100 MHz, CDCl3: δ/ppm = 55.06, 73.62, 70.61, 19.14 (d, *J* = 3.4).

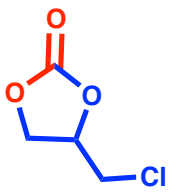

^{1}H NMR, 400 MHz, CDCl3: δ/ppm = 3.70-3.81 (m, 2H), 4.38-4.41 (dd, 1H, J=4 Hz, J=8 Hz), 4.56-4.60 (t, 1H, J=8 Hz), 4.95-5.04 (m, 1H)

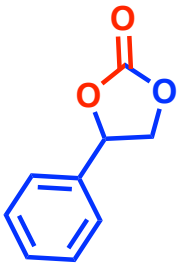

^{1}H NMR, 400 MHz, CDCl3: δ/ppm = 4.33-4.37 (t, 1H, J=8Hz), 4.78-4.82 (t, 1H, J=8 Hz), 5.66- 5.70 (t, 1H, J=8Hz), 7.36-7.37 (m, 2H), 7.44-7.45(m, 3H)

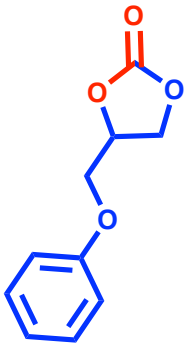

^{1}H NMR, 400 MHz, CDCl3: δ/ppm = 7.34−7.28 (2H, m, 2 x ArH), 7.02 (1H, dt, *J* = 8.3, 0.9 Hz, ArH), 6.93−6.89(2H, m, 2 x ArH), 5.06−4.99 (1H, m, OCH), 4.61 (1H, t, *J* = 8.4 Hz, OCH_2), 4.53 (1H, dd, *J* = 8.5, 5.9 Hz, OCH_2), 4.24 (1H, dd, *J* = 10.6, 4.3 Hz, CH_2OPh), 4.15 (1H, dd, *J* = 10.6, 3.6 Hz, CH_2OPh);

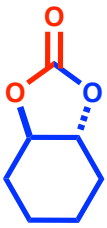

^{1}H NMR, 400 MHz, CDCl3: δ/ppm = 1.42-1.46(m,2H), 1.61-1.64(m, 2H), 1.90-1.91(m, 4H), 4.68(s, 2H)

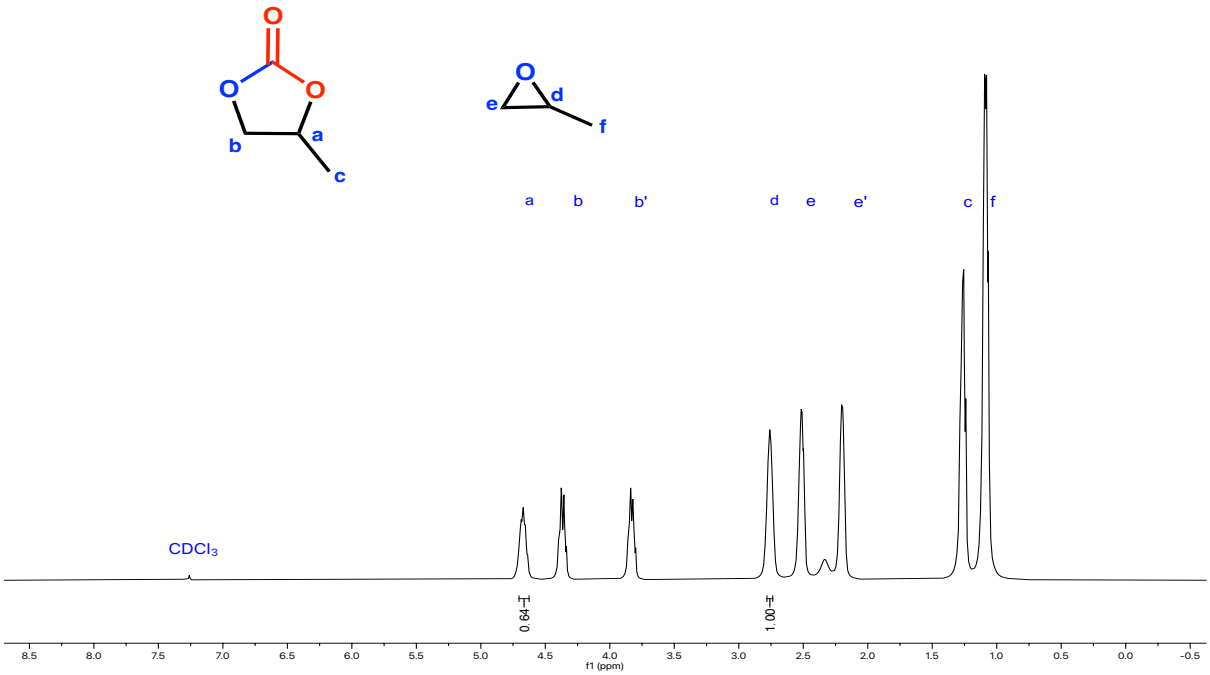

Figure S64. Crude ^{1}H NMR spectrum (400 MHz, 298 K $CDCl_3$) of propylene carbonate showing 39 % conversion based on the integration of methine resonances of unreacted epoxide (2.64 ppm) and the carbonate product (4.59 ppm).

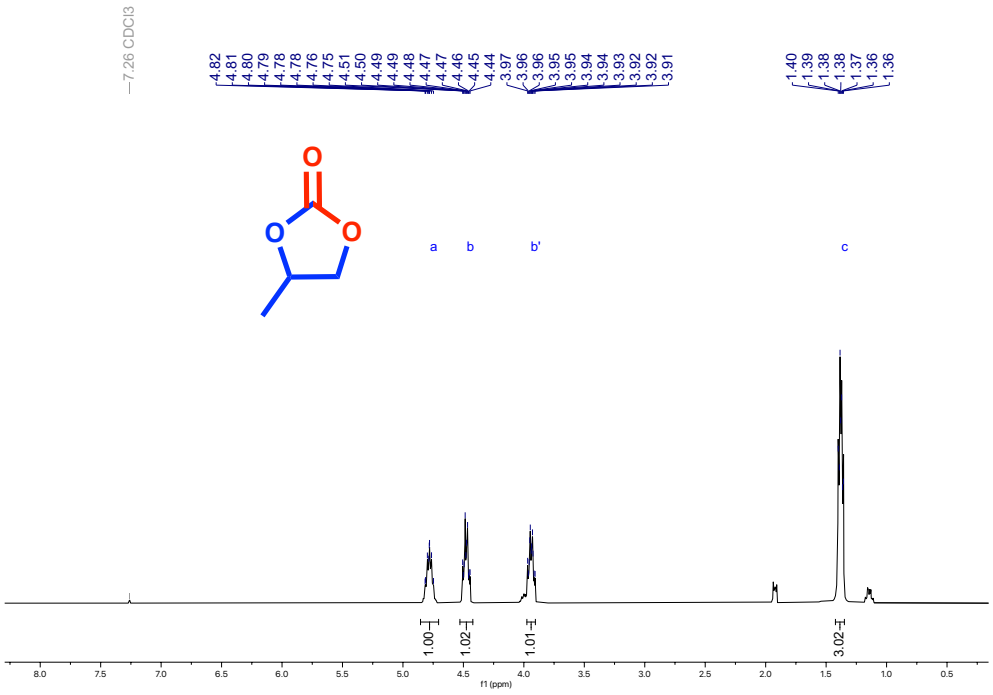

Figure S65. ^{1}H NMR spectrum (400 MHz, 298 K $CDCl_3$) of isolated propylene carbonate.

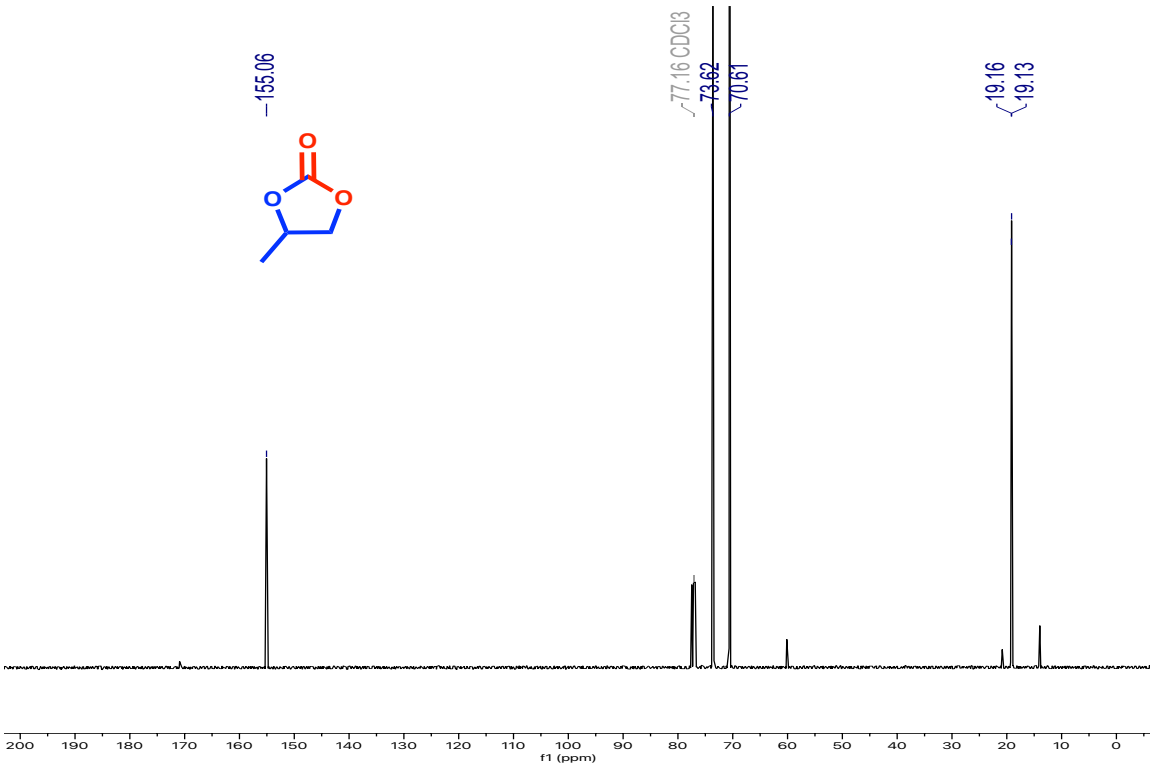

Figure S66. $^{13}C\{1H\}$ NMR (400 MHz, 298 K $CDCl_3$) of propylene carbonate

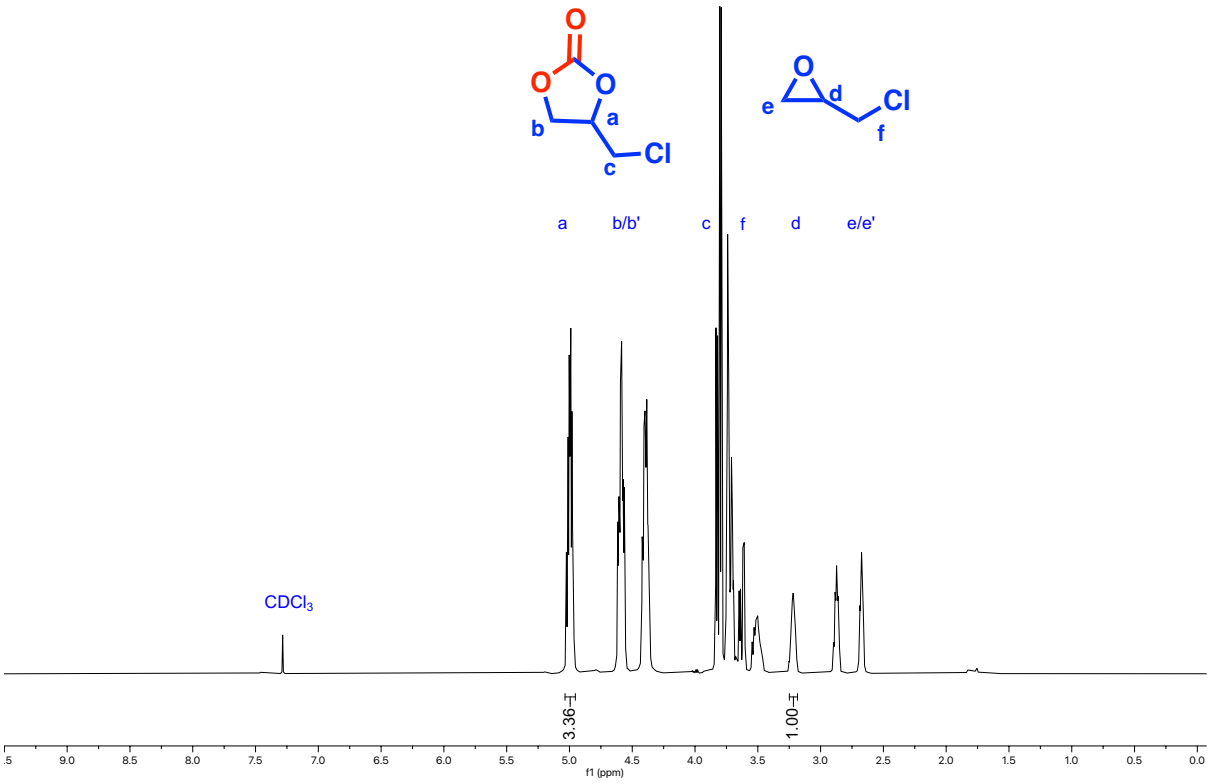

Figure S67. Crude ^{1}H NMR spectrum (400 MHz, 298 K $CDCl_3$) of 4-(chloromethyl)-1,3-dioxolan-2-one showing 77 % conversion based on the integration of resonances of unreacted epoxide at (3.22 ppm) and carbonate at (5.04-4.95 ppm).

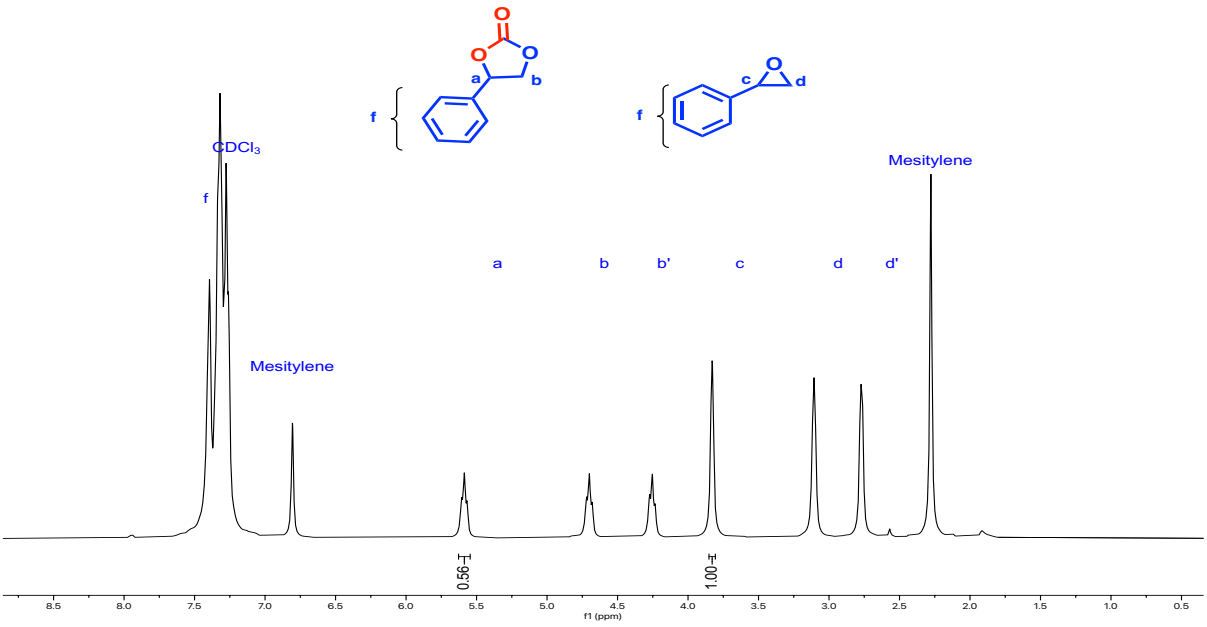

Figure S68. Crude ^{1}H NMR spectrum (400 MHz, 298 K $CDCl_3$) of styrene carbonate showing 36 % conversion based on the integration of resonances of unreacted epoxide at (3.83 ppm) and carbonate at (5.60 ppm).

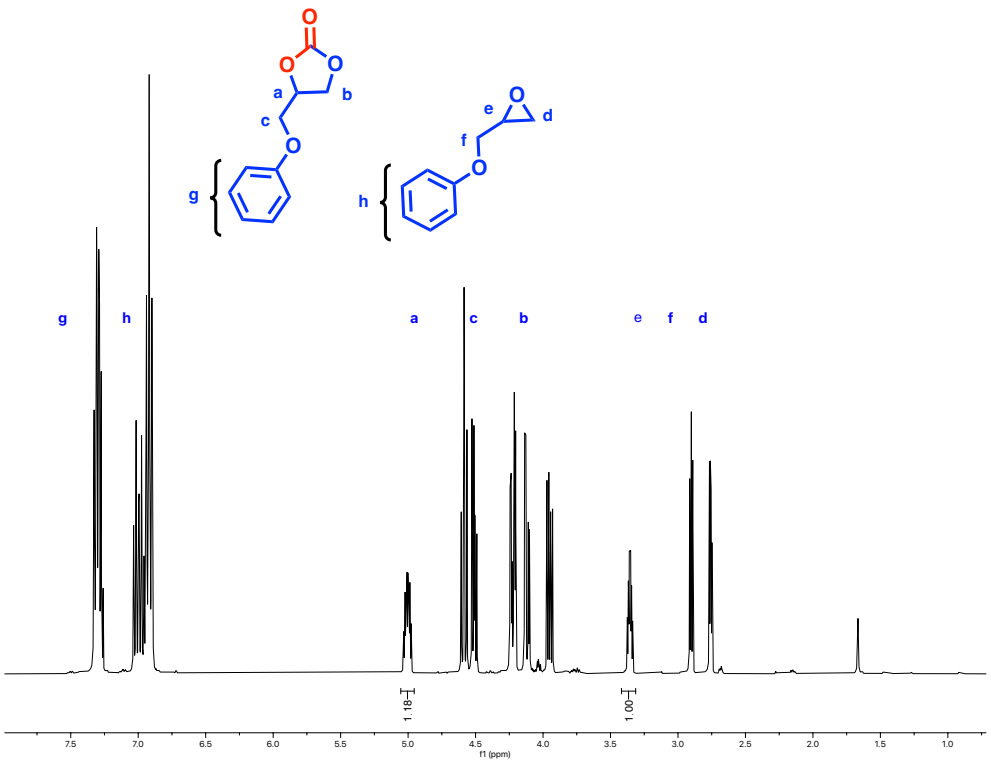

Figure S69. Crude ^{1}H NMR spectrum (400 MHz, 298 K $CDCl_3$) of phenyl glycidyl carbonate showing 54 % conversion based on the integration of resonances of unreacted epoxide at (3.38 ppm) and carbonate at (5.00 ppm).

Kinetic Procedure

Procedure:

The reaction profile was determined by fitting the data to plot the concentration ratios against peak area ratios.[1] The kinetic parameters were studied over a temperature range from 80 to 140 °C. The data were fitted to the following equations:

$$Rate = k\,[epoxide]^a[CO_2]^b[cat]^c[PPNCl]^d \quad (1)$$

$$Rate = K_{obs}[epoxide]^a \quad (2)$$

$$Rate = \frac{-d[epoxide]}{\mathrm{dt}} \quad (3)$$

Where [epoxide], [CO_2], [cat] and [PPNCl] are the propylene oxide, carbon dioxide, catalyst, and co-catalyst concentrations, respectively; a, b, c and d are the order of reactions with respect to propylene oxide, carbon dioxide, catalyst and PPNCl, respectively; *t* is time and k_{obs}

are the observed pseudo-first-order rate constant for propylene oxide conversion. To simplify the equation and solve for k, it can be assumed that the concentration of cat and PPNCl are constant during the reaction and carbon dioxide is in excess to give high dilution so that $a = 1$. Thus, the following pseudo-first-order kinetic rate law is used to simplify eqn. (2) to calculate the observed pseudo-first-order rate constant (k_{obs}) for propylene oxide conversion. [1] Combining and integrating Eqn (2) and (3) as a function of time gives the following conversion

$$-\ln[epoxide] = k_{obs}t \qquad (4)$$

Using the Arrhenius equation Eqn (5), the activation energy for the reaction can be calculated from the relationship between the observed rate constant and temperature:

$$k_{obs} = A\exp^{(-\frac{E_a}{RT})} \qquad (5)$$

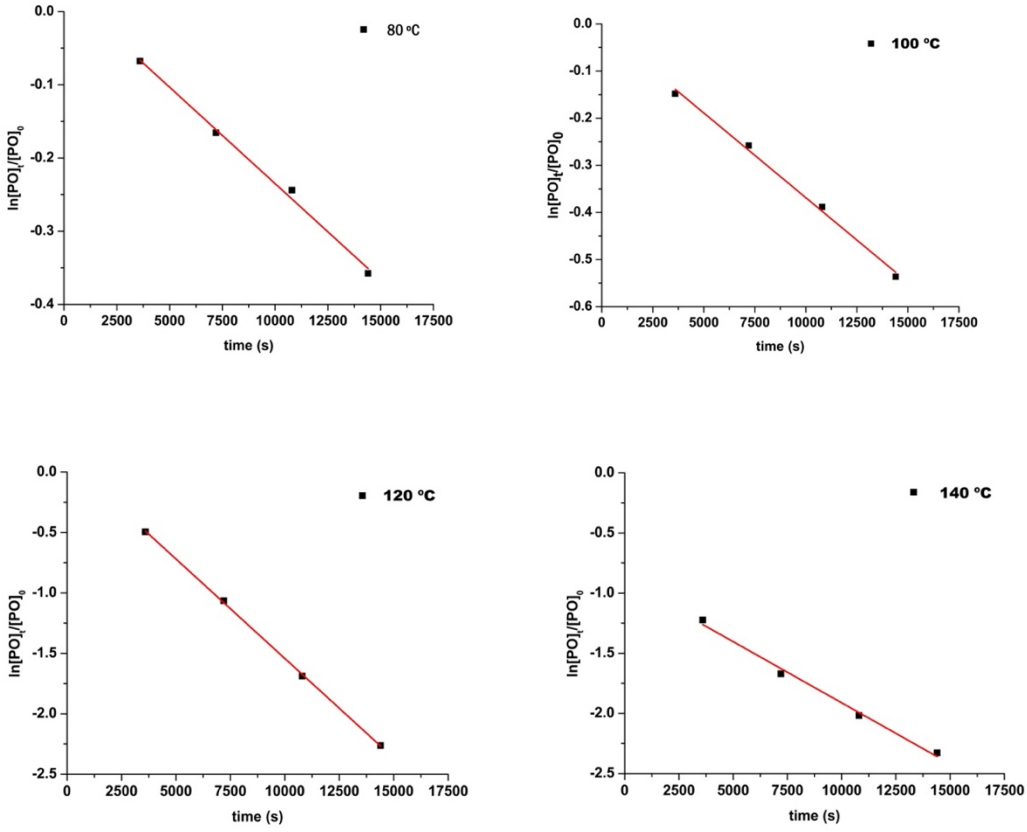

Figure S70. A semilogarithmic plot of $\ln[PO]_t/[PO]_0$ vs. time showing the initial reaction rates for PC at various temperatures with a 20 °C increment. a) 80 °C b) 100 °C c) 120 °C d) 140 °C

Table S6. Data obtained for Arrhenius analysis, linear fits, and calculated rate coefficients for CO_2/PO coupling at various temperatures.

Entry	T (K)	Y = mx + c	R^2	k_{obs} (s^{-1})
1	353	$-2.63x10^{-5} + 0.03$	0.9930	$2.63x10^{-5}$ ($\pm 0.02x10^{-5}$)
2	373	$-4.62x10^{-5} + 0.01$	0.9934	$4.62x10^{-5}$ ($\pm 0.01x10^{-5}$)
3	393	$-1.01x10^{-4} + 0.89$	0.9995	$1.01x10^{-4}$ ($\pm 0.02x10^{-4}$)
4	413	$-1.64x10^{-4} + 0.10$	0.9890	$1.64x10^{-4}$ ($\pm 0.06x10^{-4}$)

k_{obs} = slope of linear fitting of the semilogarithmic plot of $\ln[PO]_t/[PO]_0$ vs time.

Table S7. Data obtained for Eyring analysis, linear fits, and calculated apparent reaction rate *k*p for CO_2/PO coupling at various temperatures.

Entry	T (K)	k_{obs} (s^{-1})	k_p ($L\ mol^{-1}\ s^{-1}$)	Ln(k/T)
1	353	$2.63x10^{-5}$ ($\pm 0.02x10^{-5}$)	$1.07x10^{-5}$ ($\pm 0.08x10^{-5}$)	-17.3106
2	373	$4.62x10^{-5}$ ($\pm 0.01x10^{-5}$)	$1.88x10^{-5}$ ($\pm 0.03x10^{-5}$)	-16.8025
3	393	$1.01x10^{-4}$	$4.13x10^{-5}$	-16.0679

		(± 0.02x10^{-4})	(±0.01x10^{-5})	
4	413	1.64x10^{-4}	6.69x10^{-5}	-15.6352
		(±0.06x10^{-4})	(±0.06x10^{-5})	

$k_p = k_{obs}$/[cat], [cat] = 2.46 mM

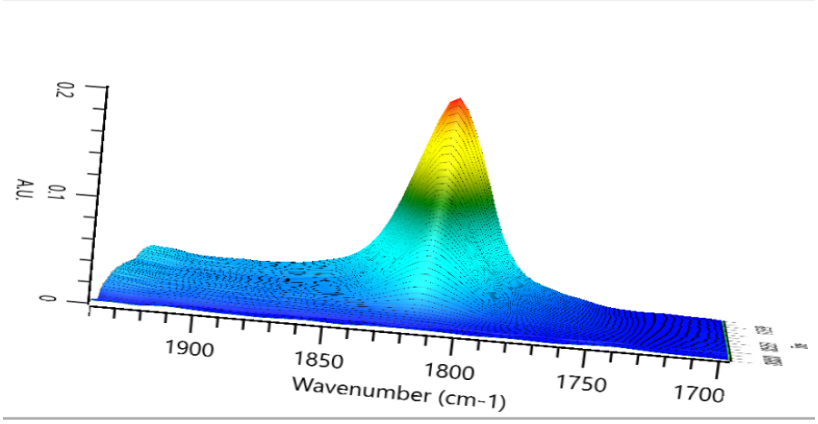

Figure S71. Three-dimensional stack plots of the IR spectra showing the variation of the intensity of the PC C=O stretching band at 1817 cm^{-1} *vs* time. Reaction conditions [cat]:[co-cat]:][PO] 1:1:6000, PCO_2 = 20 bar.

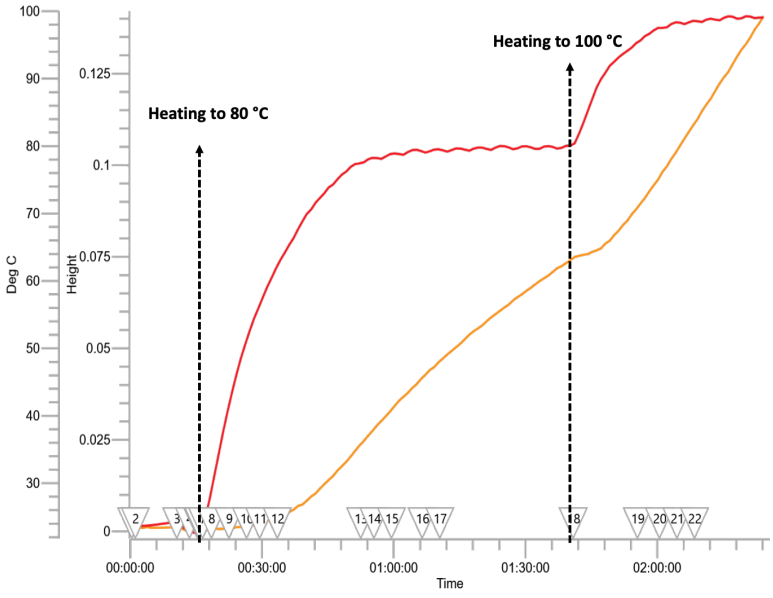

Figure S72. Growth trace of the PC at 1817 cm^{-1} (orange) and probe temperature (red).

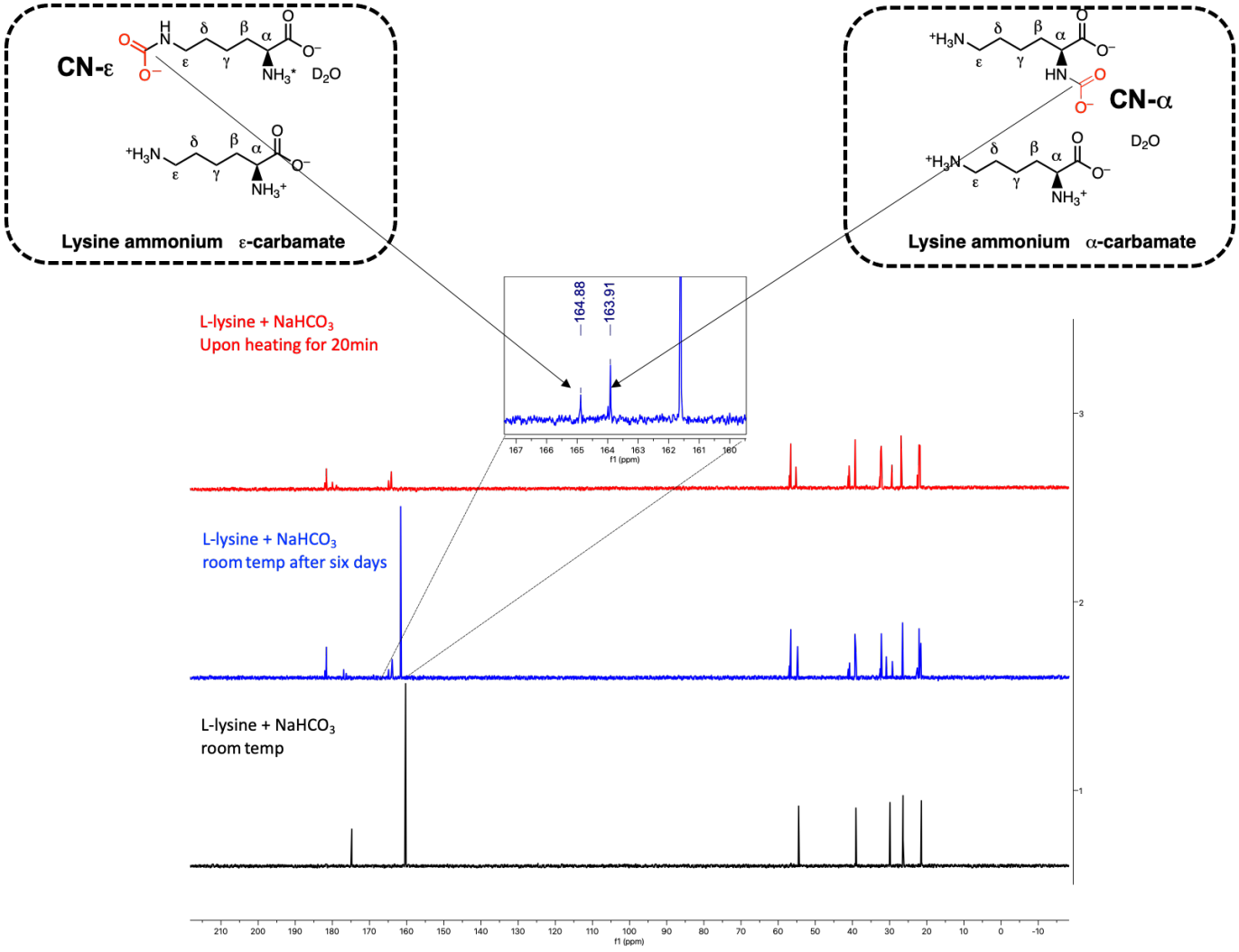

Figure S73. ^{13}C NMR spectra of L-lysine ammonium α- and ε-carbamate in D_2O. L-lysine dihydrochloride (black spectrum). After six days, the carbamate bond of L-lysine ammonium salt (blue spectrum). Upon gradually heating to 100 °C carbamates formed after 20min (red spectrum).

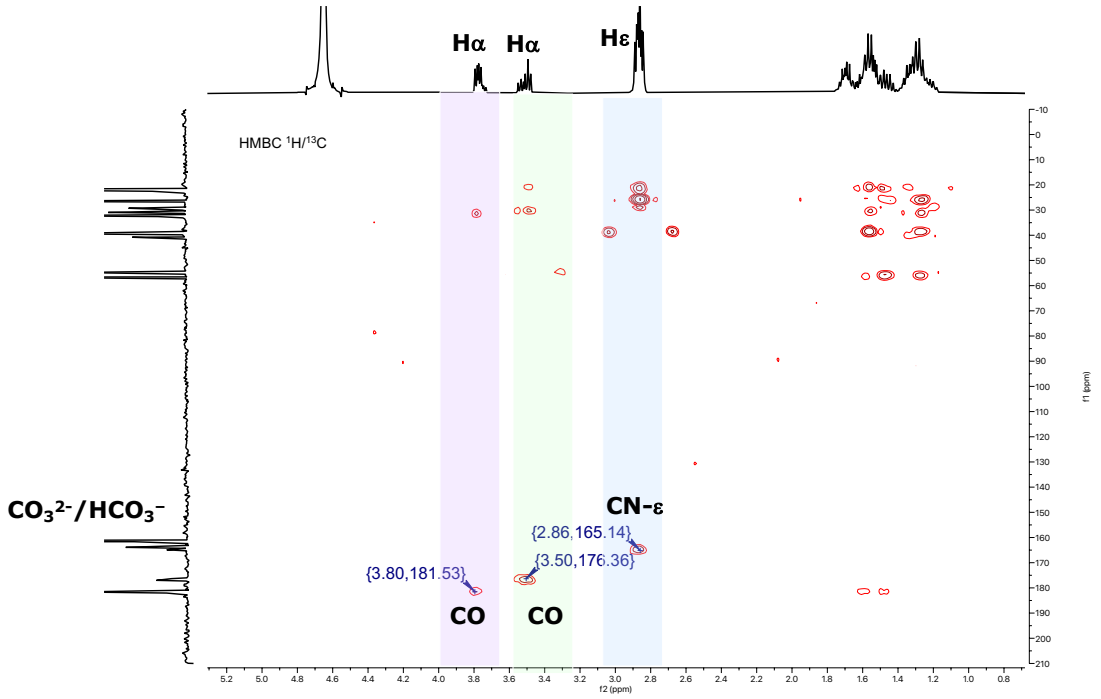

Figure S74. $^{1}H/^{13}C$ HMBC spectrum of L-lysine ammonium ε- carbamate obtained by reacting L-lysine dihydrochloride in the presence of sodium bicarbonate *after six days at room temperature.* The cross-peak between Hα (δ = 3.5 ppm) and the carboxylate carbon CO (δ = 176 ppm) is related to the formation of an α-ammonium ion. The presence of an ε-carbamate ion is confirmed by the cross-peak between Hε (δ = 2.86 ppm) and the carbamyl signal at δ = 165 ppm (CN-ε).[2,3]

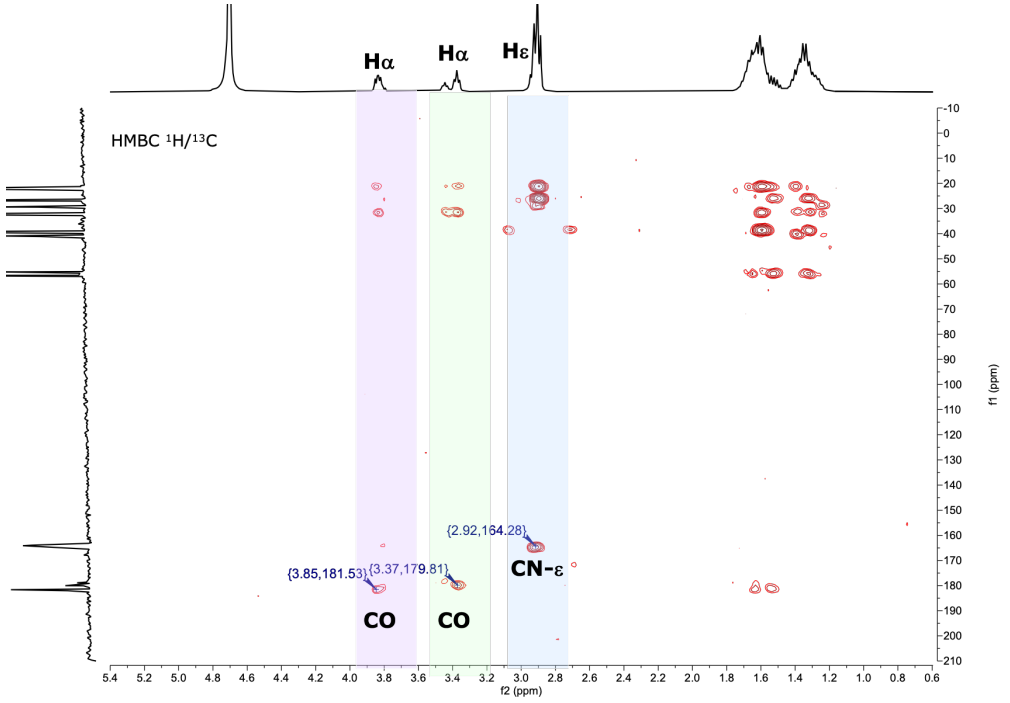

Figure S75. $^{1}H/^{13}C$ HMBC spectrum of L-lysine ammonium ε- carbamate obtained by reacting L-lysine dihydrochloride in the presence of sodium bicarbonate *after gradually heating for 20 minutes*. The cross-peak between Hα (δ = 3.37 ppm) and the carboxylate carbon CO (δ = 179.81 ppm) is related to the formation of an α-ammonium ion. The presence of an ε-carbamate ion is confirmed by the cross-peak between Hε (δ = 2.92 ppm) and the carbamyl signal at δ = 164-165 ppm (CN-ε).[2,3]

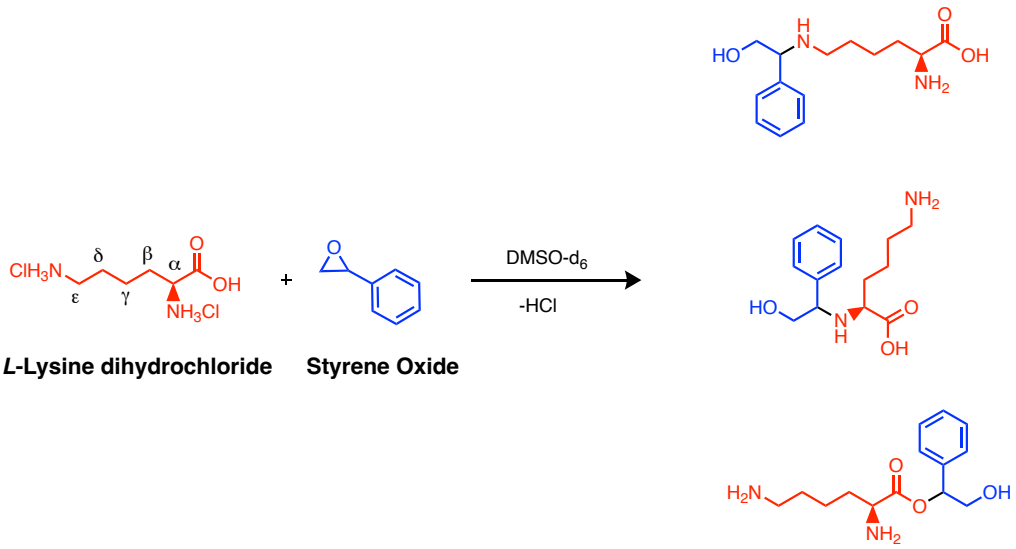

L-Lysine dihydrochloride **Styrene Oxide**

Figure S76. A possible mixture of products resulting from the reaction between *L*-lysine and styrene oxide at temperatures above 80 °C.[4]

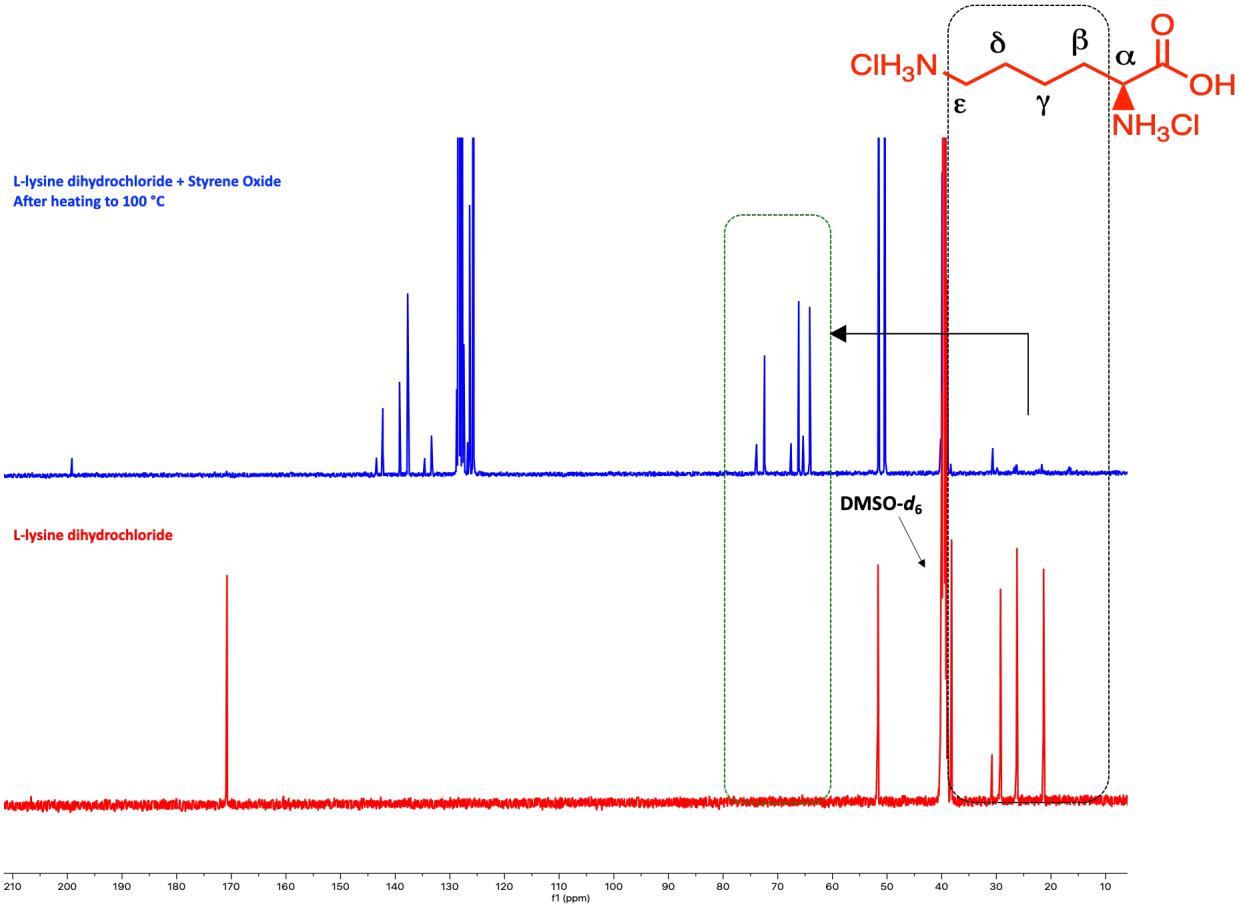

Figure S77. ^{13}C NMR spectra of L-lysine dihydrochloride in DMSO-d_6 (red spectrum) mixture of *L*-lysine dihydrochloride and styrene oxide (blue spectrum).

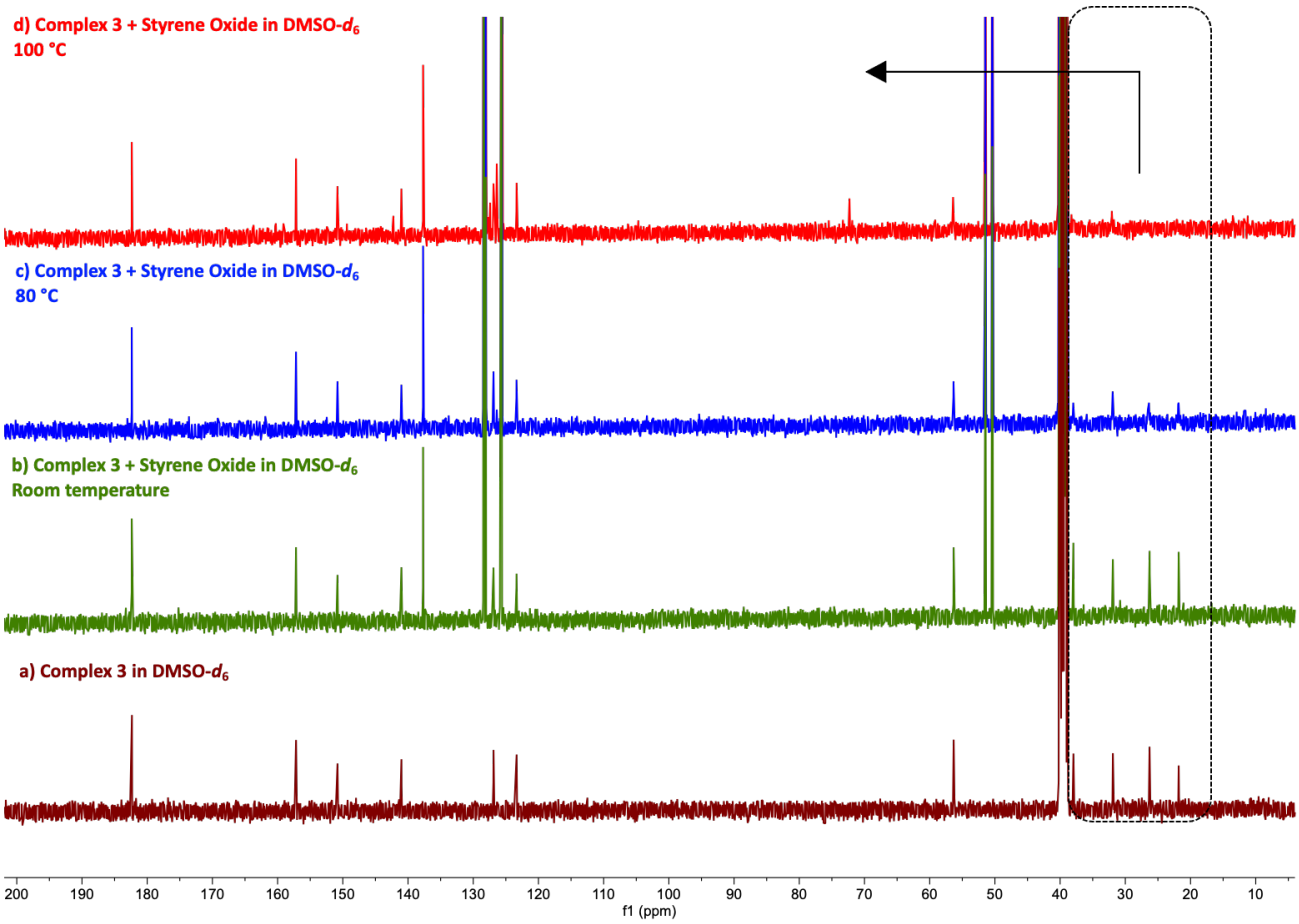

Figure S78. a) ^{13}C NMR spectra of complex 3 in DMSO-d_6 (maroon spectrum) b) mixture of complex 3 and styrene oxide at room temperature (green spectrum) c) mixture of complex 3 and styrene oxide at 80 °C (blue spectrum) mixture of complex 3 and styrene oxide at 100 °C (red spectrum).

References

(1) Supasitmongkol, S.; Styring, P. A Single Centre Aluminium(III) Catalyst and TBAB as an Ionic Organo-Catalyst for the Homogeneous Catalytic Synthesis of Styrene Carbonate. *Catal. Sci. Technol.* **2014**, *4* (6), 1622–1630. https://doi.org/10.1039/C3CY01015E.

(2) Al-Terkawi, A.-A.; Lamaty, F.; Métro, T.-X. Efficient CO_2 Sequestration by a Solid–Gas Reaction Enabled by Mechanochemistry: The Case of l -Lysine. *ACS Sustain. Chem. Eng.* **2020**, *8* (35), 13159–13166. https://doi.org/10.1021/acssuschemeng.0c00217.

(3) Wei, D.; Junge, H.; Beller, M. An Amino Acid Based System for CO_2 Capture and Catalytic Utilization to Produce Formates. *Chem. Sci.* **2021**, *12* (17), 6020–6024. https://doi.org/10.1039/D1SC00467K.

(4) M. Jágr, J. Mráz, I. Linhart, V. Stránský and M. Pospíšil, *Chem. Res. Toxicol.*, 2007, **20**, 1442-1452.